Damage detection of retrofitted beam using Frequency response function

A thesis submitted in the partial fulfillment of
requirement for the award of the degree of

MASTER OF ENGINEERING
IN
STRUCTURES

Submitted by

YOGESH KUMAR

Roll No. 800922013

Under the supervision of

Dr. Naveen Kwatra

Associate Professor

C.E.D

Thapar University

DEPARTMENT OF CIVIL ENGINEERING

THAPAR UNIVERSITY

(Established under section 3 of UGC Act, 1956)

PATIALA-147001, PUNJAB,

INDIA

CERTIFICATE

This is to certify that the Thesis titles," Damage detection of retrofitted beam by Frequency response function", being submitted by **Yogesh Kumar**, in partial fulfillment of the requirements for the award of degree of MASTER OF ENGINEERING (STRUCTURES) at THAPAR UNIVERSITY, PATIALA is a bonafide work carried out by him under my guidance and supervision and no part of this thesis submitted for the award of any other degree.

Dr Naveen Kwatra
(Associate Professor), C.E.D
Thapar University
Date: /07/2011

Dr. Maneek Kumar
(Head of department), C.E.D
Thapar University
Date: /07/2011

Dr S.K Mohapatra
(Dean of Academic Affairs)
Thapar University
Date: /07/2011

ACKNOWLEDGEMENT

This report is completed with prayer of many and love of my family and friends. However, there are few people that I would like to specially acknowledge and extend my heartfelt gratitude who have made the completion of this report possible. With the biggest contribution to this report; I would like to thank **Dr. Naveen Kwatra** had given me his full support in guiding me with stimulating suggestions and encouragement to go ahead in all the time of the seminar work.

At last but not the least my gratitude towards my parents, I would also like to thank God for not letting me down at a time of crisis and showing me the silver lining in the dark clouds.

Yogesh

YOGESH

ABSTRACT

Structures are assembles of loaded carrying members capable of safely transferring the superimposed loads to the foundations. They are constructed (e.g. buildings, bridges, dams, transmission towers, etc.) or manufactured (e.g. machines, trains, ships, aircraft, etc.) to serve specific functions during their design lives. In order to serve their designated functions, the structures must satisfy both strength and serviceability criteria throughout their stipulated design life. However, with the passage of time, some amount of deterioration and damages are bound to occur, due to variety of factors; such as environment degradation, fatigue, excessive loads etc. Knowledge of these defects with a view to detect and evaluate them and then minimizing them in the structures are essential to achieve improved and acceptable level of quality. An improvement in the structures quality increases its reliability and in turns the safety of the machines and equipment. There is, therefore, a need to have methods by which the defects in the structures can be examined without affecting their performance. Non-Destructive Testing (NDT), Non-Destructive Evaluation (NDE) and Non-Destructive Inspection (NDI) are the terms used in this connection to represent the techniques that are based on the application of physical properties employed for the purpose of detecting and assessing the irregularities and harmful defects without impairing the usefulness of such structures.

Many old building needs to be retrofitted because they have not been designed by taking in to considerations earthquake forces. SHM of such buildings is also very important in order to study the vibration characteristics. Seismic retrofitting of existing structures is one of the effective methods for improving the performance of the structure in future loading. Various terms are associated to retrofit with a marginal difference like repair, strengthening, retrofitting, remoulding, rehabilitation, reconstruction etc. But there is no consensus on them. Various retrofitting techniques are used in field and out of all plate bonding techniques are considered as the best. In the plate bonding technique the plates of different material viz Carbon Fibre Reinforced Polymer (CFRP), Glass Fibre Reinforced Polymer (GFRP), Ferro cement etc. are bonded to the surface of structural member to increase its strength. In the present work GFRP material is used for Plate bonding.

The present research deals with Damage detection of Retrofitted beams by Frequency response function. In this research we modelled RCC beam as control beam in ANSYS. The size of the beam is 117X227X4100 mm. Damage was introduced in the beam by doing the deformation controlled non-linear analysis. Retrofitted beam is modelled in ANSYS and damage of the beam is introduced using the same procedure. To model a damaged beam we used the Elastic modulus calculated using the Load deflection value observed through the non linear analysis of the beams. Retrofitted beams are modelled as stressed at 90% and 75%. Harmonic analysis is done on the control beam and retrofitted beam at different load

steps. By doing the harmonic analysis we get the frequency response function at that load step. Using the frequency response function we analysed the damage. From the research we conclude that there is increase in frequency of retrofitted beam in comparison to control beam; also the load carrying capacity of beam increases after retrofitting. We also observed increase stiffness of beam after retrofitting.

In the second phase of this research is to compare the results with the experimental results and try to identify the various effects on the RCC structural members. The result show good agreement with the experimental results.

CONTENTS

LIST OF FIGURES

CHAPTER 2

CHAPTER 3

CHAPTER 4

LIST OF TABLES

INTRODUCTION

1.1 GENERAL

Civil structures such as buildings, bridges, dams, tunnels, ports, etc. are the most expensive assets of modern society that need to be functional for a very long time under complex conditions, thus their constant monitoring is pivotal to preventing catastrophe and ensuring safety. The process of implementing a damage detection and characterization strategy for engineering structures is referred to as **Structural Health Monitoring** (SHM). Here damage is defined as changes to the material and/or geometric properties of a structural system, including changes to the boundary conditions and system connectivity, which adversely affect the system's performance (Wikipedia).

Qualitative and non-continuous methods have long been used to evaluate structures for their capacity to serve their intended purpose. Since the beginning of the 19th century, railroad wheel-tappers have used the sound of a hammer striking the train wheel to evaluate if damage was present in rotating machinery; vibration monitoring has been used for decades as a performance evaluation technique. In the last ten to fifteen years, SHM technologies have emerged creating an exciting new field within various branches of engineering.

Farrar et. al, (2006) There are many ways by which one can organize a discussion of SHM. SHM can be classified in a four step process. This following four-step process includes:

(i) operational evaluation
(ii) data acquisition, normalization and cleansing,
(iii) feature selection and information condensation, and
(iv) statistical model development for feature discrimination.

Operational evaluation

Operational evaluation attempts to answer four questions regarding the implementation of a damage identification capability.

(i) What are the life-safety and/or economic justification for performing SHM?
(ii) How is damage defined for the system being investigated and, for multiple damage possibilities, which cases are of the most concern?
(iii) What are the conditions, both operational and environmental, under which the system to be monitored functions?
(iv) What are the limitations on acquiring data in the operational environment?

Operational evaluation begins to set the limitations on what will be monitored and how the monitoring will be accomplished. This evaluation starts to tailor the damage identification process to features that are unique to the system being monitored and tries to take advantage of unique features of the damage that is to be detected.

Data acquisition, normalization and cleansing

The data acquisition portion of the SHM process involves selecting the excitation methods, the sensor types, number and locations, and the data acquisition/ storage/transmittal hardware. Again, this process will be application specific. Economic considerations will play a major role in making these decisions. The interval at which the data should be collected is another consideration that must be addressed.

As data can be measured under varying conditions, the ability to normalize the data becomes very important to the damage identification process. As it applies to SHM, data normalization is the process of separating changes in sensor reading caused by damage from those caused by varying operational and environmental conditions. One of the most common procedures is to normalize the measured responses by the measured inputs. When environmental or operational variability is an issue, the need can arise to normalize the data in some temporal fashion to facilitate the comparison of data measured at similar times of an environmental or operational cycle. Sources of variability in the data acquisition process and with the system being monitored need to be identified and minimized to the extent possible. In general, not all sources of variability can be eliminated. Therefore, it is necessary to make the appropriate measurements such that these sources can be statistically quantified. Variability can arise from changing environmental and test conditions, changes in the data reduction process and unit-to-unit inconsistencies.

Data cleansing is the process of selectively choosing data to pass on to or reject from the feature selection process. The data cleansing process is usually based on the knowledge gained by individuals directly involved with the data acquisition. As an example, an inspection of the test set-up may reveal that a sensor was loosely mounted and, hence, based on the judgment of the individuals performing the measurement, this set of data or the data from that particular sensor may be selectively deleted from the feature selection process. Signal processing techniques such as filtering and resampling can also be thought of as data cleansing procedures**. Lynch (2007), Sohn (2007), Park and Inman (2007), Todd et. al. (2007)**

*Feature extraction and information condens*ation

The area of the SHM process that receives the most attention in the technical literature is the identification of data features that allows one to distinguish between the undamaged and damaged structure. As such, numerous articles in this theme issue are devoted to the feature extraction portion of SHM (**Fassois & Sakellariou 2007; Friswell 2007; Mal et al. 2007; Staszewski & Robertson 2007**). Inherent in this feature selection process is the condensation of the data. The best features for damage identification are, again, application specific.

One of the most common feature extraction methods is based on correlating measured system response quantities, such as vibration amplitude or frequency, with the first-hand observations of the degrading system. Another method of developing features for damage identification is to apply engineered flaws, similar to ones expected in actual operating

conditions, to systems and develop an initial understanding of the parameters that are sensitive to the expected damage. The flawed system can also be used to validate that the diagnostic measurements are sensitive enough to distinguish between features identified from the undamaged and damaged system. The use of analytical tools such as experimentally validated finite element models can be a great asset in this process. In many cases, the analytical tools are used to perform numerical experiments where the flaws are introduced through computer simulation. Damage accumulation testing, during which significant structural components of the system under study are degraded by subjecting them to realistic loading conditions, can also be used to identify appropriate features. This process may involve induced-damage testing, fatigue testing, corrosion growth or temperature cycling to accumulate certain types of damage in an accelerated fashion. Insight into the appropriate features can be gained from several types of analytical and experimental studies as described above and is usually the result of information obtained from some combination of these studies.

The operational implementation and diagnostic measurement technologies needed to perform SHM produce more data than traditional uses of structural dynamics information. A condensation of the data is advantageous and necessary when comparisons of many feature sets obtained over the lifetime of the structure are envisioned.

Feature Extraction and Data Compression

The area of the SHM process that receives the most attention in the technical literature is the identification of data features that allows one to distinguish between the undamaged and damaged structure. Inherent in this feature selection process is the condensation of the data. The best features for damage identification are, again, application specific.

One of the most common feature extraction methods is based on correlating measured system response quantities, such a vibration amplitude or frequency, with the first-hand observations of the degrading system. Another method of developing features for damage identification is to apply engineered flaws, similar to ones expected in actual operating conditions, to systems and develop an initial understanding of the parameters that are sensitive to the expected damage. The flawed system can also be used to validate that the diagnostic measurements are sensitive enough to distinguish between features identified from the undamaged and damaged system. The use of analytical tools such as experimentally-validated finite element models can be a great asset in this process. In many cases the analytical tools are used to perform numerical experiments where the flaws are introduced through computer simulation. Damage accumulation testing, during which significant structural components of the system under study are degraded by subjecting them to realistic loading conditions, can also be used to identify appropriate features. This process may involve induced-damage testing, fatigue testing, corrosion growth, or temperature cycling to accumulate certain types of damage in an accelerated fashion. Insight into the appropriate features can be gained from several types of analytical and experimental studies as described above and is usually the result of information obtained from some combination of these studies.

The operational implementation and diagnostic measurement technologies needed to perform SHM produce more data than traditional uses of structural dynamics information. A condensation of the data is advantageous and necessary when comparisons of many feature sets obtained over the lifetime of the structure are envisioned. Also, because data will be acquired from a structure over an extended period of time and in an operational environment, robust data reduction techniques must be developed to retain feature sensitivity to the structural changes of interest in the presence of environmental and operational variability. To further aid in the extraction and recording of quality data needed to perform SHM, the statistical significance of the features should be characterized and used in the condensation process.

Statistical Model Development

The portion of the SHM process that has received the least attention in the technical literature is the development of statistical models for discrimination between features from the undamaged and damaged structures. Statistical model development is concerned with the implementation of the algorithms that operate on the extracted features to quantify the damage state of the structure. The algorithms used in statistical model development usually fall into three categories. When data are available from both the undamaged and damaged structure, the statistical pattern recognition algorithms fall into the general classification referred to as supervised learning. Group classification and regression analysis are categories of supervised learning algorithms. Unsupervised learning refers to algorithms that are applied to data not containing examples from the damaged structure. Outlier or novelty detection is the primary class of algorithms applied in unsupervised learning applications. All of the algorithms analyze statistical distributions of the measured or derived features to enhance the damage identification process. **Hayton et. al (2007), Sohn (2007), Worden and Manson (2007**)

1.2 FREQUENCY RESPONSE FUNCTION

Irvine, (2000) for successful structural health monitoring and damage assessment, at least four levels needs to be considered: existence, location, extent and prediction. However, the key issue for on-line structural health monitoring is to diagnose the state of the structure; healthy or damaged, by comparing the current dynamic response measurements with those made previously. In recent years, the discipline of novelty detection has been introduced to identify from measured data if a machine or structure has deviated from normal conditions. The method used for damage identification is based on frequency response function sensitivities to the stiffness variations. The frequency response function sensitivities method also quantifies the decrease in stiffness, due to damage i.e. the decrease in Young's Modulus.

A *frequency response function* (FRF) is a transfer function, expressed in the frequency domain. Frequency response functions are complex functions, with real and imaginary components. They may also be represented in terms of magnitude and phase. A frequency response function can be formed from either measured data or analytical functions. A frequency response function expresses the structural response to an applied force as a function of frequency. The response may be given in terms of displacement, velocity, or

acceleration. Based on this line of arguments, Schultz et al. Proposed SHM methods classifying the structure in various damages states based on the differences between the vibration features extracted from the measured responses of the structure in the damaged and undamaged states.

1.3 OBJECTIVE

1. To determine analytically the dynamic characteristics of reinforced concrete beams subjected to different level of damage. The dynamic characteristics envisaged to be investigated are natural time period, Frequency Response Function (FRF) etc, by doing the harmonic analysis using ANSYS.
2. To determine analytically the dynamic characteristics of retrofitted beams subjected to different damage levels, after strengthening using GPRP sheets.
3. To assess the suitability of FRF technique for heath monitoring of retrofitted beams.

1.4 SCOPE OF WORK

The FRF characteristics of the model of reinforced concrete beams will be determined for both original and retrofitted beams. The following parameters will be observed:

1. Nonlinear static load deflection behaviour
2. Frequency Response Function

1.5 METHEDOLOGY

Beams of size (127X117X4100mm) will be modelled in ANSYS. Method of two point loading will be used for loading of beams. The FRF will be studied while increasing the load from 0kN to ultimate load. Then beams will be stressed up to 75, 90 of their respective loads and they will be retrofitted with GFRP model and their FRF will be studied.

1.6 OUTLINE OF THESIS

Following the introduction to thesis in chapter 1, Chapter 2 will discuss the Literature review i.e., work done by the people in the same field and gaps in the work.
All the modelling procedure will be discussed in Chapter 3.
Results and discussion of the present study will be discussed in Chapter 4 and finally salient conclusion of the present study is given in Chapter 5.

LITERATURE REVIEW

2.1 ANALYTICAL WORK

Irvine, (2000) in his paper "An introduction to frequency response function" defined FRF as a transfer function, expressed in the frequency domain. Frequency response functions are complex functions, with real and imaginary components. They may also be represented in terms of magnitude and phase. A frequency response function expresses the structural response to an applied force as a function of frequency. The response may be given in terms of displacement, velocity, or acceleration.

Frequency Response Function Model

Consider a linear system as represented by the diagram in Figure 2.1.

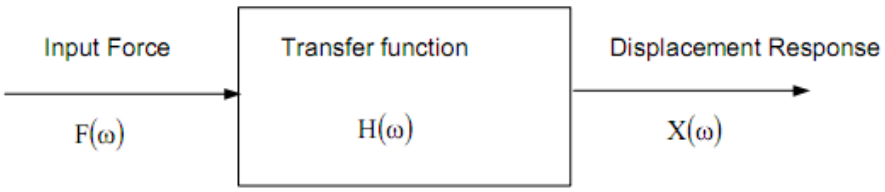

Fig 2.1 Linear system

F(ω) is the input force as a function of the angular frequency ω .H(ω) is the transfer function. X(ω) is the displacement response function. Each function is a complex function, which may also be represented in terms of magnitude and phase. Each function is thus a spectral function. There are numerous types of spectral functions. For simplicity, consider each to be a Fourier transform.

The relationship in Figure 2.1 can be represented by the following equations:

$$X(\omega) = H(\omega) \cdot F(\omega) \qquad \text{eq. 2.1}$$

$$H(\omega) = \frac{X(\omega)}{F(\omega)} \qquad \text{eq. 2.2}$$

Similar transfer functions can be developed for the velocity and acceleration responses.

There are six basic transfer functions as shown in Tables 2.1.

Dimension	Displacement/Force	Velocity/Force	Acceleration/Force
Name	Admittance, Compliance, Receptance	Mobility	Accelerance, Inertance

Table 2.1 Basic transfer function

Dimension	Force/Displacement	Force/Velocity	Force/Acceleration
Name	Dynamic Stiffness	Mechanical Impedance	Apparent Mass, Dynamic Mass

Table 2.1 Basic transfer function (Cont)

Analytical Frequency Response Function

Consider a single-degree-of-freedom system subjected to a force excitation as shown in Figure 2.2. The free-body diagram is shown in Figure 2.3.

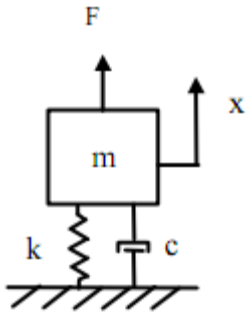

Fig 2.2 Single-degree-of-freedom system

The variables are

m = mass,
c = viscous damping coefficient,
k = stiffness,
x = absolute displacement of the mass,
F = applied force.

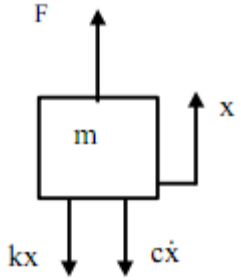

Fig 2.3 Free-body diagram

Summation of forces in the vertical direction

$$\sum F = m\ddot{x} \qquad \text{eq 2.3}$$

$$m\ddot{x} = -c\dot{x} - kx + F \qquad \text{eq 2.4}$$

$$m\ddot{x} + c\dot{x} + kx = F \qquad \text{eq 2.5}$$

$$\ddot{x} + (c/m)\dot{x} + (k/m)x = F/m \qquad \text{eq 2.6}$$

By convention,

$$(c/m) = 2\xi\omega_n \qquad \text{eq 2.7}$$

$$(k/m) = \omega_n{}^2 \qquad \text{eq 2.8}$$

where ω_n is the natural frequency in (radians/sec), and ξ is the damping ratio.

Substituting the convention terms into equation 2.6

$$\ddot{x} + 2\xi\omega_n \dot{x} + \omega_n{}^2 x = \omega_n{}^2 F/k \qquad \text{eq 2.9}$$

The Fourier transform of each side of equation 2.9 may be taken to derive the steady-state transfer function for the absolute response displacement.

After many steps, the resulting transfer function is

$$\frac{X(\omega)}{F(\omega)} = \left[\frac{1}{k}\right]\left[\frac{\omega_n{}^2}{\omega_n{}^2 - \omega^2 + j(2\xi\omega\omega_n)}\right] \qquad \text{eq 2.10}$$

This transfer function, which represents displacement over force, is sometimes called the receptance function.

Saifullah et. al (2011) in their paper focused on the behaviour of reinforced concrete beam for different pattern of shear reinforcement to evaluate the effective shear reinforcement pattern and also compare the variation in behaviour of reinforced concrete beam for with and without shear reinforcement with a simulation. To carry out the analysis, six 3D beams without and with different patterns of shear reinforcement was built using comprehensive computer software **ANSYS 10 © 2005 SAS IP, Inc** package. The static non linear analysis was done to find out ultimate capacity, formation of first crack and its distance from support, initiation of diagonal crack and its distance from support. Load deflection response was also closely observed and compared with the result from theoretical calculation.

Size of concrete beam was 10X18 in.^{2} and 15 ft long. Bottom r/f of 4 bars of 8mm each and stirrups of 3@9". Concrete beam was modelled in ANSYS with material properties shown in Table 2.2. Solid 65 element was used for Concrete, Solid 45 for steel plate and support, and link 8 was used for reinforcement. FEM model can be seen in Fig .Development of cracks was studied and various load deflection curve were studied. In this study it was found that for a beam without shear reinforcement diagonal tension crack initiates at larger distance from support with compared to others.. It was also observed that the theoretical calculation and ANSYS give almost same results for steel stressing at 1st crack and also from combined load deflection curve, the 1st cracking point and the steel yielding point for with and without different patterns of shear reinforcement are almost same.

Material Model Number	Element Type	Material Properties	
1	Solid65		
		Linear Isotropic	
		EX	3604974.865
		PRXY	0.25
			Strain
		Concrete	
		ShrCf-Op	0.3
		ShrCf-Cl	1
		UnTensSt	474.34
		UnCompSt	-1
		BiCompSt	0
		HydroPs	0
		BiCompSt	0
		UnTensSt	0
		TenCrFac	0
2	Solid45	Linear Isotropic	
		EX	29,000,000 psi
		PRXY	0.3
3	Link8		
		Linear Isotropic	
		EX	29,000,000 psi
		PRXY	0.3
		Bilinear Isotropic	
		Yield Stress	60,000 psi
		Tangent Modulus	2,900 psi

Table 2.2 Material properties of elemet (Saifullah et. al (2011))

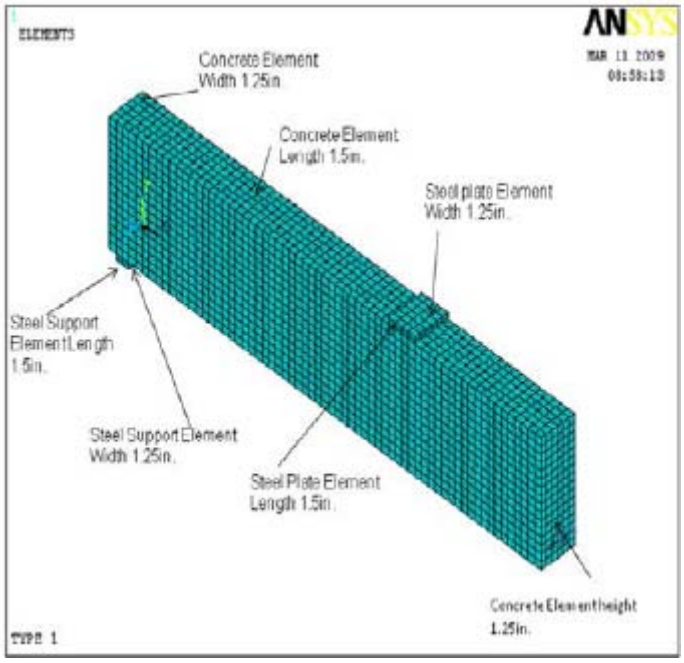

Fig 2.4 Ansys model of concrete beam (Saifullah et. al (2011))

Ibrahim and Mahmood (2009) in their paper did analysis of reinforced concrete beams externally reinforced with fibre reinforced polymer (FRP) laminates using finite elements method adopted by ANSYS.

The finite element models are developed using a smeared cracking approach for concrete and three dimensional layered elements for the FRP composites. The results obtained from the ANSYS finite element analysis are compared with the experimental data for six beams with different conditions from researches (all beams are deficient shear reinforcement). The comparisons are made for load-deflection curves at mid-span; and failure load. The results from finite element analysis were calculated at the same location as the experimental test of the beams. The accuracy of the finite element models is assessed by comparison with the experimental results, which are to be in good agreement.

	B1, B1C-90, B1G-90	B2, B2C-90, B2C-90-0
Steel yield strength f_y (N/mm^2)	420	414
Steel modulus of elasticity E_s (N/mm^2)	200000	200000
Steel Poisson's ratio v_s	0.3	0.3
Concrete compressive strength f_c (N/mm^2)	27.54	31
Concrete Poisson's ratio v_c	0.2	0.2

Table 2.3 Summary of material properties of selected beam (Ibrahim and Mahmood)

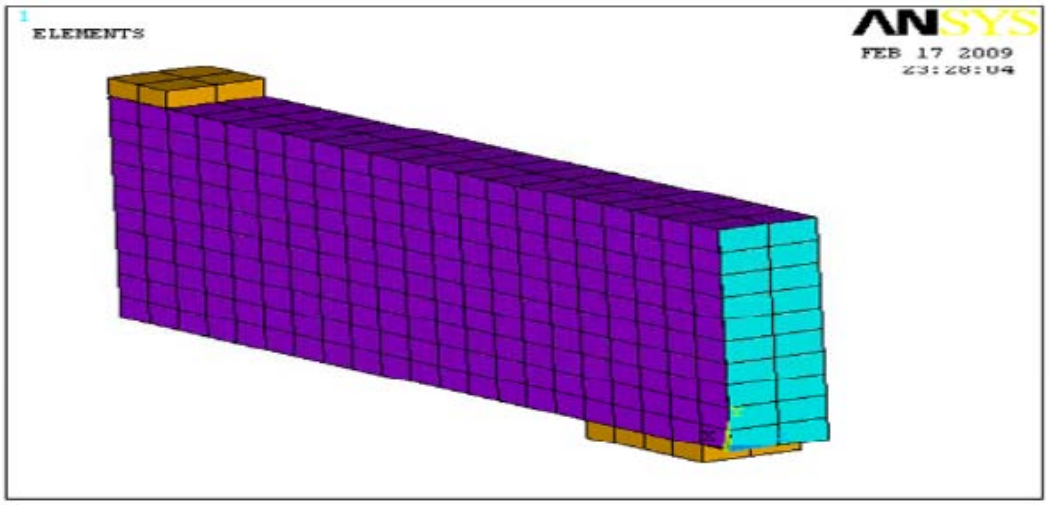

Fig 2.5 F.E.M modelling of beam (Ibrahim and Mahmood)

Symbol	Description	FRP Lamination thickness
B1	As built beam (control beam)	……
B1C-90	Strengthen by one layer of unidirectional transverse laminates CFRP inclined at an angle of 90º to the longitudinal axis [carbon/epoxy	1.6
B1G-90	Strengthen by two layers of unidirectional transverse E-glass/epoxy laminates GFRP inclined at an angle of 90º to the longitudinal axis	2.1
B2	As built beam (control beam)	……
B2C-90	Strengthen by warping with one layer of CFRP inclined at an angle of 90^0 to the longitudinal axis	0.18
B2C-90-0	Strengthen by warping with one layer of CFRP inclined at an angle of 90^o with an additional layer of CFRP on both sides of the web inclined at an angle of 0^0 to the longitudinal axis	0.18

Table 2.4 Summary of six beams (Ibrahim and Mahmood)

Beam	Experimental ultimate load (kN)	Numerical ultimate load (kN)	% Difference	Increased in ultimate load of strengthened
B1	69	66	4.3	1
B1C-90	125	119	4.8	1.6
B1G-90	116	107	7.8	1.8
B2	416	405	2.6	1
B2C-90	435	414	4.8	1.02
B2C-90-0	445	420	5.6	1.03

Table 2.5 Comparsions between experimental and finite element ultimate loads, and ultimate capacity of the strengthened beams with ultimate capacity of the control *beams*. (Ibrahim and Mahmood)

In their study they concluded that the numerical solution which was adopted to evaluate the ultimate shear strength of the reinforced concrete beams reinforced with FRP laminates in simple, cheap and rapid way compared with experimental full scale test. The general behaviours of the finite element models show good agreement with observations and data from the experimental full-scale beam tests. The addition of FRP reinforcement to the control beam shifts the behaviour of the control beams from shear failure near the ends of the beam to flexure failure at the midspan. The results obtained demonstrate that carbon fibre polymer is efficient more than glass fibre polymer in strengthening the reinforced concrete beams for shear. The present finite element model can be used in additional studies to develop design rules for strengthening reinforced concrete members using FRP laminates.

Lee et. al. (2004) developed a structural damage identification method (SDIM) for cylindrical shells and the numerically simulated damage identification tests are conducted to study the feasibility of the proposed SDIM. The SDIM is derived from the frequency response function solved from the structural dynamic equations of damaged cylindrical shells. A damage distribution function is used to represent the distribution and magnitudes of the local damages within a cylindrical shell. In contrast with most existing modal parameters-based SDIMs which require the modal parameters measured in both intact and damaged states, the present SDIM requires only the FRF-data measured in the damaged state. By virtue of utilizing FRF-data, one is able to make the inverse problem of damage identification well-posed by choosing as many sets of excitation frequency and FRF measurement point as needed to obtain a sufficient number of equations.

To investigate the effects of damage on the natural frequencies and also to test the feasibility of the present SDIM, a cylindrical shell simply supported at both end edges is considered. The cylindrical shell has the radius R=0.125 m, length L=0.3 rn, thickness h=0.003 m, Young's Modulus E=206 *GPa,* and the mass density p = 7850 *kg/m 3.* As shown in Fig. 3, two cases are considered: the first case is when the shell has one local damage D=0.3, and the second case is when the shell has three local damages D1=0.3, Dz=0.4 and /93=0.2. To compute the inertance FRF required for structural damage identification, the cylindrical shell is excited by applying a harmonic point force at the point (x=.15m)

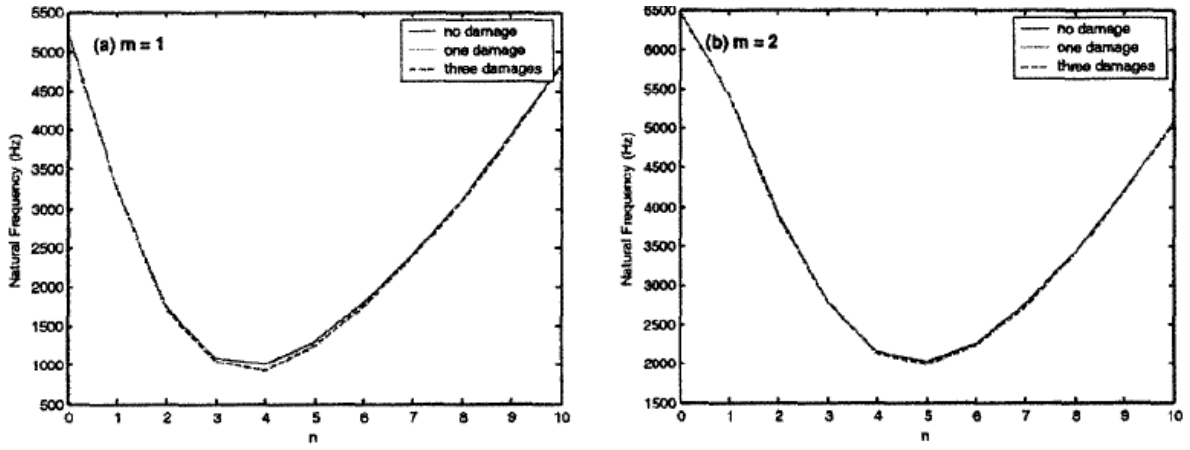

Fig 2.6 The effect of damage on natural frequency (Lee et. al)

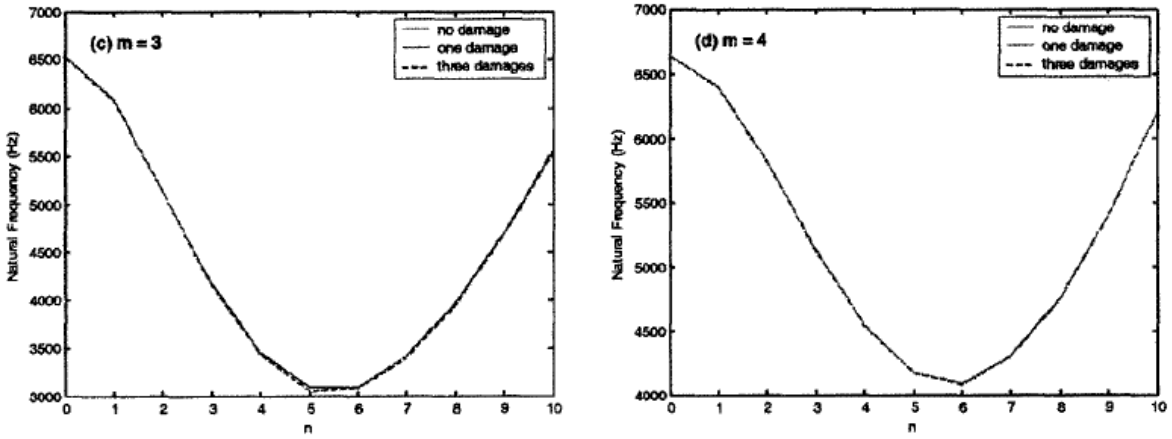

Fig 2.6(cont.) The effect of damage on natural frequency (Lee et. al)

In their paper they concluded that (1) FRF data, instead of modal data is required for the damaged state. (2) To form a well posed damage identification problem, a sufficient number of linear algebraic equations can be readily obtained by simply varying the combination of excitation frequency and FRF measurement point. (3) Many local damages can be located and quantified simultaneously.

Maia et. al. (2003) in their paper addressed the subject of damage detection in structures. A series of numerical simulations on a simple beam are made in order to compare various damage detection methods based on mode shape changes. A generalisation of these methods to the whole frequency ranges of measurement is proposed, i.e. methods based on mode shape changes become based on operational mode shapes. The objective of such a study was to ascertain the possibility of using various damage detection methods without the need for modal identification. Here, some of that work is applied to the FRF-based methods which are compared and discussed. Numerical simulated examples will be used, as well as an experimental test case, where damage is inflicted in a free–free beam.

A FE model of 99 beam elements and 100 nodes of a free–free beam were used. The beam dimensions are 100X64X65, Young's modulus is 220 GPa and density is 7896 kg/m3. The constant damping ratio of the beam is 0.01. A force of 1N is applied at node 34 in the direction of the smallest dimension. To simulate damage, three other models were generated with reductions of 25, 50 and 75% of the Young's modulus at element 70. With these models, modal and harmonic analyses for a frequency range of 0–1600 Hz and 1600 frequency lines were performed in ANSYS. Results of these mode shape damage detection method and FRF based detection method (0-1600Hz) were studied.

For the experimental example a steel beam was used, with constant rectangular cross section, of dimensions 1005X60X6. The test item was suspended by soft springs to simulate free–free end conditions. Fifty equally spaced points for translation response measurements were considered. The test item was excited by a shaker (B&K 4809) with pseudo-random signal (0–800 Hz, 3200 frequency lines) at location 34. The force transmitted was measured by a force transducer (B&K 8200) and the response was measured by a CCLD accelerometer

(B&K 4507). The signals were fed into the Multichannel Data Acquisition Unit B&K 2816 (PULSE) and analysed directly with the software B&K Pulse from the attached PC (Compaq DP4000). To simulate a damage it was decided to cut the beam 33% deep, 1.5mm wide, in the middle of locations 16 and 17 (32 and 34% of the length). Results of FRF based damage detection methods (0-800 Hz) were studies.

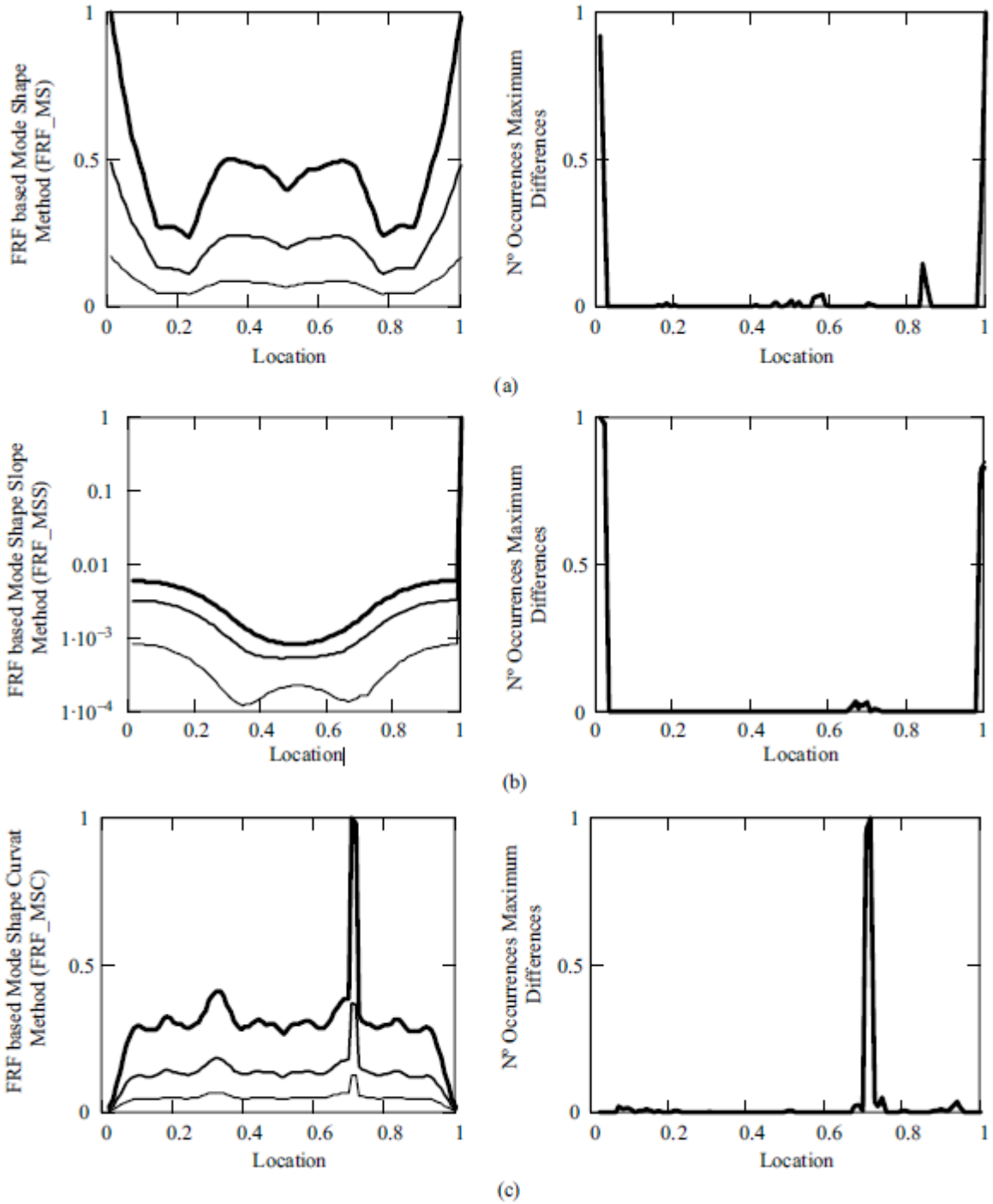

Fig 2.7 FRF based damage detection method (0-1600Hz). (a) FRF-based mode shape method; (b) FRF based mode shape slope method; (c) FRF-based mode shape curvature method;

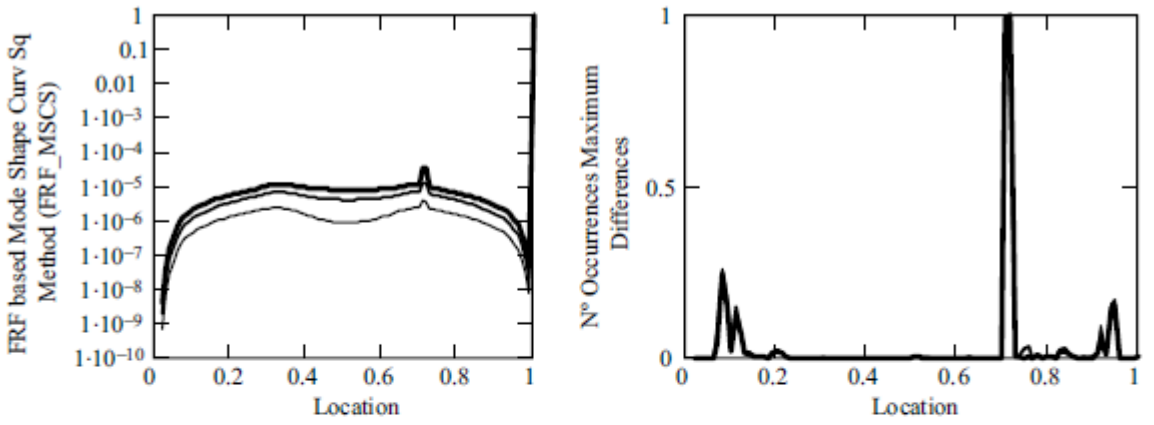

(d)

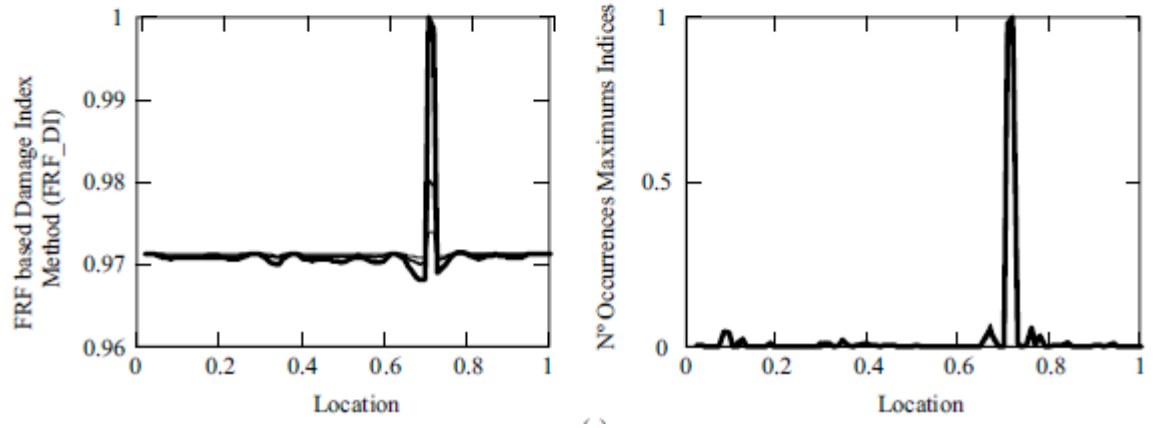

Fig 2.7 (cont.) FRF-based damage detection methods (0–1600 Hz). (d) FRF-based mode shape curvature square method; (e) FRF-based damage index method; 25% damage between 0.70 and 0.71; , 50% damage between 0.70 and 0.71; , 75% damage between 0.70 and 0.71.

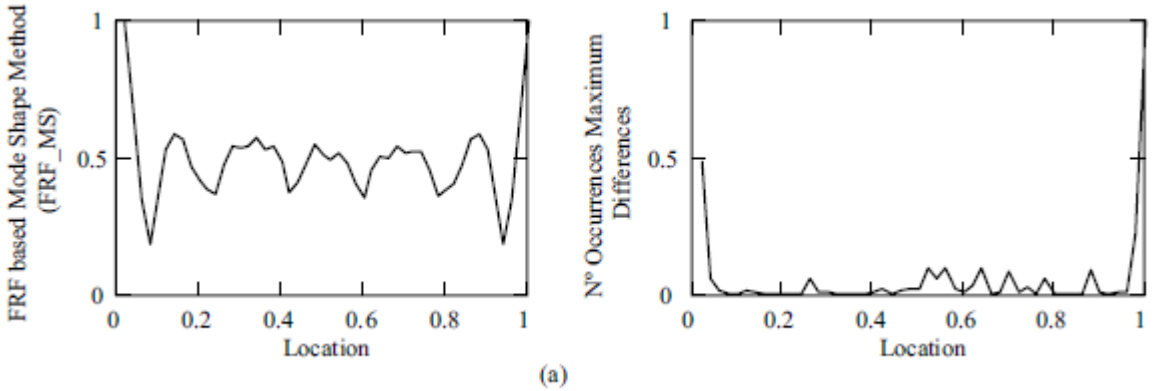

(a)

Fig 2.8 FRF-based damage detection methods (0–800 Hz). (a) FRF-based mode shape method;

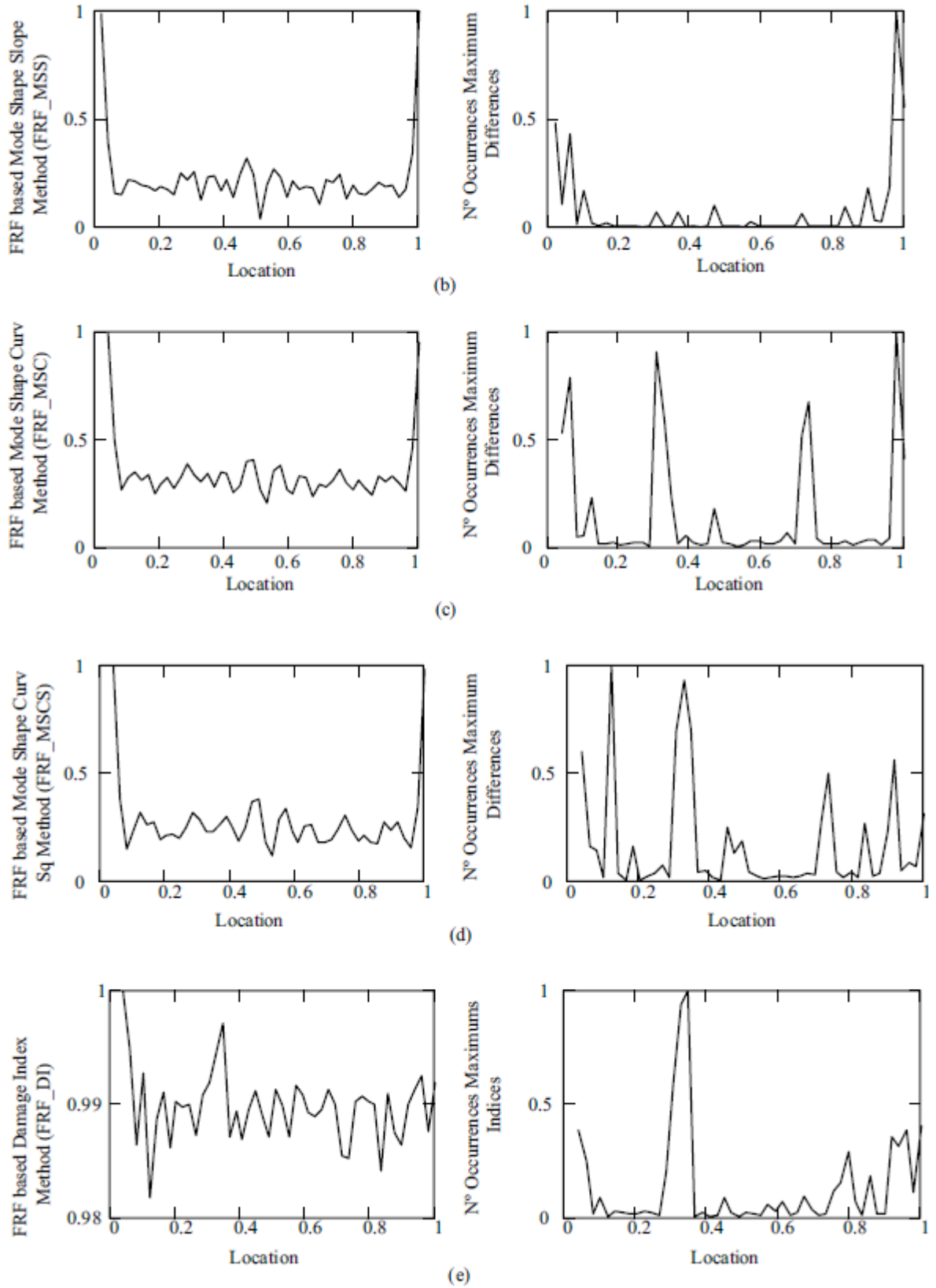

Fig 2.8 (cont.). FRF-based damage detection methods (0–800 Hz). (b) FRFbased mode shape slope method; (c) FRF-based mode shape curvature method; (d) FRF-based mode shape curvature square method; (e) FRF-based damage index method; }, 33% damage between 0.32 and 0.34.

In their paper they concluded that FRF based damage index method was the best.

Balamuralikrishnana R and Jeyasehar C A (2009) In their paper explores the flexural behaviour of carbon fiber reinforced polymer (CFRP) strengthened reinforced concrete (RC) beams. For flexural strengthening of RC beams, total ten beams were cast and tested over an effective span of 3000 mm up to failure under monotonic and cyclic loads. The beams were designed as under-reinforced concrete beams. Eight beams were strengthened with bonded CFRP fabric in single layer and two layers which are parallel to beam axis at the bottom under virgin condition and tested until failure; the remaining two beams were used as control specimens. Static and cyclic responses of all the beams were evaluated in terms of strength, stiffness, ductility ratio, energy absorption capacity factor, compositeness between CFRP fabric and concrete, and the associated failure modes. The theoretical moment-curvature relationship and the load-displacement response of the strengthened beams and control were predicted by using FEA software ANSYS. Comparison had been made between the numerical (ANSYS) and the experimental results. The results showed that the strengthened beams exhibit increased flexural strength, enhanced flexural stiffness, and composite action until failure.

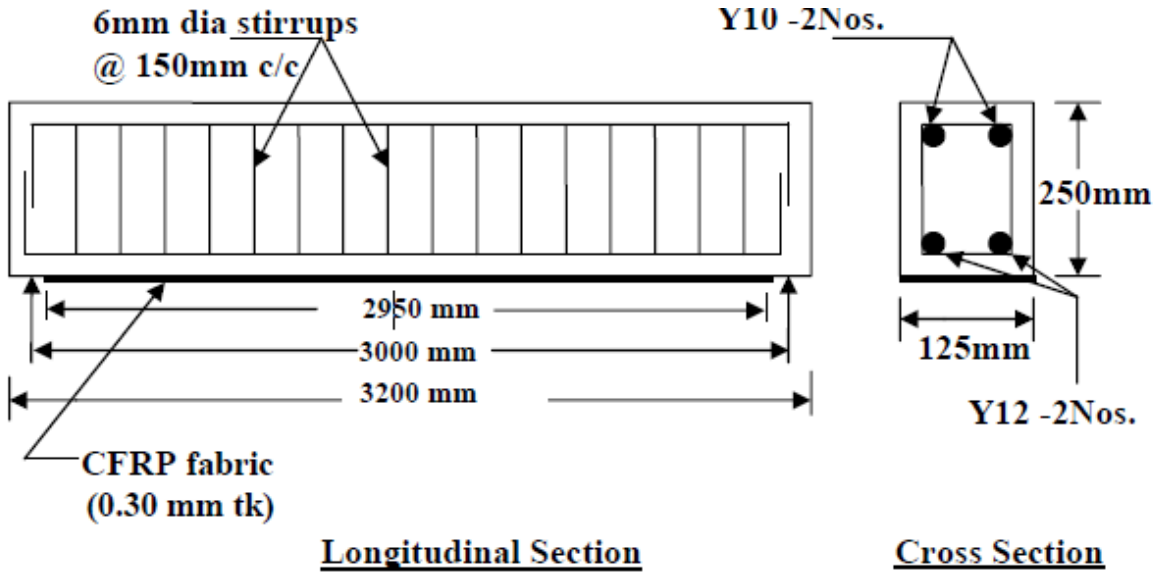

Fig 2.9 Longitudinal and cross section of strengthened beam

FEA software ANSYS is adopted for predicting the load displacement response of the control and strengthened beams numerically. The mesh model defined 375 nodes and 47 elements. The programme offers solid 65 for beam element, link 8 for steel element and solid 45 for CFRP fabric element. The generated models for beams are CB1, RB1 and RB3. The element discretization, loading pattern and boundary conditions in FEA model (ANSYS) for RB3 beam is shown in Fig. 2.9. The experimental and numerical (ANSYS) load deflection curves are compared for both control beam CB1 and strengthened beams RB1 and RB3 are shown in Fig. 2.10. It can be seen that the predicted deflections are in close agreement with the experimental results.

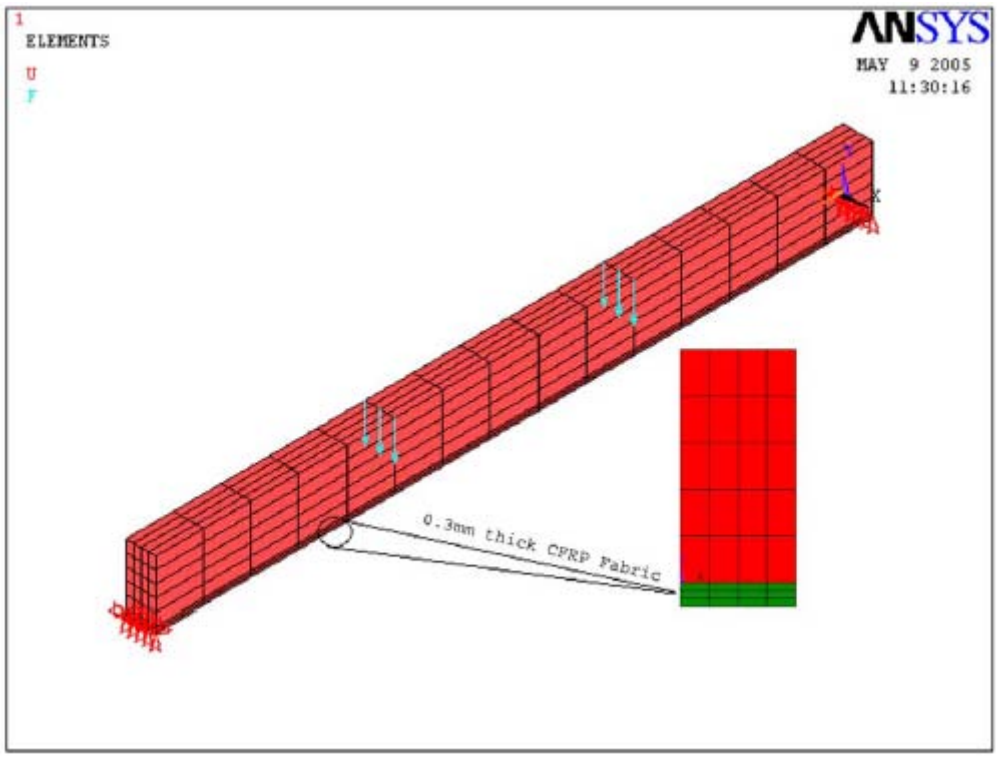

Fig 2.10 Element Discretization, Loading Pattern and Boundary Conditions (RB3).

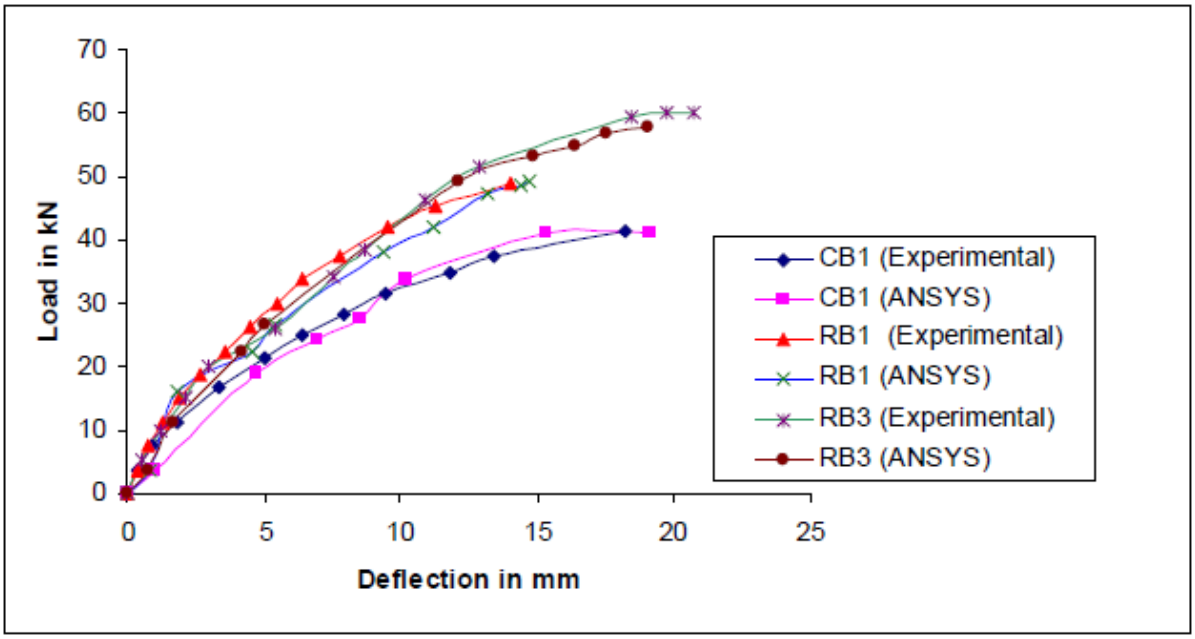

Fig 2.11 Load – Deflection Curve for Control Beam CB1 and Strengthened beams RB1 and RB3

Tavio T and Tata A (2009) presented a nonlinear finite element modelling and analysis of rectangular normal-strength reinforced concrete columns confined with transverse steel under axial compressive loading. In this study, the columns were modelled as discrete elements using ANSYS nonlinear finite element software. Concrete was modelled with 8-noded SOLID65 elements that can translate either in the *x*-, *y*-, or *z*-axis directions from ANSYS

element library. Longitudinal and transverse steels were modelled as discrete elements using 3D-LINK8 bar elements available in the ANSYS element library. The nonlinear constitutive law of each material was also implemented in the model.

The results indicate that the stress-strain relationships obtained from the analytical model using ANSYS are in good agreement with the experimental data. This has been confirmed with the insignificant difference between the analytical and experimental, i.e. 5.65 and 2.80 percent for the peak stress and the strain at the peak stress, respectively. The comparison shows that the ANSYS nonlinear finite element program is capable of modelling and predicting the actual nonlinear behaviour of confined concrete column under axial loading. The actual stress-strain relationship, the strength gain and ductility improvement have also been confirmed to be satisfactorily.

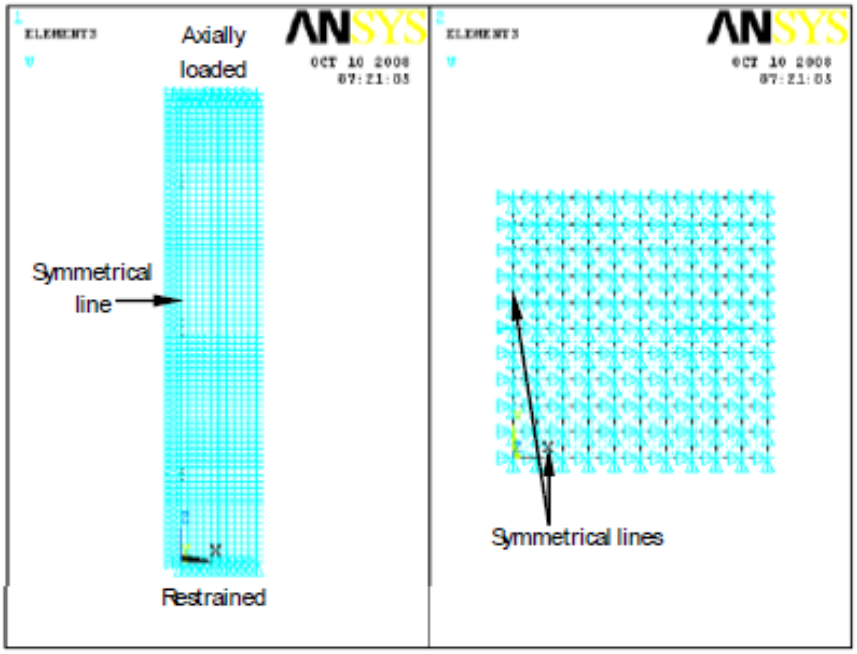

Fig 2.12 Boundary conditions of a symmetrical quarter of a column model: (a) elevation; (b) cross section

Column ID	Cross Section (mm)	Height (mm)	f_c' (MPa)	ρ (%)	f_{yl} (MPa)	f_{yh} (MPa)	Spacing,s (mm)	Volumetric ratio (%)
(1)	(2)	(3)	(4)	(5)	(6)	(7)	(8)	(9)
LS0	500 × 500	1500	24.3	—	—	—	—	—
LS1	500 × 500	1500	24.3	0.95	295	235	60	1.73
LS2	500 × 500	1500	24.3	0.95	295	235	75	2.19
LS3	500 × 500	1500	24.3	0.95	295	235	40	2.60

Note: f_c' = compressive strength of concrete; ρ = ratio of longitudinal steel; f_{yl} = yield strength of longitudinal steel; f_{yh} = yield strength of transverse steel.

Table 2.6 Summary of geometrical and mechanical properties of the column specimens

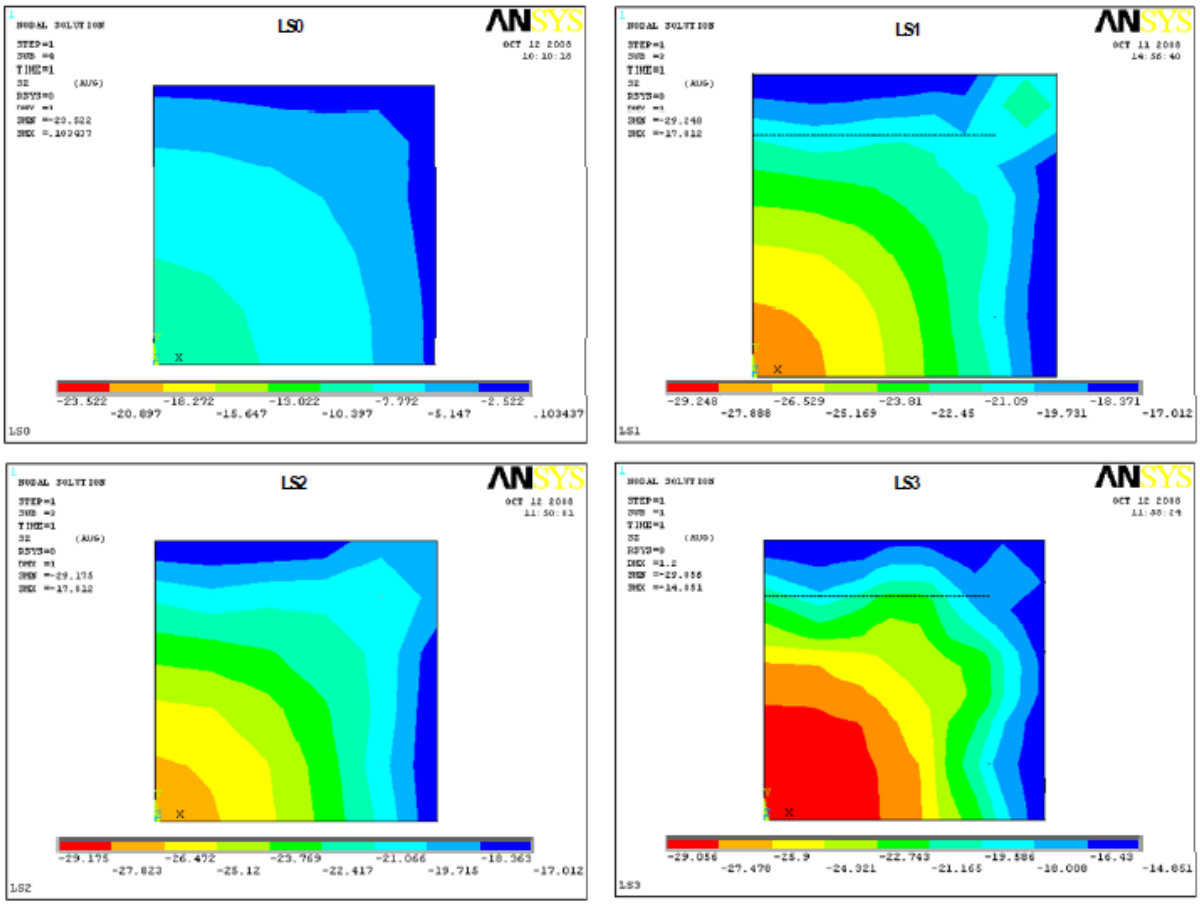

Fig 2.13 Axial stress distributions over the mid-height cross section of quarter column specimens LS0, LS1, LS2, and LS3

Barbosa A.F and Ribeiro G.O (1998) considered the practical application of nonlinear models in the analysis of reinforced concrete structures. The results of some analyses performed using the reinforced concrete model of the general purpose finite element code Ansys were presented and discussed.

The differences observed in the response of the same reinforced concrete beam as some variations are made in a material model that is always basically the same are emphasized.

Analysis	Concrete Model		Reinforcing steel model	
	Tension	Compression	Representation	Material model
Case 2f	Cracking	Linear elastic + crushing	Discrete	Linear elastic
Case 2m	Cracking	Elastic perfectly plastic (Drucker-Prager)	Discrete	Elastic perfectly plastic
Case 2k	Cracking	Multilinear work hardening (von Mises)	Discrete	Elastic perfectly plastic
Case 2L	Cracking	Multilinear work hardening + crushing	Discrete	Elastic perfectly plastic
Case 3m	Cracking	Linear elastic + crushing	Smeared	Linear elastic
Case 3n	Cracking	Elastic perfectly plastic (Drucker-Prager)	Smeared	Elastic perfectly plastic
Case 3p	Cracking	Multilinear work hardening (von Mises)	Smeared	Elastic perfectly plastic
Case 3o	Cracking	Multilinear work hardening + crushing	Smeared	Elastic perfectly plastic

Table 2.7 Summary of model analysed

The consequences of small changes in modelling are discussed and it is shown that satisfactory results may be obtained from relatively simple and limited models.

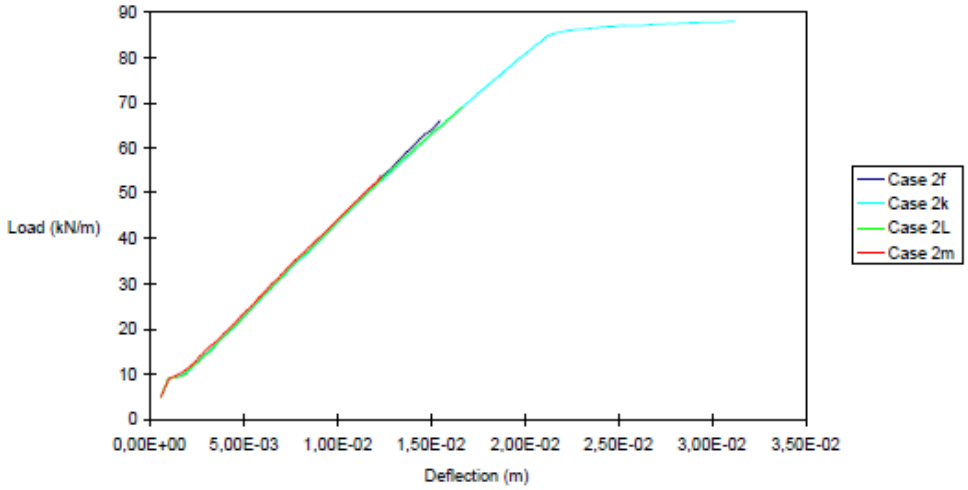

Fig 2.14 Load-deflection curves for models with discrete reinforcement.

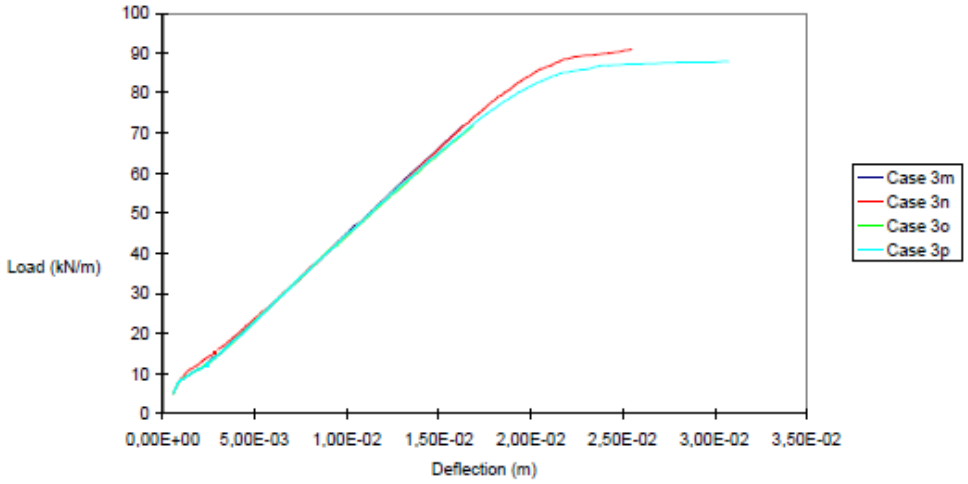

Fig 2.15 Load-deflection curves for models with smeared reinforcement

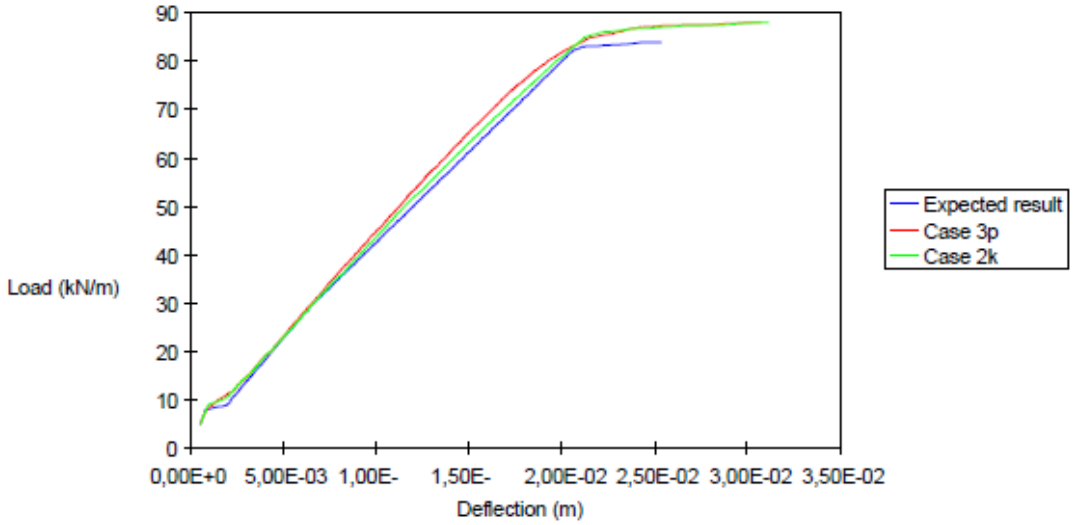

Fig 2.16 Comparison between l-d curves of models with discrete reinforcement and smeared reinforcement.

Liu X et. al. (2009) did the utilisation of structural shape signals for damage localisation has shown some promise, especially in the applications where an accurate finite element model of the structure is not available. For this purpose, traditional shape signals, like mode shapes, flexibility matrices, uniform load surface (ULS) and operational deflection shapes (ODS) have been widely used. Using frequency response function (FRF) shapes for structural damage localisation is however, a relatively new but promising technique. Unlike mode shapes, ULS and ODS, FRF shapes are defined on broadband data and so have potential to reveal damage location more clearly. Another advantage of using FRF shapes is that the test data can be directly used without the necessity of conducting modal identification.

Nevertheless, some problems associated with this approach still remain to be solved. No solid foundation or deduction about the use of FRF shapes for damage localisation has been given in any literature so far. In addition, it has been observed that this method only works for a low-frequency range. This limitation of FRF shapes has not been explained or well treated so far. In this study, a scheme of using FRF shapes for structural damage localisation is proposed. Methods within this scheme include some important modifications like using the imaginary parts of FRF shapes and normalising FRF shapes before comparison. The theoretical explanation of using FRF shapes for damage localisation is presented and the limitations of the previous FRF shape methods have been overcome. The proposed methods have shown great potential in structural damage localisation.

The full FRF matrix of a system with n DOFs in a n by n matrix:

$$FRF(\omega_f) = \begin{bmatrix} \alpha_{11}(\omega_f) & \alpha_{12}(\omega_f) & \dots & \alpha_{1n}(\omega_f) \\ \alpha_{21}(\omega_f) & \alpha_{22}(\omega_f) & \dots & \alpha_{2n}(\omega_f) \\ \vdots & & \dots & \\ \alpha_{n1}(\omega_f) & \alpha_{n2}(\omega_f) & \dots & \alpha_{nm}(\omega_f) \end{bmatrix} \qquad \text{eq 2.11}$$

Where,

$$\alpha_{ij}(\omega_f) = \sum_{k=1}^{n} \frac{\phi_{ik}\phi_{jk}}{(\omega_k^2 - \omega_f^2) + 2j\xi_k\omega_k\omega_f}$$

$$= \sum_{k=1}^{n} \frac{\phi_{ik}\phi_{jk}(\omega_k^2 - \omega_f^2)}{(\omega_k^2 - \omega_f^2)^2 + (2\xi_k\omega_k\omega_f)^2} - j\sum_{k=1}^{n} \frac{2\phi_{ik}\phi_{jk}\xi_k\omega_k\omega_f}{(\omega_k^2 - \omega_f^2)^2 + (2\xi_k\omega_k\omega_f)^2} \qquad \text{eq 2.12}$$

Saikia et al. (2005) has discussed about strength and serviceability performance of beams reinforced with GFRP bars in flexure. According to them Glass fibre reinforced polymer (GFRP) rebars have been identified as an alternate construction material for reinforcing concrete during the last decade primarily due to its strength and durability related characteristics. These materials have strength higher than steel, but exhibit linear stress-strain response up to failure. Furthermore, the modulus of elasticity of GFRO is significantly lower than that of steel. This reduced stiffness often controls the design of the GFRP reinforced concrete elements. In the present investigation, GFRP reinforced beams designed based on limit state principles have been examined to understand their strength and serviceability

performance. A block type rotation failure was observed for GFRP reinforced beams, while flexural failure was observed in geometrically similar control beams reinforced with steel rebars. An analytical model has been proposed for strength assessment accounting for the failure was observed for GFRP reinforced beams. The serviceability criteria for design of GFRP reinforced beams appear to be governed by maximum crack width. An empirical model has beam proposed for predicting the maximum width of the cracks. Deflection of these GFRP rebar reinforced beams has been predicted using an earlier model available in the literature. The results predicted by the analytical model compare well with the experimental data.

2.2 GAP IN RESERCH AREA

There are many available developed procedures, which are based on measuring change in frequencies, mode shapes, or **other** structural properties before and after the occurrence of natural hazards. The concept of structural health monitoring is rapidly growing to enable early identification of damage and provide warning of unsafe conditions. Current evaluation methods and the damage detection of structures vary according to the materials used in construction of building. Some researchers have investigated using only experimental approaches. But health monitoring of a building is difficult to do at experimentally. Also experiments without analysis can lead to result that are difficult to understand. For these reasons, analytical approach using nonlinear static analysis software is proposed to be adopted for the research envisaged. The structural health monitoring is defined as the measurement of critical response of a structure under operating and loading environments, to evaluate the symptoms of operational incidents, deterioration or damage indicator that may impair operation.

2.3 DIRECTION FOR PRESENT RESERCH

This research is concerned with retrofitting the reinforced beams using GFRP sheets. The use of advanced materials like GFRP sheets for reinforced concrete structural repair and strengthening applications has been studied extensively in previous researches. However all studies of strengthened structural elements have reported only load-deflection behaviour. But frequency response function has never been reported analytically. In this research frequency response function of control beam and retrofitted beam in damaged state has been developed using Finite element analysis software, Ansys.

In the second phase the results of analytical work is compared with the experimental work done by **GOYAL (2007).**

FINITE ELEMENT MODELING IN ANSYS

3.1 INTRODUCTION

ANSYS is engineering simulation software based on the Finite element method and is capable of performing static (stress) analysis, thermal analysis, modal analysis, frequency response analysis, transient simulation and also coupled field analysis. The Ansys multiphysics can couple various physical domains such as structural, thermal and electromagnetic.

In this chapter we will discuss about how we model a concrete beam in Ansys. Element types used in the models ant the constitutive equations, assumptions, and parameters for the various materials. Loading and boundary conditions, Nonlinear analysis procedure and convergence criteria will be explained. Also will be given the procedure to get FRF graph.

To create a Model in Ansys we need to know these 4 steps:

1. Element type
2. Real constants
3. Material properties
4. Geometry

3.2 ELEMENT TYPE

3.2.1 *Reinforced Concrete*

An eight-node solid element, Solid65, was used to model the concrete. The solid element has eight nodes with three degrees of freedom at each node – translations in the nodal x, y, and z directions. The element is capable of plastic deformation, cracking in three orthogonal directions, and crushing. The geometry and node locations for this element type are shown in Figure 3.1.

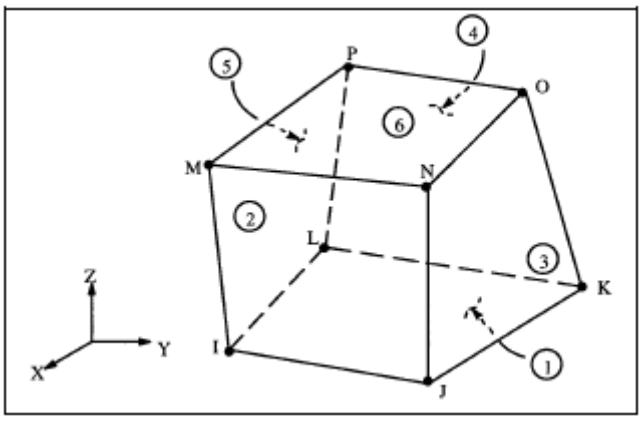

Fig. 3.1 Solid65 – 3-D reinforced concrete solid (ANSYS)

A Beam23 element was used to model the steel reinforcement. Two nodes are required for this element. Each node has three degree of freedom- translations in the nodal x and y

direction and rotation about the nodal z-axis. The element has plastic, creep, and swelling capabilities. The geometry of this element type is shown in fig. 3.2.

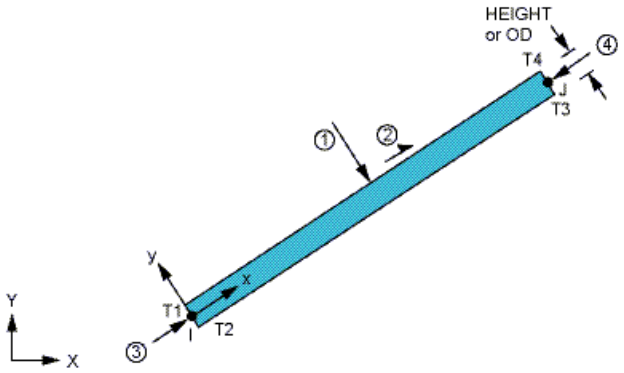

Fig 3.2 Beam 23 element (ANSYS)

3.2.2 *FRP Composites*

A layered solid element, Solid46 (fig 3.3), was used to model the FRP composites. The element allows for up to 100 different material layers with different orientations and orthotropic material properties in each layer. The element has three degrees of freedom at each node and translations in the nodal x, y, and z directions.

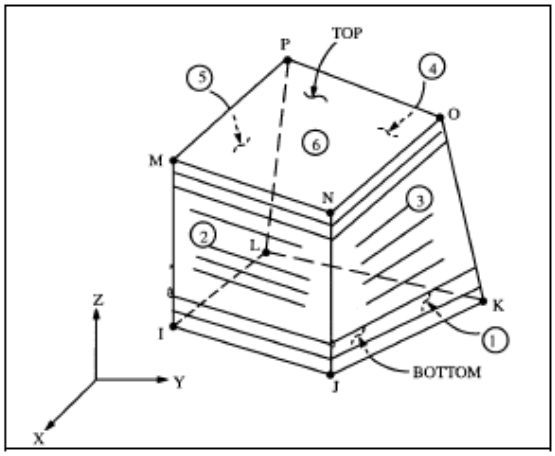

Fig. 3.3 Solid46 – 3D layered structural solid (ANSYS)

3.3 REAL CONSTANTS

Real constants of various materials are as follows:

3.3.1 *Solid65* can incorporate we are going to incorporate the stirrups as smeared. The real constants of the concrete are given below:

Real constant for bar 1	
Material No.	2
Volume ratio	0.00166
Orientation angle (ϕ_1)	90
Orientation angle (ϕ_2)	0

Real constant for bar 2	
Material No.	2
Volume ratio	0.00322
Orientation angle (ϕ_1)	0
Orientation angle (ϕ_2)	90

Table 3.1 Real constants for concrete

3.3.2 For *steel reinforcement* we have to define its radius in the real constants.

1) For rebar 1

Diameter of bar (m)	0.010

2) For rebar 2

Diameter of bar (m)	0.008

3.4 MATERIAL PROPERTIES

3.4.1 *Concrete*

Development of a model for the behaviour of concrete is a challenging task. Concrete is a quasi-brittle material and has different behaviour in compression and tension. The tensile strength of concrete is typically 8-15% of the compressive strength (Shah, et al. 1995). Figure 3.4 shows a typical stress-strain curve for normal weight concrete (Bangash 1989).

In compression, the stress-strain curve for concrete is linearly elastic up to about 30 percent of the maximum compressive strength. Above this point, the stress increases gradually up to the maximum compressive strength. After it reaches the maximum compressive strength σ_{cu}, the curve descends into a softening region, and eventually crushing failure occurs at an ultimate strain ε_{cu}. In tension, the stress-strain curve for concrete is approximately linearly elastic up to the maximum tensile strength. After this point, the concrete cracks and the strength decreases gradually to zero (Bangash 1989).

FEM Input data

For concrete, ANSYS require input data properties as follows:
1. Elastic modulus (Ec).
2. Ultimate uniaxial compressive strength (f'c).
3. Ultimate uniaxial tensile strength (modulus of rupture)fr)
4. Poisson's ratio (ν).
5. Shear transfer coefficient (βt).
6. Compressive uniaxial stress-strain relationship for concrete.

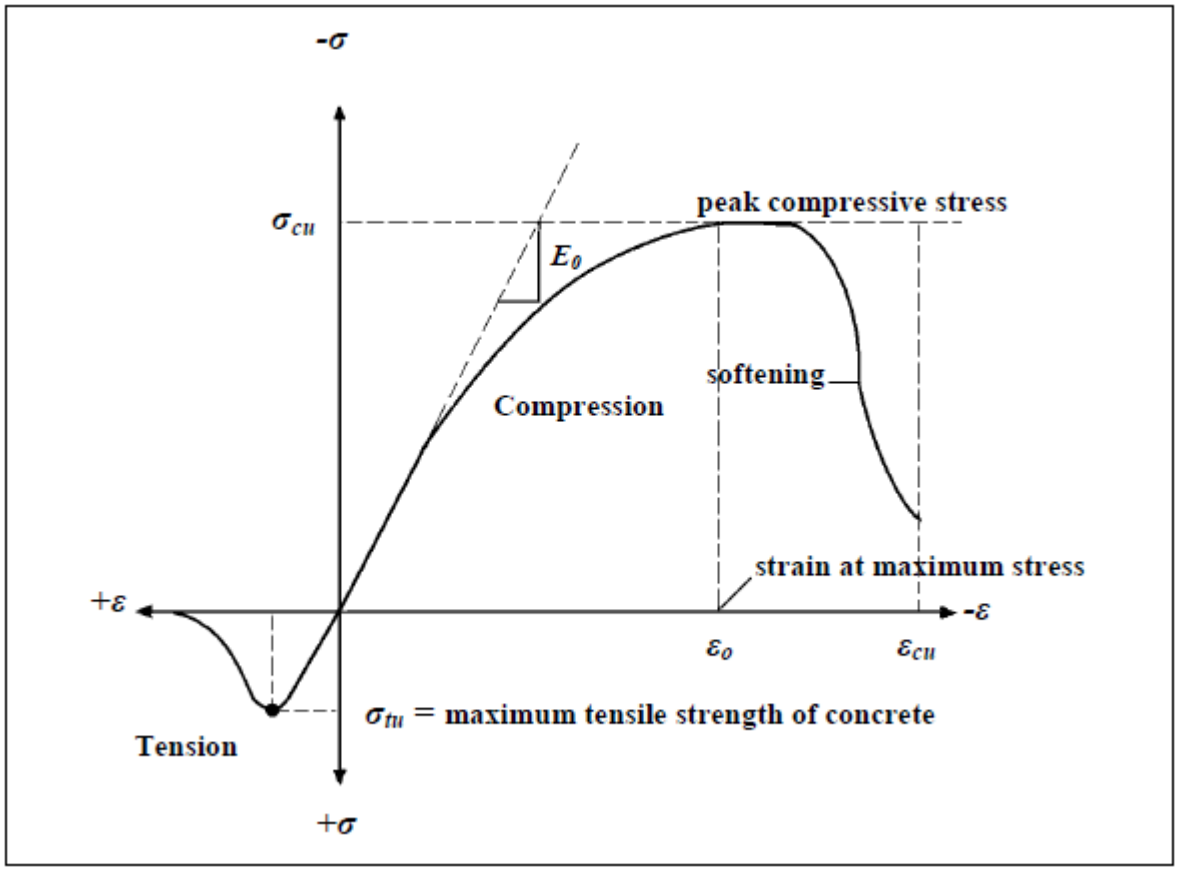

Figure 3.4: Typical uniaxial compressive and tensile stress-strain curve for concrete (Bangash 1989)

For the full-scale beam tests (Kachlakev and McCurry 2000), an effort was made to accurately estimate the actual elastic modulus of the beams using the ultrasonic pulse velocity method (ASTM 1983, ASTM 1994). A correlation was made between pulse velocity and compressive elastic modulus following the ASTM standard methods. From this work, it was noted that each experimental beam had a slightly different elastic modulus; therefore, these values were used in the finite element modelling.

From the elastic modulus obtained by the pulse velocity method, the ultimate concrete compressive and tensile strengths for each beam model were calculated by Equations 3.1, and 3.2, respectively (ACI 318, 1999).

$$f_c' = \left(\frac{E_c}{57000} \right)^2 \qquad \text{eq. 3.1}$$

$$f_r = 7.5\sqrt{f_c'} \qquad \text{eq 3.2}$$

where: E_c, f_c and f_r are in psi.

Poisson's ratio for concrete was assumed to be 0.2 (Bangash 1989)

The shear transfer coefficient, β_t, represents conditions of the crack face. The value of β_t ranges from 0.0 to 1.0, with 0.0 representing a smooth crack (complete loss of shear transfer)

and 1.0 representing a rough crack (no loss of shear transfer) (ANSYS 1998). The value of β_t used in many studies of reinforced concrete structures, however, varied between 0.05 and 0.25 (Bangash 1989; Huyse, et al. 1994; Hemmaty 1998). A number of preliminary analyses were attempted in this study with various values for the shear transfer coefficient within this range, but convergence problems were encountered at low loads with β_t less than 0.2. Therefore, the shear transfer coefficient used in this study was equal to 0.2.

For damaged beam we took the load deflection curve of the control beam and from there we evaluated the change in Elastic Modulus and used the new elastic modulus corresponding to that load in the beam. Also for the stressed beam we reduced the Elastic modulus.

Compressive uniaxial stress-strain relationship for concrete

The ANSYS program requires the uniaxial stress-strain relationship for concrete in compression. Numerical expressions (Desayi and Krishnan 1964), Equations 3.3 and 3.4 were used along with Equation 4-5 (Gere and Timoshenko 1997) to construct the uniaxial compressive stress-strain curve for concrete in this study.

$$f = \frac{E_c \varepsilon}{1 + \left(\frac{\varepsilon}{\varepsilon_0}\right)^2} \qquad \text{eq. 3.3}$$

$$\varepsilon_0 = \frac{2 f'_c}{E_c} \qquad \text{eq. 3.4}$$

$$E_c = \frac{f}{\varepsilon} \qquad \text{eq. 3.5}$$

where:

f = stress at any strain ε, psi
ε = strain at stress f
ε_0 = strain at the ultimate compressive strength f_c'

Figure 3.5 shows the simplified compressive uniaxial stress-strain relationship that was used in this study.

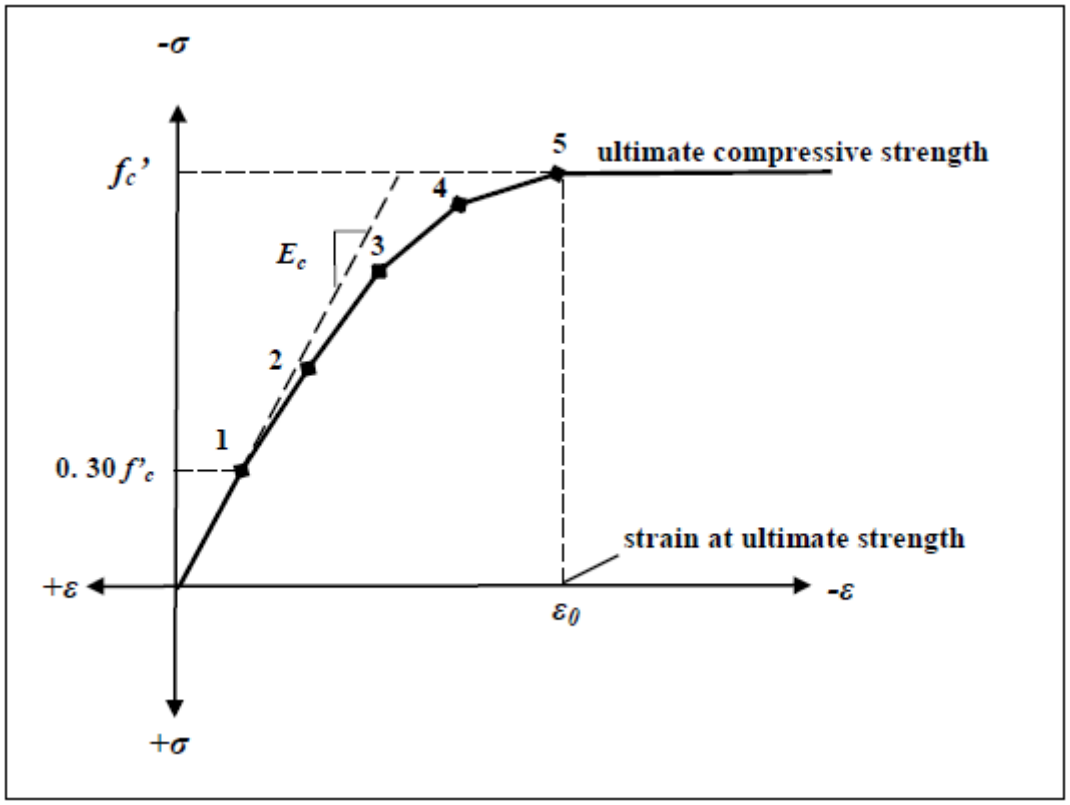

Fig. 3.5 Simplified compressive uniaxial stress-strain curve for concrete

The simplified stress-strain curve for each beam model is constructed from six points connected by straight lines. The curve starts at zero stress and strain. Point No. 1, at 0.30 f'_c, is calculated for the stress-strain relationship of the concrete in the linear range (Equation 4-5). Point Nos. 2, 3, and 4 are obtained from Equation 3.3, in which ε_0 is calculated from Equation 3.4. Point No. 5 is at ε_0 and f'_c. In this study, an assumption was made of perfectly plastic behaviour after Point No. 5.

Failure Criteria for Concrete

The model is capable of predicting failure for concrete materials. Both cracking and crushing failure modes are accounted for. The two input strength parameters – i.e., ultimate uniaxial tensile and compressive strengths – are needed to define a failure surface for the concrete. Consequently, a criterion for failure of the concrete due to a multiaxial stress state can be calculated (William and Warnke 1975).

A three-dimensional failure surface for concrete is shown in Figure 3.6. The most significant nonzero principal stresses are in the x and y directions, represented by σ_{xp} and σ_{yp}, respectively. Three failure surfaces are shown as projections on the σ_{xp}-σ_{yp} plane. The mode of failure is a function of the sign of σ_{zp} (principal stress in the z direction). For example, if σ_{xp} and σ_{yp} are both negative (compressive) and σ_{zp} is slightly positive (tensile), cracking would be predicted in a direction perpendicular to σ_{zp}. However, if σ_{zp} is zero or slightly negative, the material is assumed to crush (ANSYS 1998).

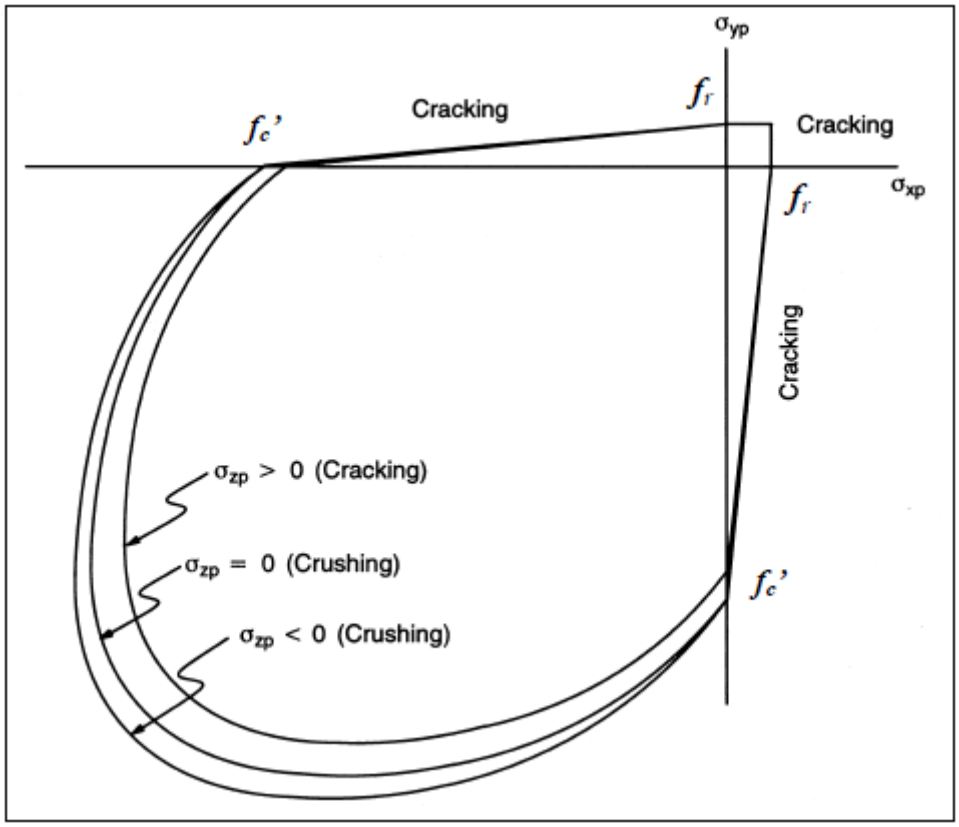

Fig. 3.6 3-D failure surface for concrete (ANSYS)

In a concrete element, cracking occurs when the principal tensile stress in any direction lies outside the failure surface. After cracking, the elastic modulus of the concrete element is set to zero in the direction parallel to the principal tensile stress direction. Crushing occurs when all principal stresses are compressive and lie outside the failure surface; subsequently, the elastic modulus is set to zero in all directions (ANSYS 1998), and the element effectively disappears.

During this study, it was found that if the crushing capability of the concrete is turned on, the finite element beam models fail prematurely. Crushing of the concrete started to develop in elements located directly under the loads. Subsequently, adjacent concrete elements crushed within several load steps as well, significantly reducing the local stiffness. Finally, the model showed a large displacement, and the solution diverged.

A pure “compression” failure of concrete is unlikely. In a compression test, the specimen is subjected to a uniaxial compressive load. Secondary tensile strains induced by Poisson’s effect occur perpendicular to the load. Because concrete is relatively weak in tension, these actually cause cracking and the eventual failure (Mindess and Young 1981; Shah, et al. 1995). Therefore, in this study, the crushing capability was turned off and cracking of the concrete controlled the failure of the finite element models.

3.4.2 *Steel Reinforcement*

Steel reinforcement in the experimental beams was constructed with typical Grade 60 steel reinforcing bars. Properties, i.e., elastic modulus and yield stress, for the steel reinforcement used in this FEM study follow the design material properties used for the experimental investigation (Kachlakev and McCurry 2000). The steel for the finite element models was assumed to be an elastic-perfectly plastic material and identical in tension and compression. Poisson's ratio of 0.3 was used for the steel reinforcement in this study (Gere and Timoshenko 1997). Figure 3.7 shows the stress-strain relationship used in this study. Material properties for the steel reinforcement for all four models are as follows:

Elastic modulus, E_s = 200,000 MPa (29,000 ksi)
Yield stress, f_y = 410 MPa (60,000 psi)
Poisson's ratio, v = 0.3

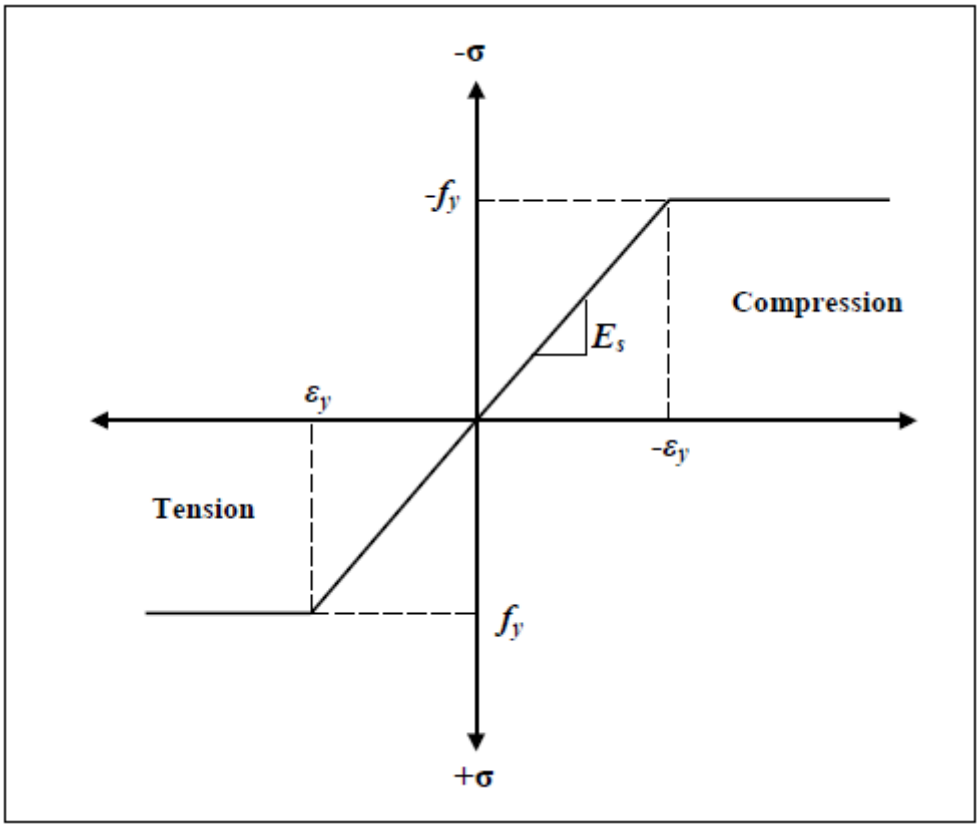

Fig 3.7 Stress-Strain curve for steel reinforcement

3.4.3 *FRP composite*

FRP composites are materials that consist of two constituents. The constituents are combined at a macroscopic level and are not soluble in each other. One constituent is the reinforcement, which is embedded in the second constituent, a continuous polymer called the matrix (Kaw 1997). The reinforcing material is in the form of fibers, i.e., carbon and glass, which are typically stiffer and stronger than the matrix. The FRP composites are anisotropic materials; that is, their properties are not the same in all directions. Figure 3.8 shows a schematic of FRP composites.

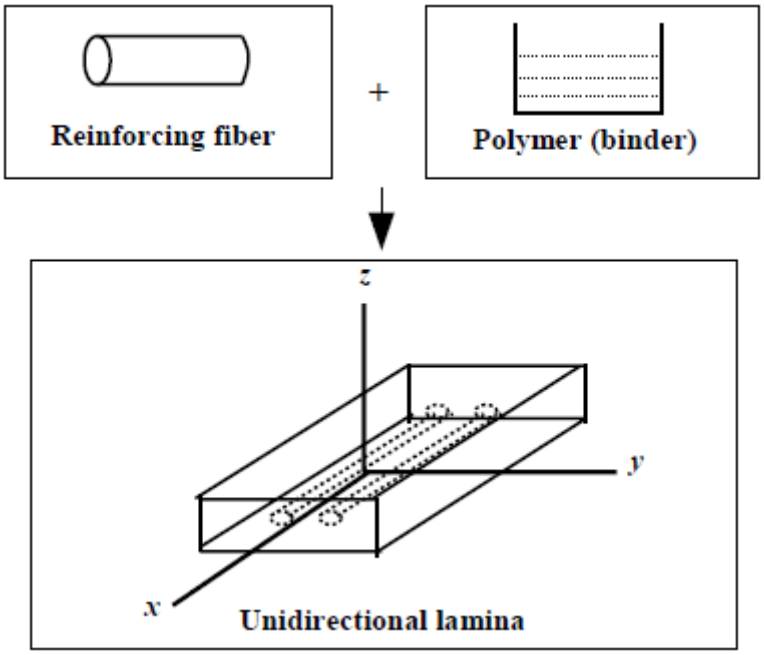

Fig. 3.8 Schematic of FRF composites (Gibson 1994, Kaw 1997)

As shown in Figure 4.8, the unidirectional lamina has three mutually orthogonal planes of material properties (i.e., xy, xz, and yz planes). The xyz coordinate axes are referred to as the principal material coordinates where the x direction is the same as the fiber direction, and the y and z directions are perpendicular to the x direction. It is a so-called specially orthotropic material (Gibson 1994, Kaw 1997). In this study, the specially orthotropic material is also transversely isotropic, where the properties of the FRP composites are nearly the same in any direction perpendicular to the fibres. Thus, the properties in the y direction are the same as those in the z direction. In our study Glass fibre polymer was used, the stress-strain curve used in this study for the FRP composites in the direction of the fibre is shown in Fig. 3.9.

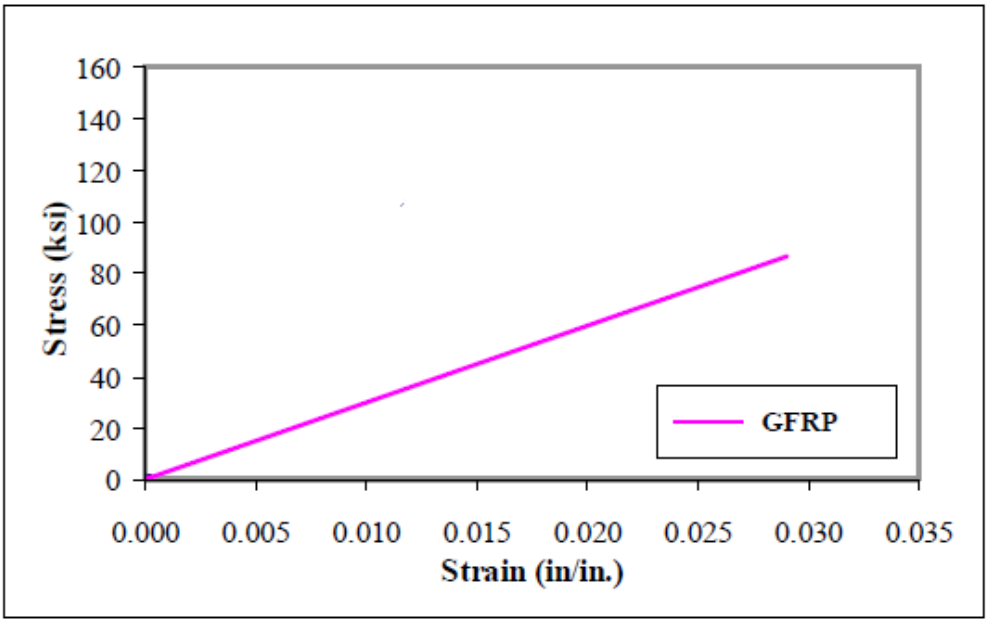

Fig 3.9 Stress-strain curves for the FRP composites in the direction of the fibers

Input data needed for the FRP composites in the finite element models are as follows:

1) No. of layers.
2) Thickness of each layer.
3) Orientation of the fibre direction for each layer
4) Elastic modulus
5) Poisson's Ratio

The properties of isotropic materials, such as elastic modulus and Poisson's ratio, are identical in all directions; therefore no subscripts are required. This is not the case with specially orthotropic materials. For example, $E_x \neq E_y$ and $\nu_{xy} \neq \nu_{yx}$. E_x is the elastic modulus in the fibre direction, and E_y is the elastic modulus in the y direction perpendicular to the fibre direction. The use of Poisson's ratios for the orthotropic materials causes confusion; therefore, the orthotropic material data are supplied in the ν_{xy} or major Poisson's ratio format for the ANSYS program. The major Poisson's ratio is the ratio of strain in the y direction to strain in the perpendicular x direction when the applied stress is in the x direction. The quantity ν_{yx} is called a minor Poisson's ratio and is smaller than ν_{xy}, whereas E_x is larger than E_y. Equation 2-6 shows the relationship between ν_{xy} and ν_{yx} (Kaw 1997).

$$\nu_{yx} = \frac{E_y}{E_x}\nu_{xy} \qquad \text{eq. 4.6}$$

where:

vyx = Minor Poisson's ratio
E_x = Elastic modulus in the x direction (fiber direction)
E_y = Elastic modulus in the y direction
ν_{xy} = Major Poisson's ratio

A summary of material properties used for the modelling is shown in Table

FRP Composite	Elastic Modulus (MPa)	Tensile Strength (MPa)	Poisson's Ratio	Thickness of laminate (mm)
GFRP	21000	600	.36	1

Table 3.2 Material properties of FRP

3.5 GEOMETRY

The dimensions of the full-size beams were 127 mm x 227 mm x 4100 mm. The span between the two supports was 3750 mm. Figure 3.10 illustrates typical dimensions for the beams before FRP reinforcing.

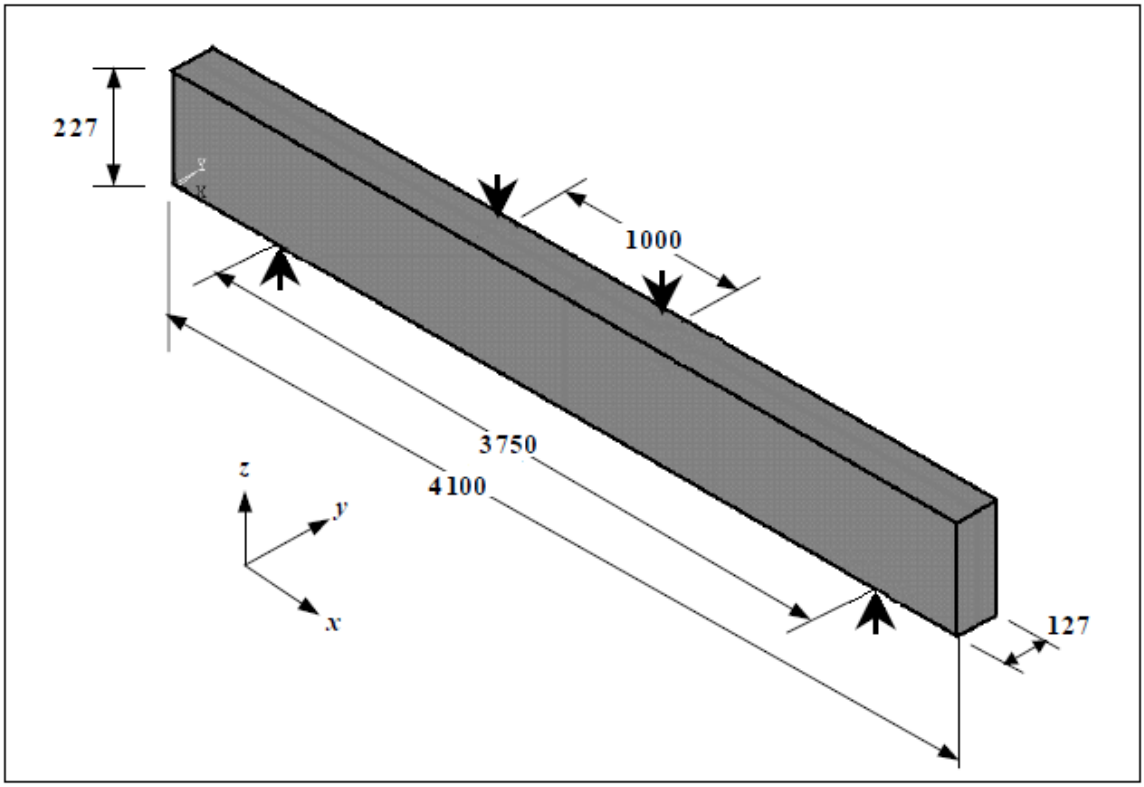

Fig. 3.10 Typical beam dimension (not to scale)

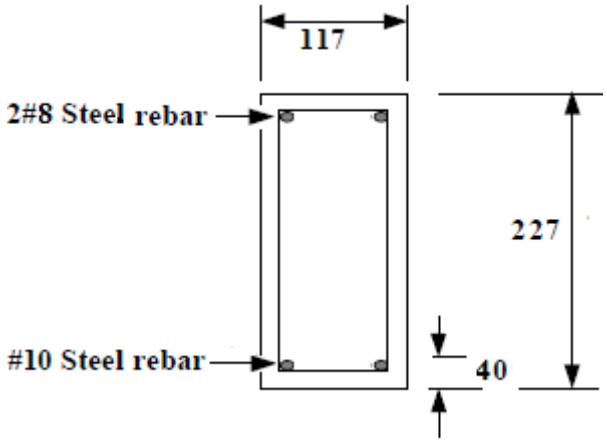

Fig 3.11 Section

Ideally, the bond strength between the concrete and steel reinforcement should be considered. However, in this study, perfect bond between materials was assumed. To provide the perfect bond, the link element for the steel reinforcing was connected between nodes of each adjacent concrete solid element, so the two materials shared the same nodes. The same approach was adopted for FRP composites. The high strength of the epoxy
used to attach FRP sheets to the experimental beams supported the perfect bond assumption.

In the finite element models, layered solid elements, Solid46, were used to model the FRP composites. Nodes of the FRP layered solid elements were connected to those of adjacent concrete solid elements in order to satisfy the perfect bond assumption. Figure 3.12 illustrates the element connectivity.

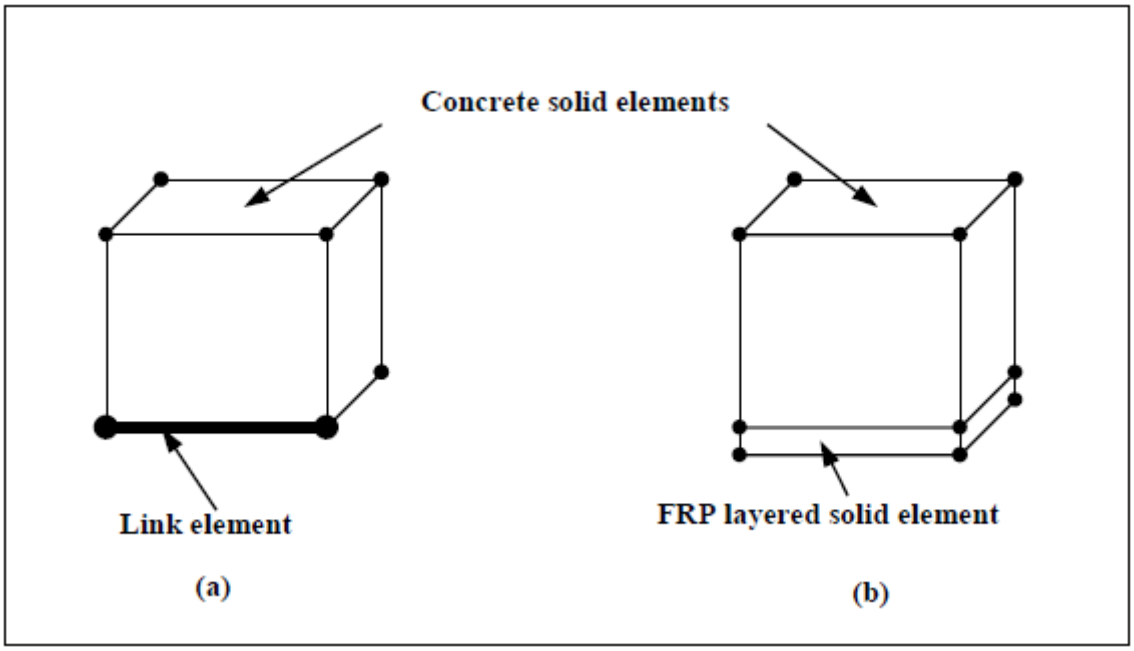

Figure 3.12 Element connectivity: (a) concrete solid and link elements; (b) concrete solid and FRP layered solid elements

Fig 3.13 and Fig 3.14 shows the beam model of simple beam and retrofitted beam respectively

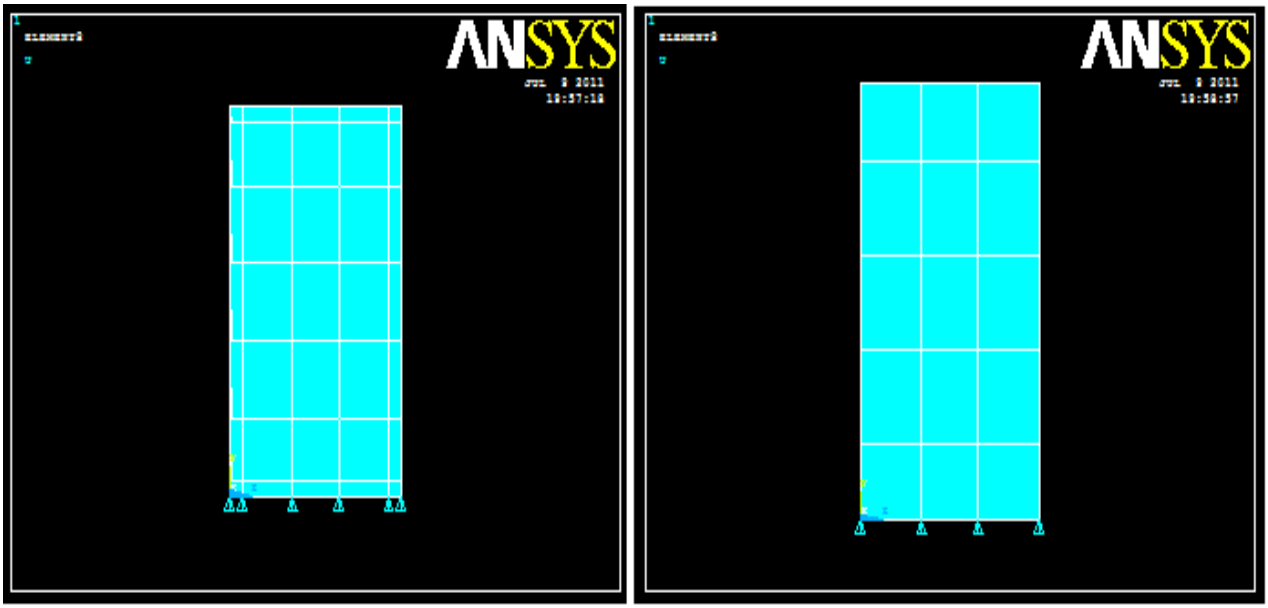

Fig 3.13 Cross section of retrofitted beam and control beam (ANSYS)

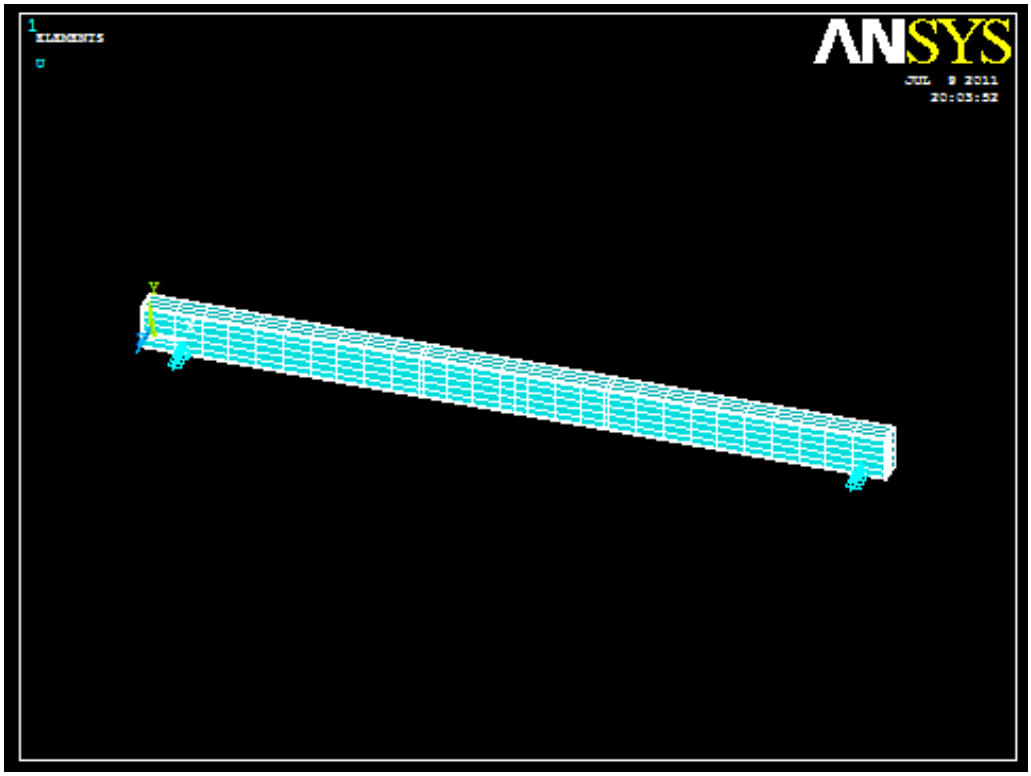

Fig 3.14 (a) Retroffired beam

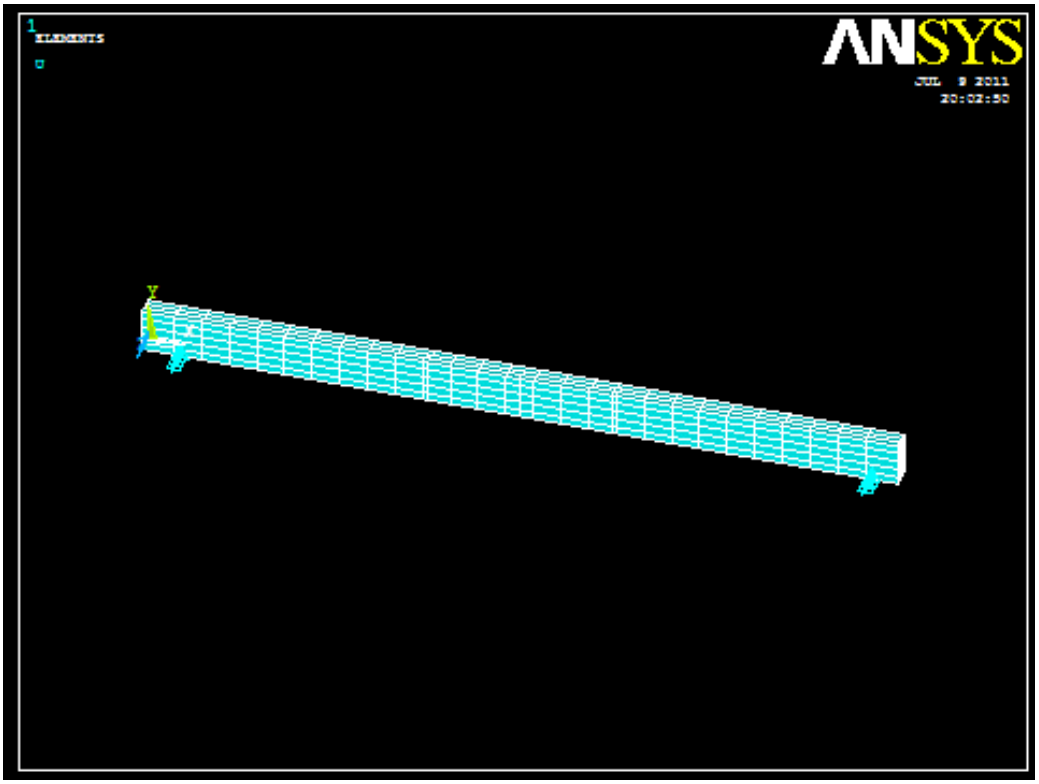

Fid 3.14 (b) Control beam

3.6 LOADING AND BOUNDARY CONDITION

For the load deflection curve we analysed the beam as deformation controlled analysis. Value of displacement in y direction at support nodes were used to create the support. Fig 4.15 shows the boundary condition for a typical model.

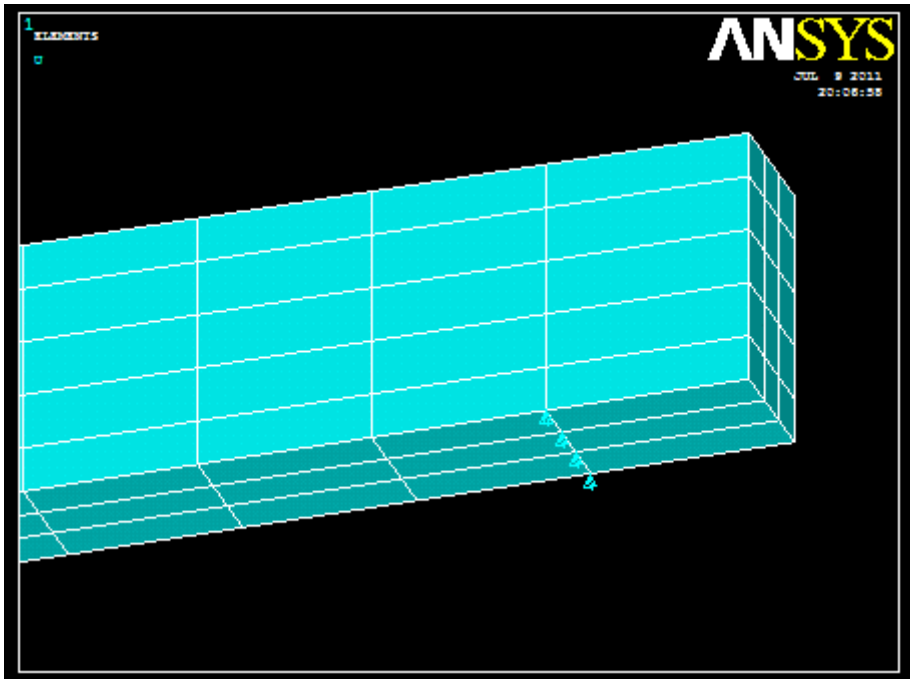

Fig 4.15 Boundary condition of control beam

3.7 NON LINEAR ANALYSIS

In nonlinear analysis, the total displacement applied to a finite element model is divided into a series of increments called load steps. At the completion of each incremental solution, the stiffness matrix of the model is adjusted to reflect nonlinear changes in structural stiffness before proceeding to the next load increment. The ANSYS program (ANSYS 1998) uses Newton-Raphson equilibrium iterations for updating the model stiffness.

Newton-Raphson equilibrium iterations provide convergence at the end of each load increment within tolerance limits. Figure 3.16 shows the use of the Newton-Raphson approach in a single degree of freedom nonlinear analysis.

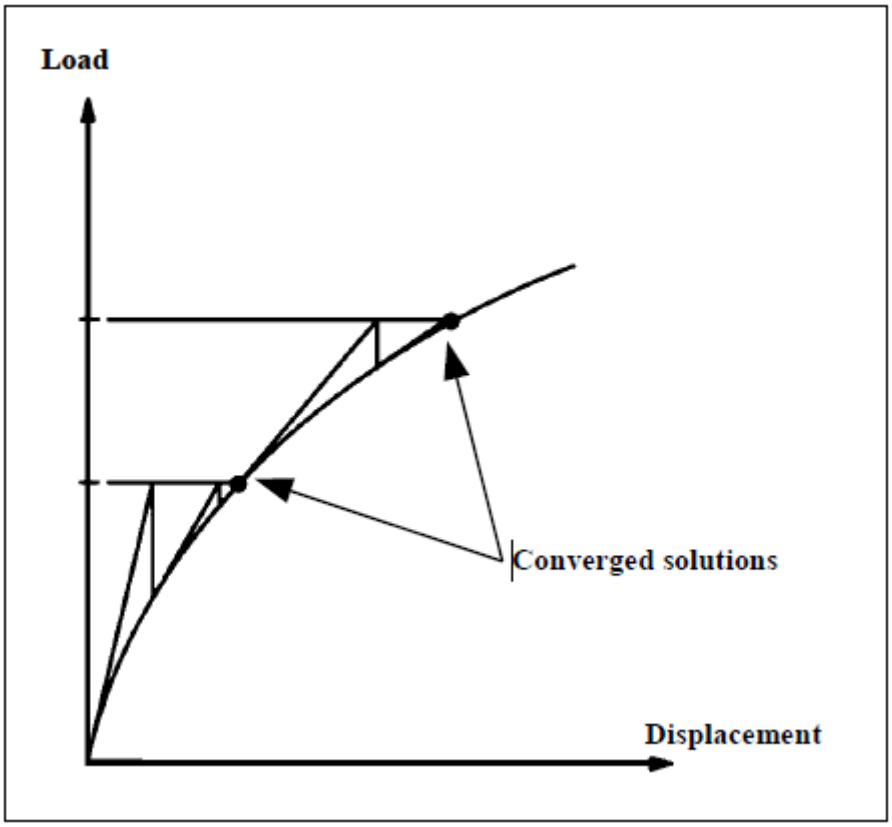

Fig 3.16 Newton-Raphson iterative solution (2 load increments) (ANSYS)

Prior to each solution, the Newton-Raphson approach assesses the out-of-balance load vector, which is the difference between the restoring forces (the loads corresponding to the element stresses) and the applied loads. Subsequently, the program carries out a linear solution, using the out-of-balance loads, and checks for convergence. If convergence criteria are not satisfied, the out-of-balance load vector is re-evaluated, the stiffness matrix is updated, and a new solution is attained. This iterative procedure continues until the problem converges (ANSYS).

3.8 MODAL ANALYSIS

A modal analysis is performed to determine the vibration characteristics (i.e., the natural frequencies and mode shapes) of a structure. In ANSYS, a modal analysis is also the starting point for other, more detailed, dynamic analyses, such as a harmonic response or a transient analysis.

3.9 HARMONIC ANALYSIS

An harmonic response analysis yields solutions of time-dependent equations of motion associated with linear structures undergoing steady-state vibration. To this end, all loads and displacements are assumed to vary sinusoidal at the same known frequency.

The results of the harmonic analysis can be plotted in a graph of amplitude vs. frequency using the Time-history Postprocessor. This graph of amplitude vs. frequency is the FRF of that structure.

3.10 MODELLING OF DAMAGED BEAM

In our analytical work we have to model damaged beams at various load increments. To model a damaged beam we have made an assumption that the damage in the beam is changing the Elastic modulus of the beam.

To model a damaged beam we did a deformation controlled non-linear analysis on the beam and find out its Load-Deflection curve, and then find out the value of E corresponding to the load respectively. The following procedure has been used to find out the damaged beam elastic modulus.

Let P be the load at a particular deformation Δ,

Then stiffness k,

$$k = P/\Delta \qquad \text{eq 3.7}$$

We know that,
Maximum deformation in a 2 point loading is

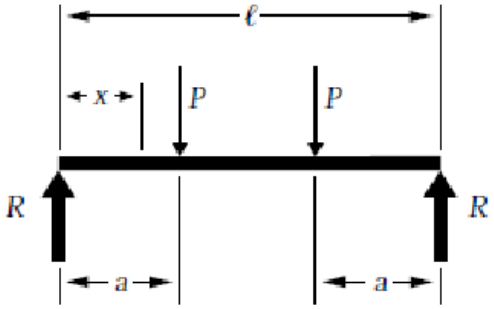

Fig 3.17 Two point load

$$\Delta_{max}\ (\text{at center}) = \frac{Pa}{24EI}(3\ell^2 - 4a^2) \qquad \text{eq 3.8}$$

where,
E = Elastic modulus of beam
I = Moment of Inertia

From eq 3.8,

$$E = \frac{Pa}{24\Delta I}(3\ell^2 - 4a^2) \qquad \text{eq 3.9}$$

We can find out value of E corresponding to the value of load and deflection at the corresponding load. This new value of bean is then used in the FEM model to the damaged beam.

RESULTS

4.1 RESULTS

In this chapter, discussions on the results of the analytical work have been presented. The result has been illustrated below.

4.1.1 Control beam

Here is the plot of FRF graph of the beam. The graph is plotted with respect to different load i.e. 0kN, 5.6kN, 8.4kN, 13.2kN, 15.2kN, 19.9kN. These loads are incorporated in the beam by decreasing the elastic modulus of the beam model in ANSYS. By doing the non-linear analysis, the load deflection curve of the beam is plotted, which we have used to find the modified elastic modulus value as per the load step. These modified elastic modulus value represent the damage in the beam when the corresponding load is applied.

After the non-linear analysis, modal analysis is done to find out the frequency and harmonic analysis to find out the FRF graph. The various FRF graph are plotted below.

CONTROL BEAM	
LOAD (kN)	DEFLECTION (mm)
0	0
5.6	2.42
8.4	4.44
13.2	12.26
15.2	15.08
19.9	43.43

Table 4.1 Load deflection of control beam

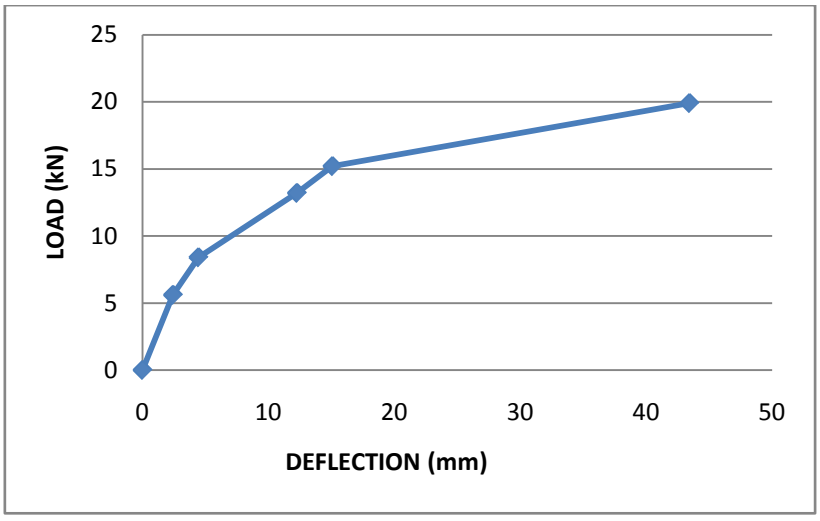

Fig 4.1 Load deflection curve

4.1.1.1. <u>No load.</u>

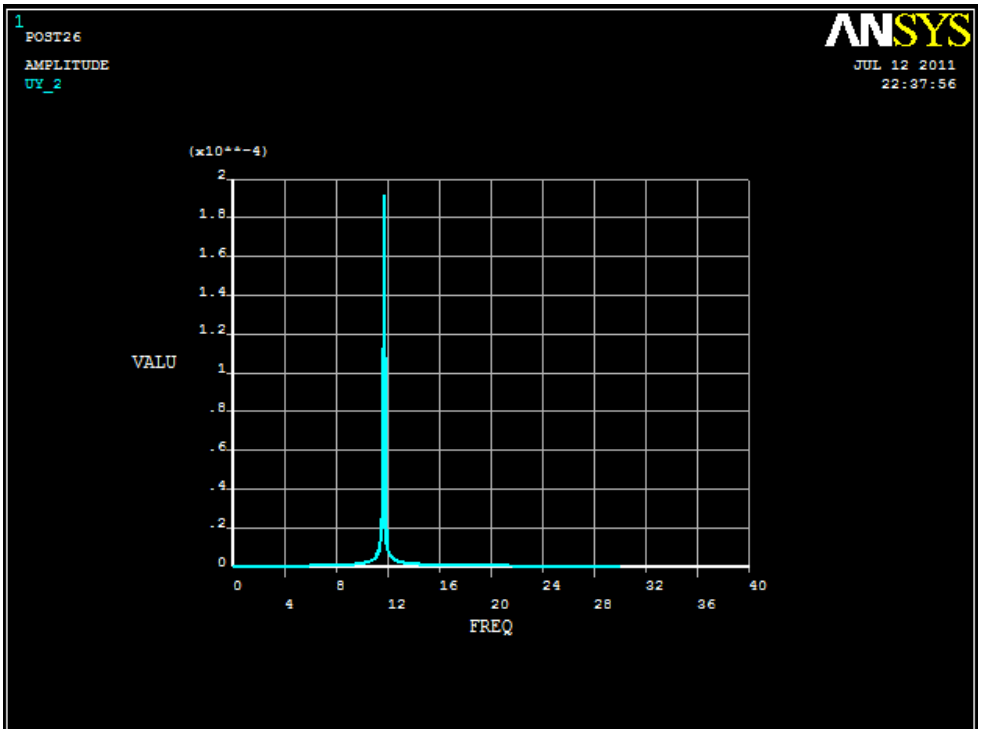

Fig 4.2 FRF graph of control beam when load is 0 kN

4.1.1.2 <u>Load 5.6 kN</u>

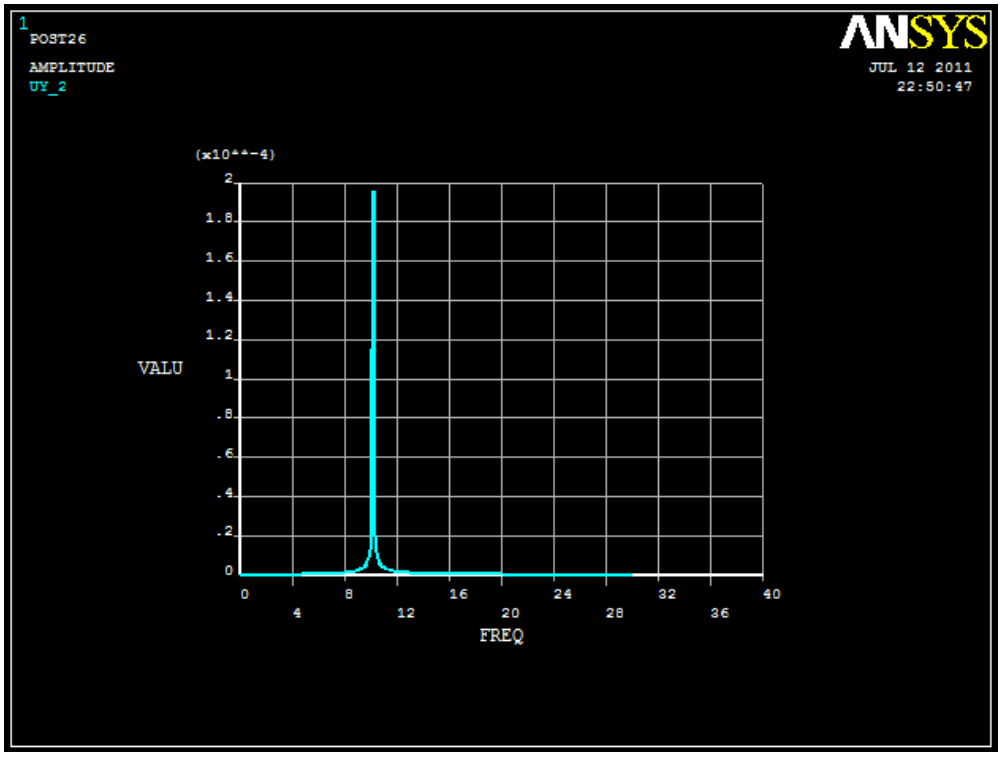

Fig 4.3 FRF graph of control beam when load is 5.6Kn

4.1.1.3 Load 8.4 kN

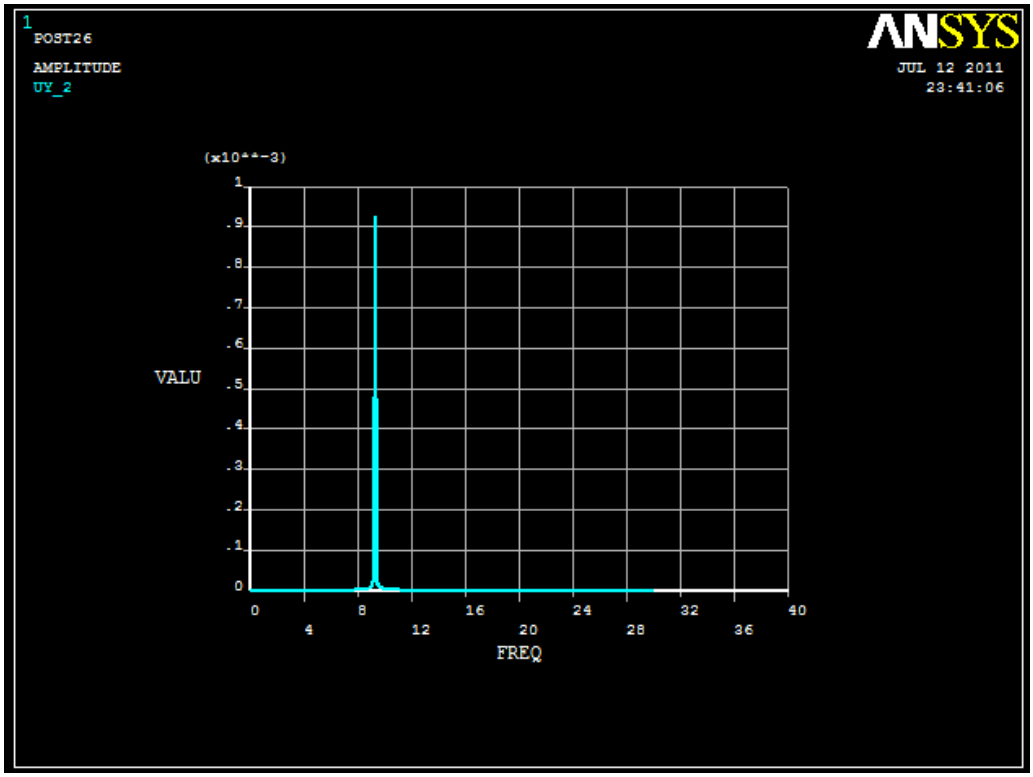

Fig 4.4 FRF graph of control beam when load 8.4 kN

4.1.1.4 Load 13.2

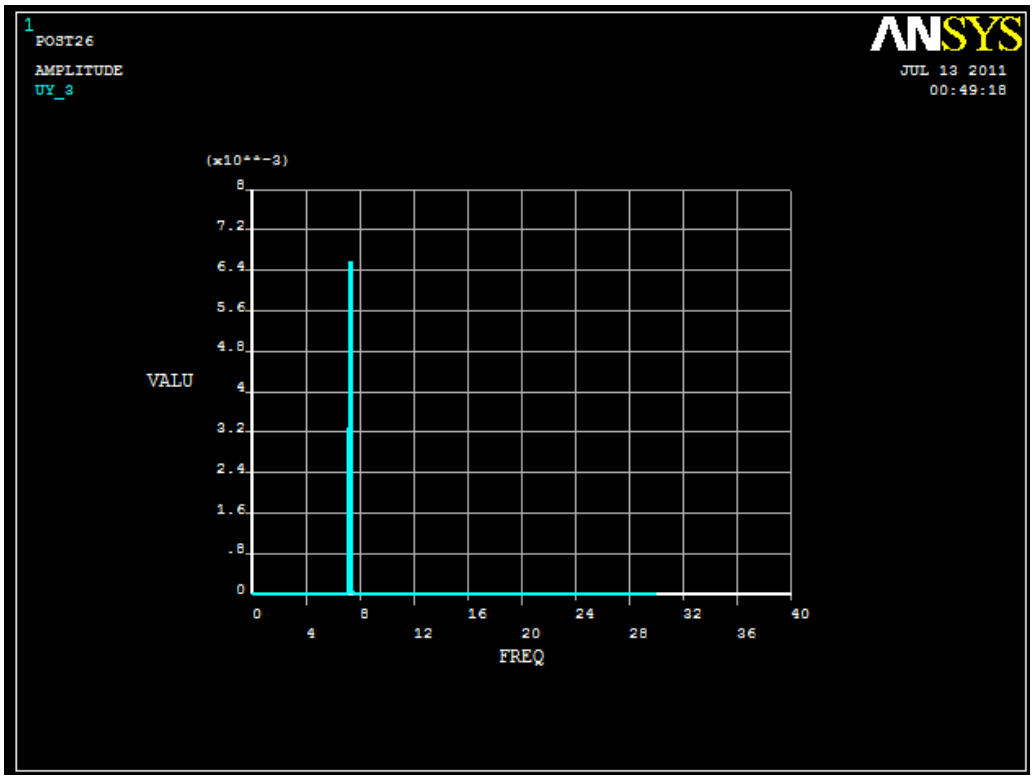

Fig 4.5 FRF graph of control beam when load is 13.2kN

4.1.1.5 Load 15.2

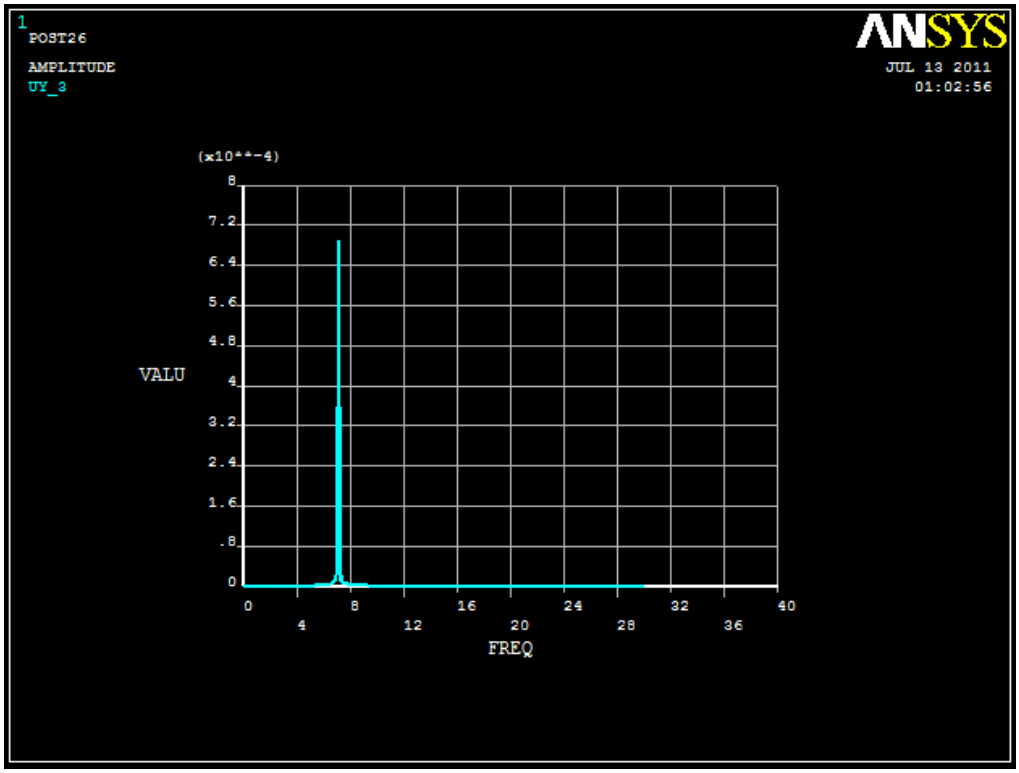

Fig 4.6 FRF graph of control beam when load is 15.2kN

4.1.1.6 Load 19.9

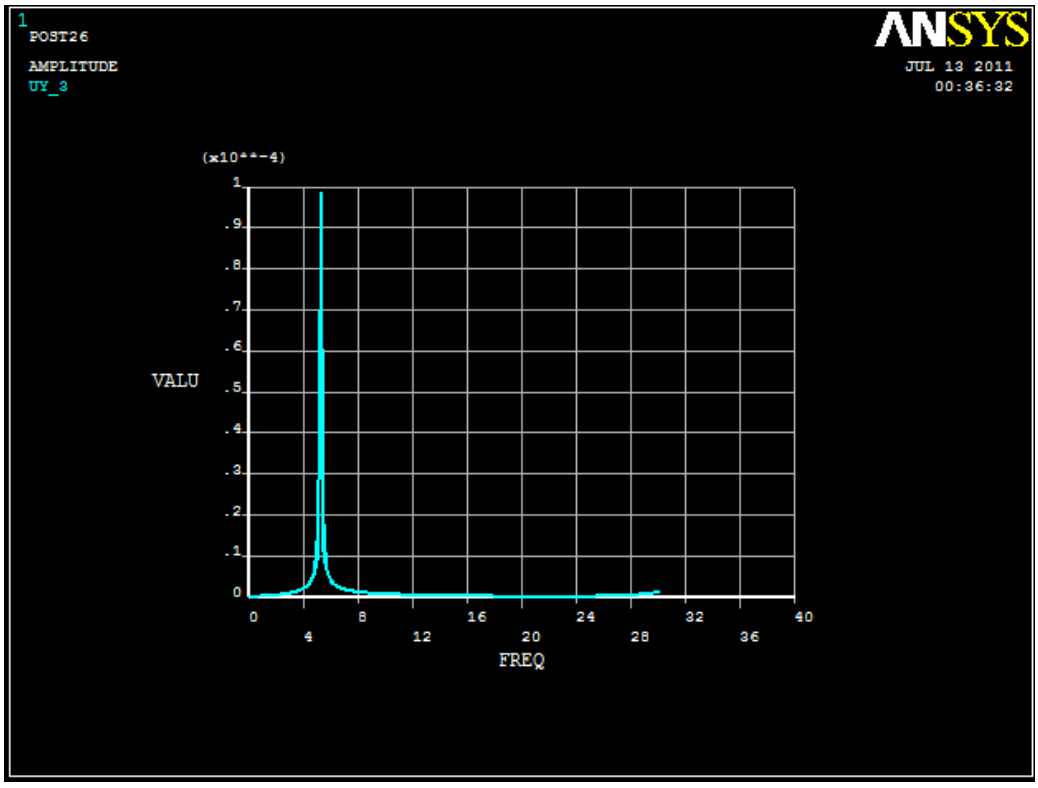

Fig 4.7 FRF graph of control beam when load is 19.9k

From the above graphs we can deduce the following

CONTROL BEAM		
Load (kN)	Amplitude (mm)	Frequency
0	1.91E-04	11.7
5.6	1.95E-04	10.2
8.4	9.24E-04	9.3
13.2	6.55E-03	7.3
15.2	6.86E-04	7.1
19.9	9.88E-05	5.3

Table 4.2 Results of the control beam

From the above table we can deduce that there is decrease in the frequency as there is increase in load.

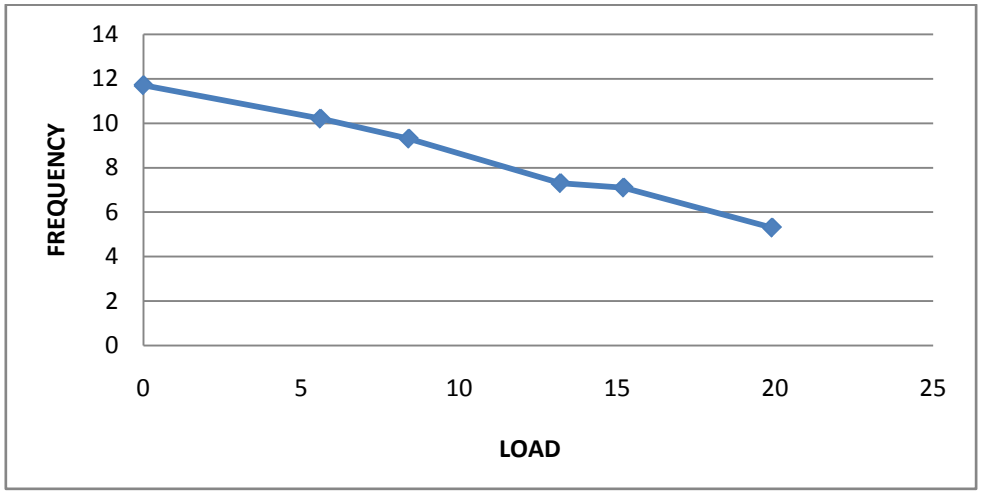

Fig 4.8 Load-frequency graph

From the above table we can see that there is increase in deflection with increase in frequency but it starts to decrease after it reaches 13.2 kN.

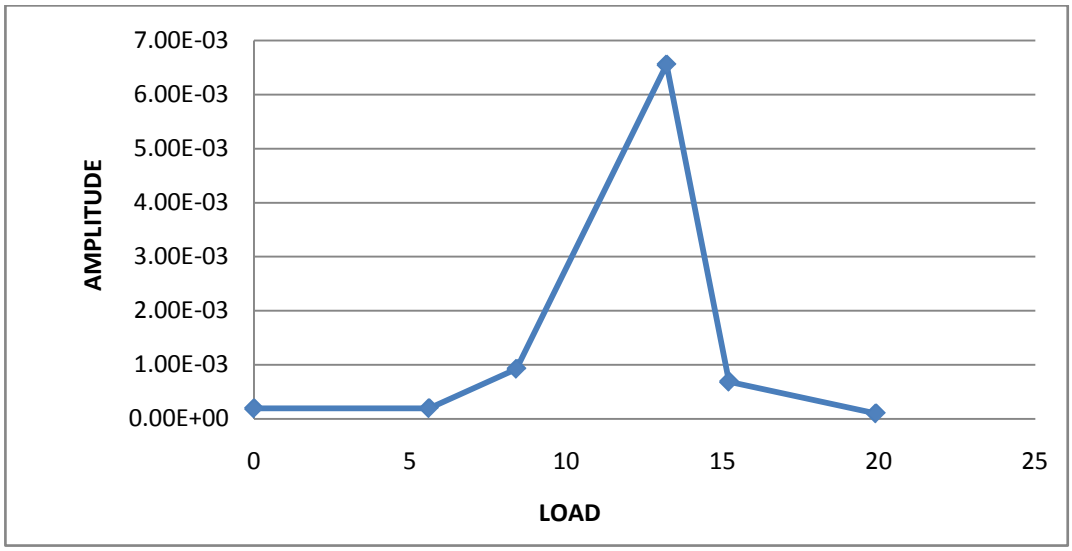

Fig 4.9 Amplitude-frequency graph

From the above table it can be observed that there is decrease in the frequency of the beam ass we increase the load. For load 5.6kN, 8.4kN, 13.2kN, 15.2kN, 19.9kN and the decrease in frequency is 12.5%, 20.5% 37.6%, 39.3%, 54.7%.

4.1.2 Retrofitted beam stressed at 90%

Here the study of FRF of retrofitted beam which are stressed at 90% is presented. To model this beam a model of retrofitted beam incorporating the concrete beam with fibre composite in made in ANSYS and then a deformation controlled non-linear analysis is performed. From the non-linear analysis we find out the load-deflection curve, which is used to find the modified elastic modulus which represents the damage at that load step. This elastic modulus is incorporated in the beam to model a damaged beam. Harmonic analysis is done to plot the frequency response graph which is shown below.

RETROFITTED BEAM 90%	
LOAD (kN)	DEFLECTION (mm)
0	0
4.6	8.2
8.4	14.77
13	23
16	28
16.8	29.5
23.4	44.2
25.6	62.4
29	79.8
31.6	96.3

Table 4.3 Load deflection of retrofitted beam stressed at 90 %

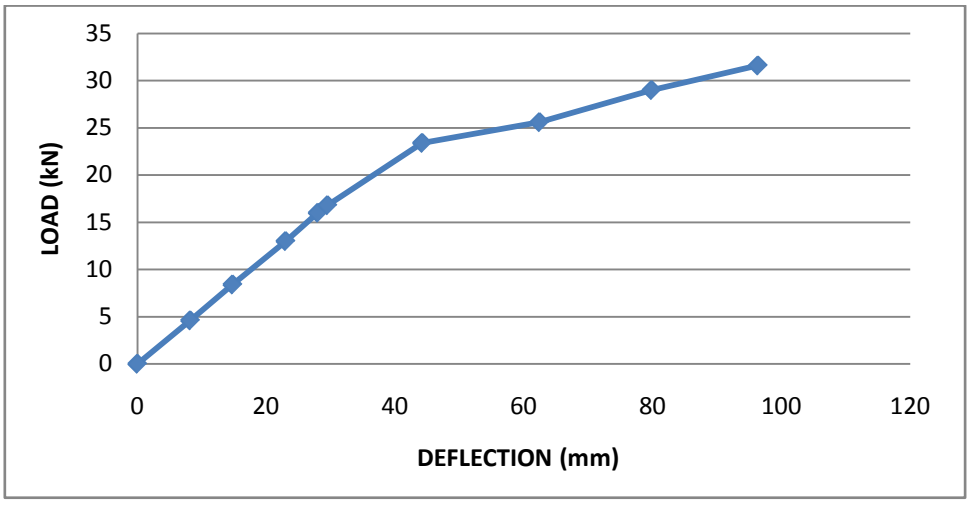

Fig 4.10 Load Deflection graph

4.1.2.1 Load 0kN

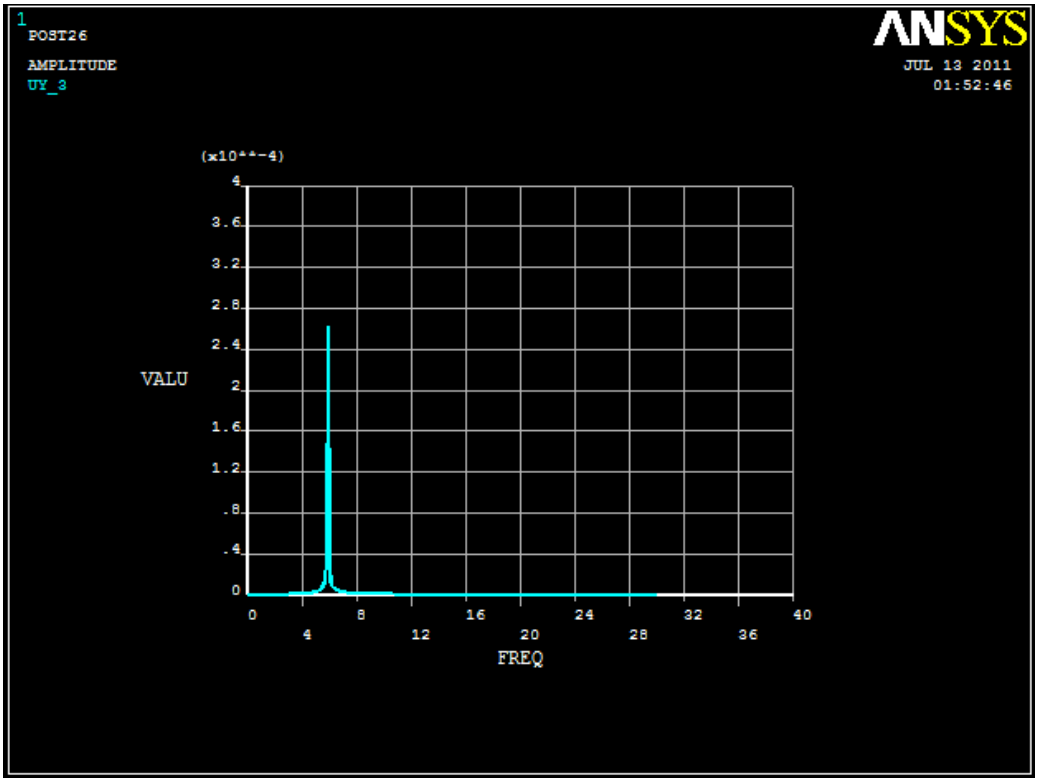

Fig 4.11 FRF graph of retrofitted beam 90% stressed at load 0 kN

4.1.2.2 Load 4.6kN

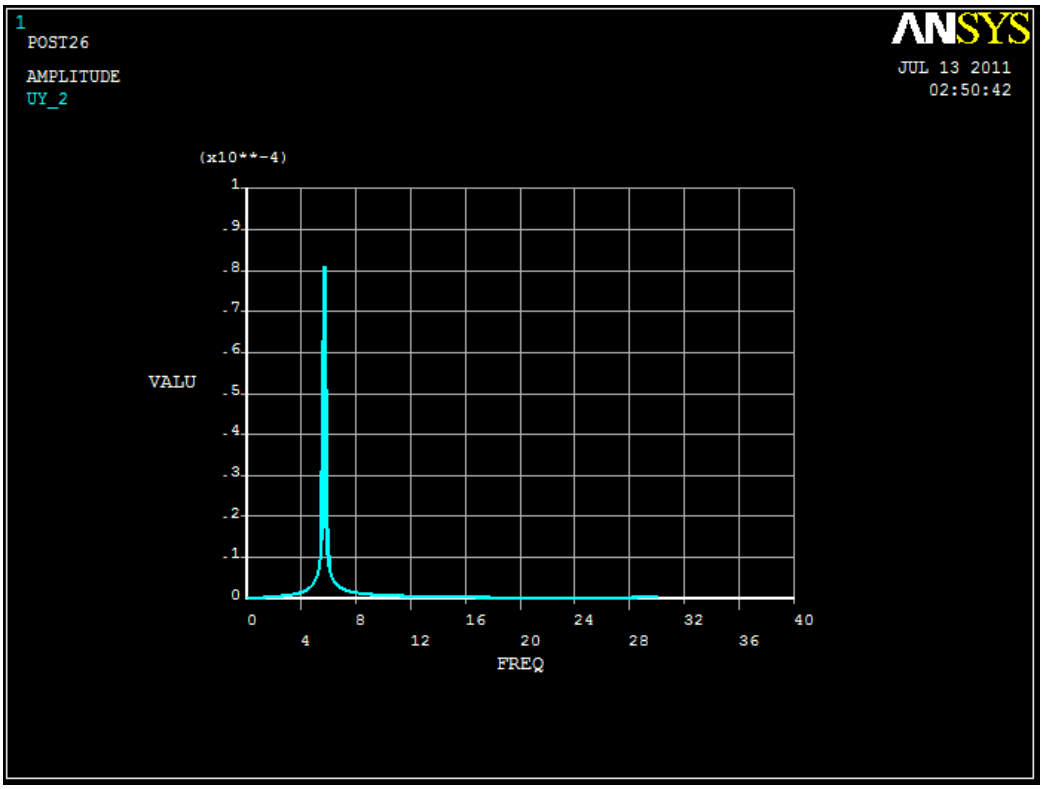

Fig 4.12 FRF graph of retrofitted beam 90% stressed at load 4.6kN

4.1.2.3 Load 8.4kN

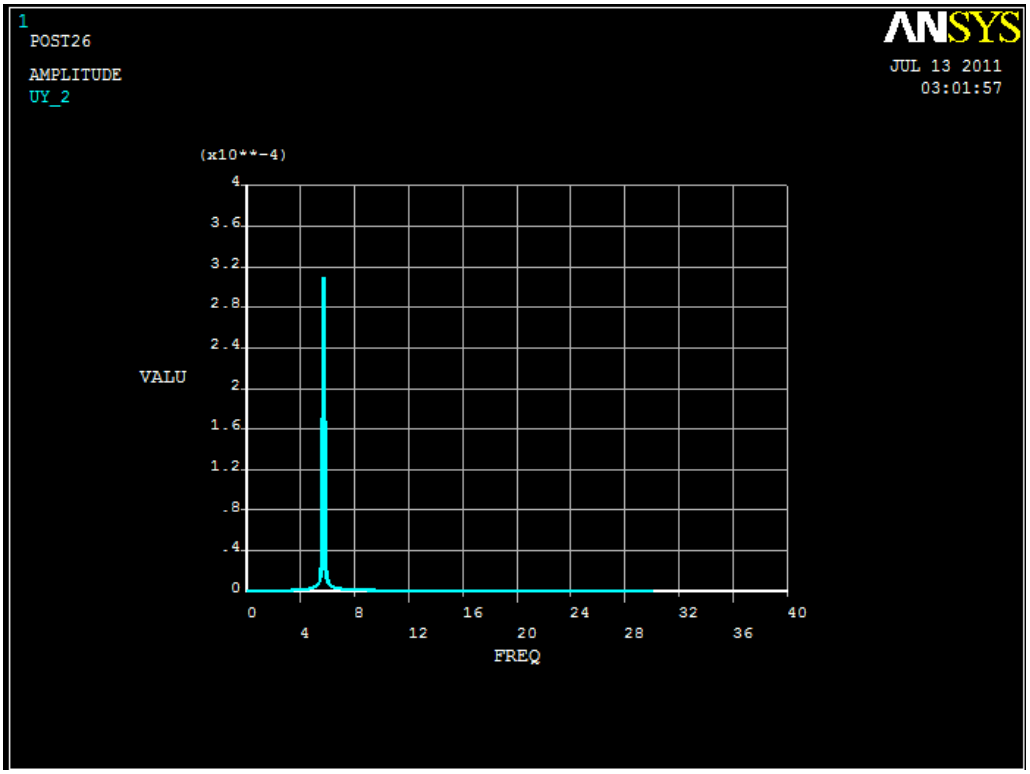

Fig 4.13 FRF graph of retrofitted beam 90% stressed at load 8.4kN

4.1.2.4 Load 13kN

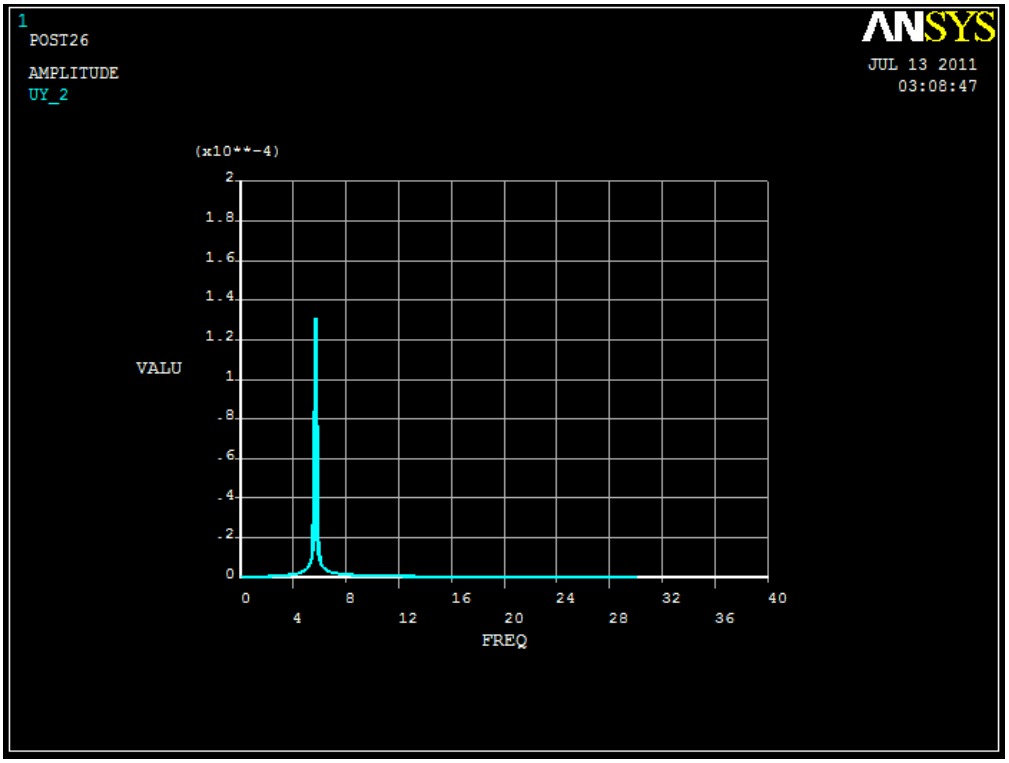

Fig 4.14 FRF graph of retrofitted beam 90% stressed at load 13kN

*4.1.2.5 Load 16*kN

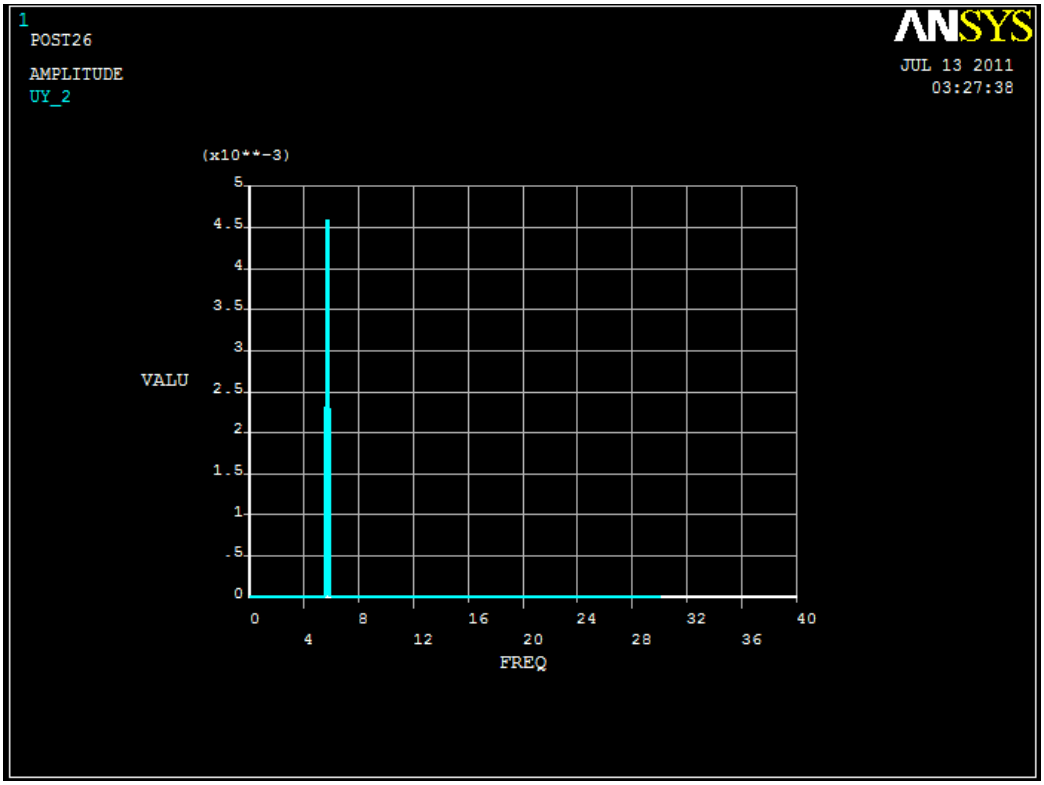

Fig 4.15 FRF graph of retrofitted beam 90% stressed at load 16kN

4.1.2.6 Load 23.4kN

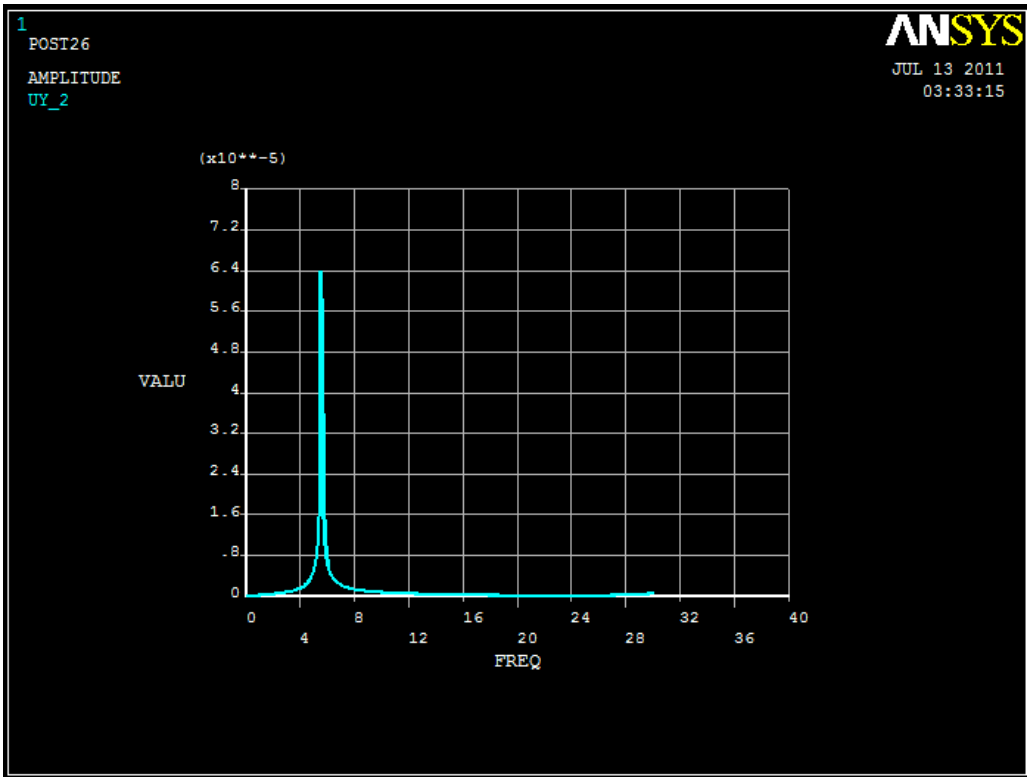

Fig 4.16 FRF graph of retrofitted beam 90% stressed at load 23.4kN

4.1.2.7 Load 31.6kN

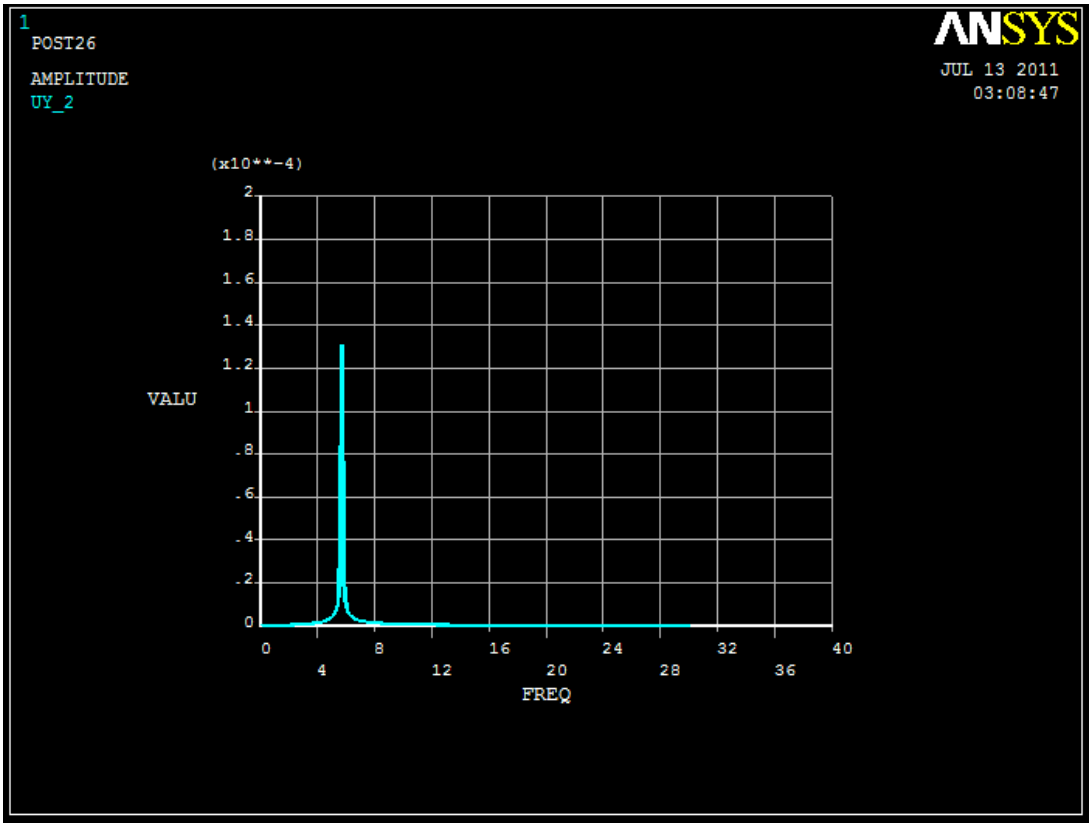

Fig 4.17 FRF graph of retrofitted beam 90% stressed at load 31.6 kN

From the above graphs we can deduce the following:

RETROFFIED BEAM AT 90%		
Load (kN)	Amplitude (mm)	Frequency
0	2.63E-04	5.9
4.6	8.10E-05	5.7
8.4	3.20E-04	5.7
13	1.31E-04	5.7
16	4.60E-03	5.7
23.4	6.38E-05	5.5
25.6	1.21E-04	5.1
31.6	1.39E-04	4.7

Table 4.4 Results of the retrofitted beam at 90% stressed

From the above table we can see that there is decrease in the frequency as there is increase in load. There is increase in the amplitude from load step from 13kN to 16kN.

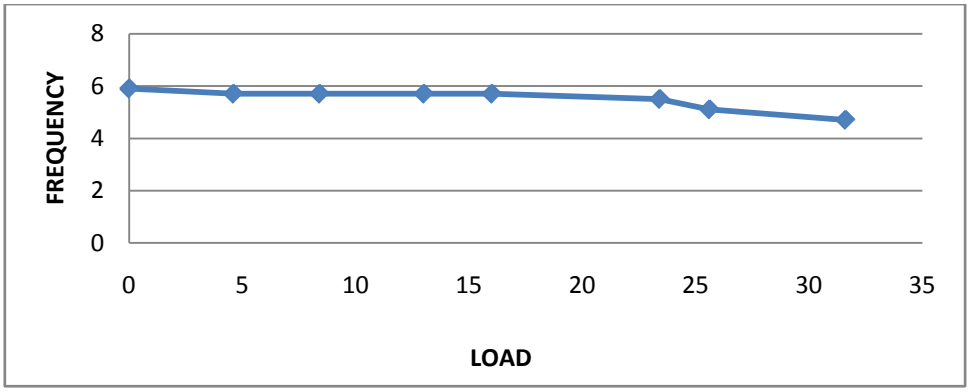

Fig 4.18 Load-frequency graph

From the above table we can see the variation in displacement with respect to frequency

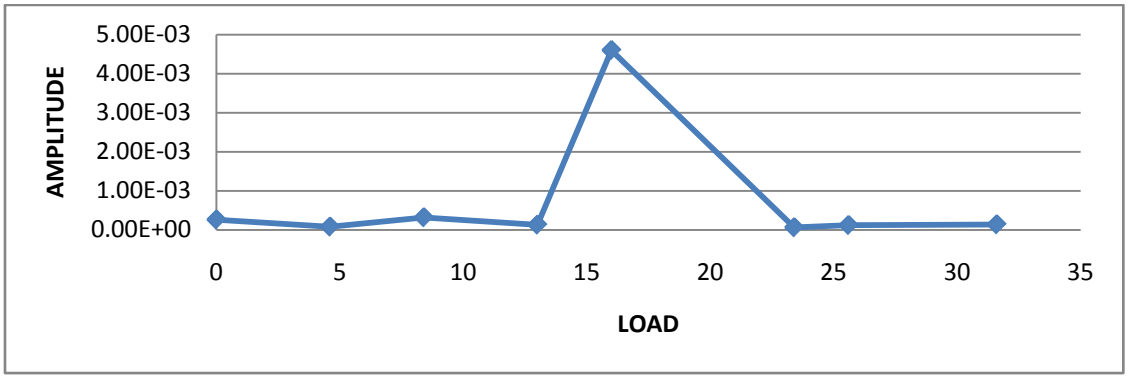

Fig 4.19 Amplitude-frequency graph

From the above table it can be observed that there is decrease in the frequency of the beam ass we increase the load. For load 8.2kN, 14.77kN, 23kN, 28kN, 44.2kN, 62.4kN, 96.3kN and the decrease in frequency is 3.3%, 3.3%,3.3%, 3.3%, 6.7%, 13.5%, 20.3%.

4.1.3 RETROFITTED BEAM STRESSED AT 75%

Similar procedure was done for retrofitted beam stressed at 75 %.

RETROFITTED BEAM 75%	
LOAD (kN)	DEFLECTION (mm)
0	0
4.6	7
8.4	13
13	20.1
15.4	23.66
16.8	26.02
24.8	39.13
30.1	79.85
32	97.6
33.6	115.1

Table 4.5 Load-deflection of retrofitted beam at 75 %

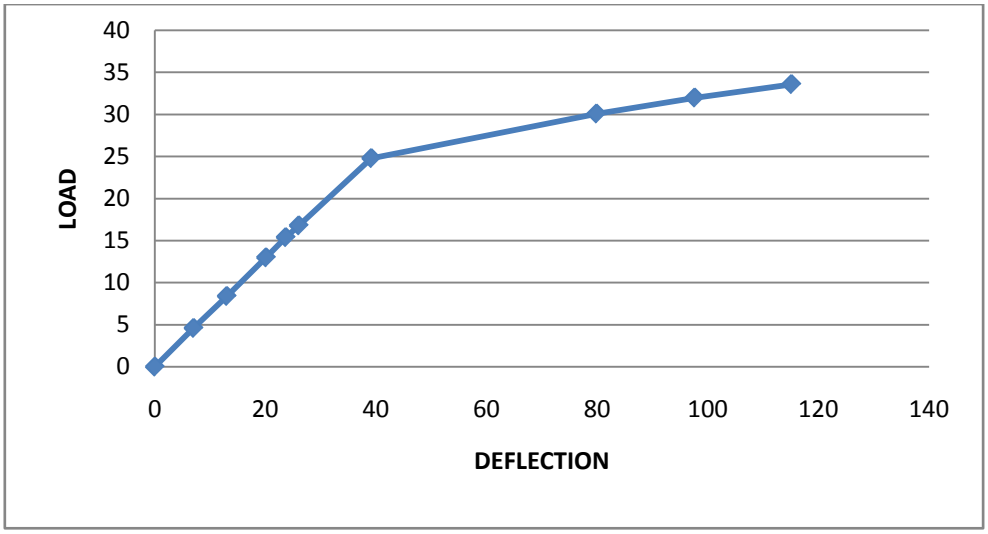

Fig 4.20 Load deflection curve

4.1.3.1 Load 0kN

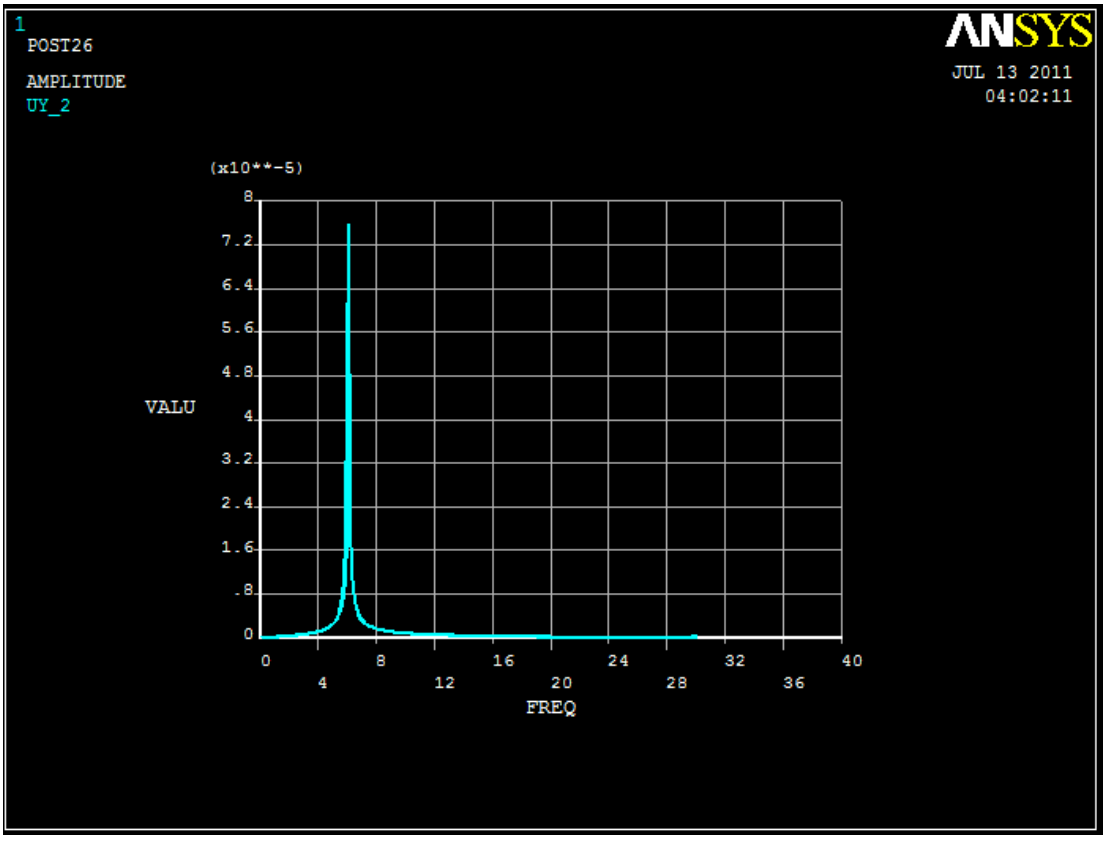

Fig 4.21 FRF graph of retrofitted beam 75% stressed at load 0kN

4.1.3.2 Load 4.6kN

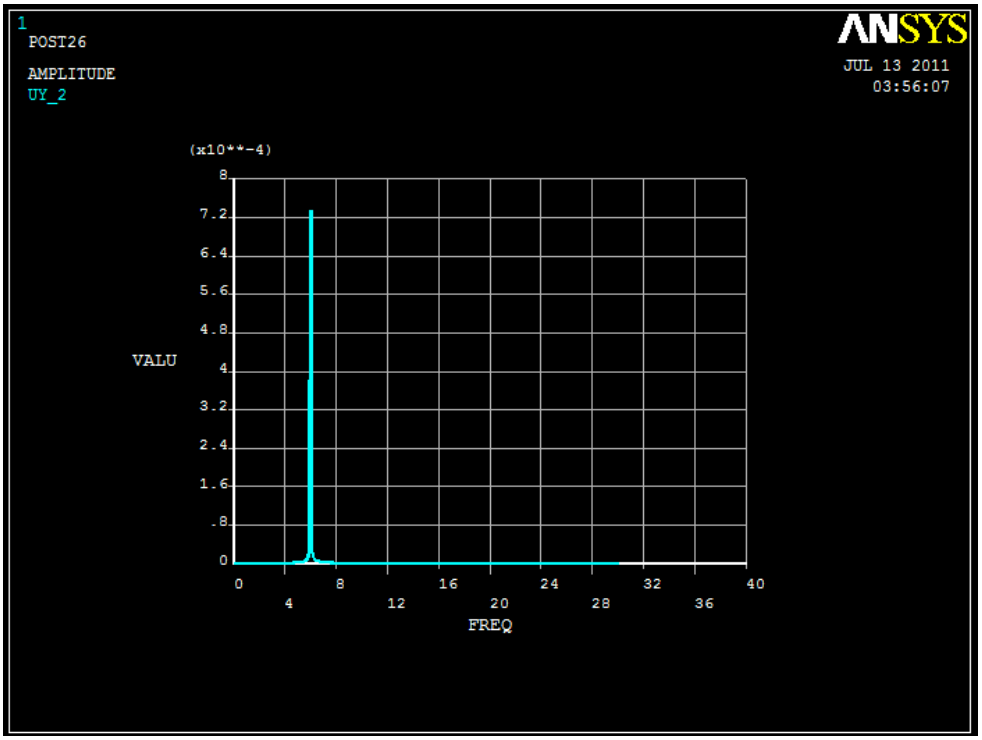

Fig 4.22 FRF graph of retrofitted beam 75% stressed at load 4.6kN

4.1.3.3 Load 8.4kN

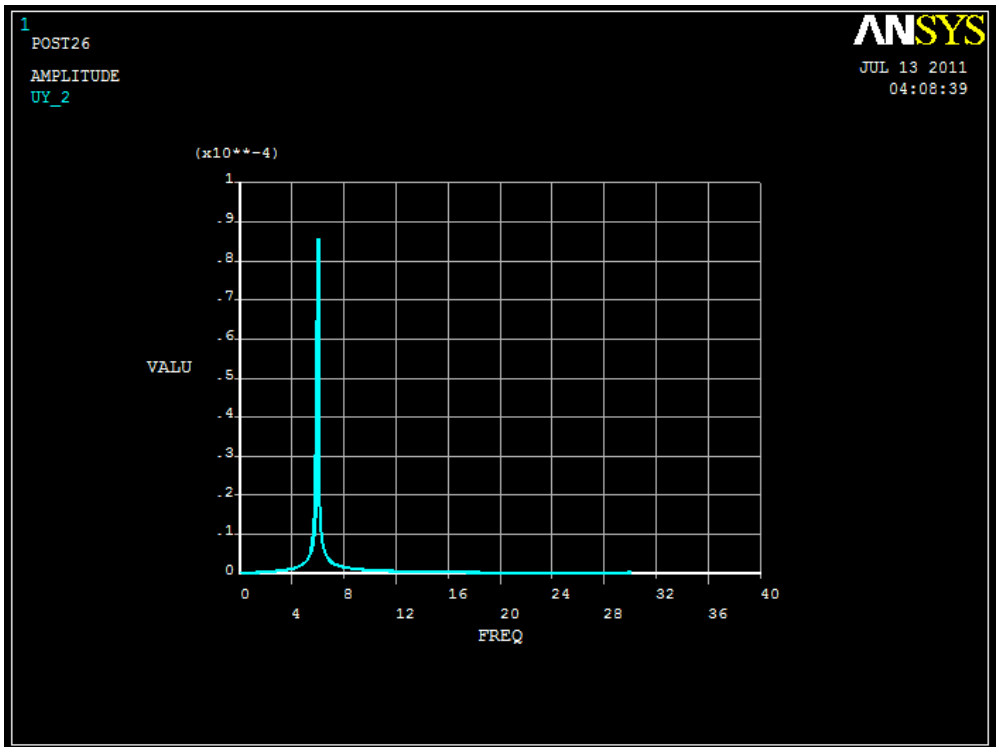

Fig 4.23 FRF graph of retrofitted beam 75% stressed at load 8.4kN

4.1.3.4 Load 13kN

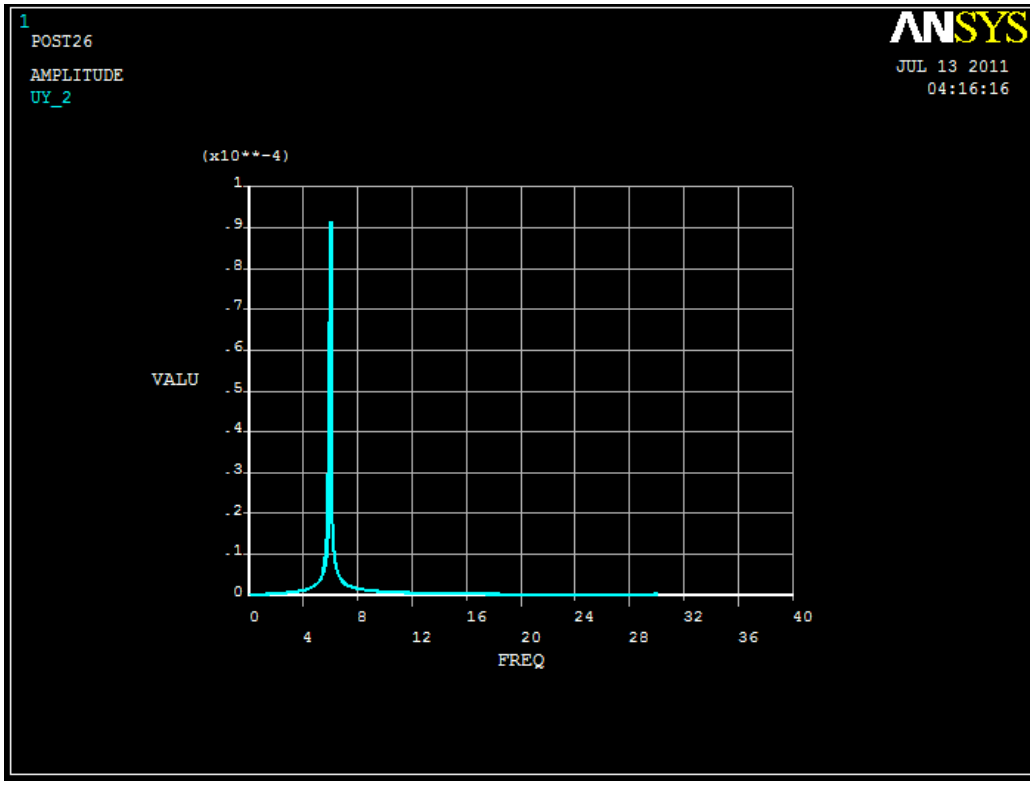

Fig 4.24 FRF graph of retrofitted beam 75% stressed at load 13kN

4.1.3.5 Load 15.4kN

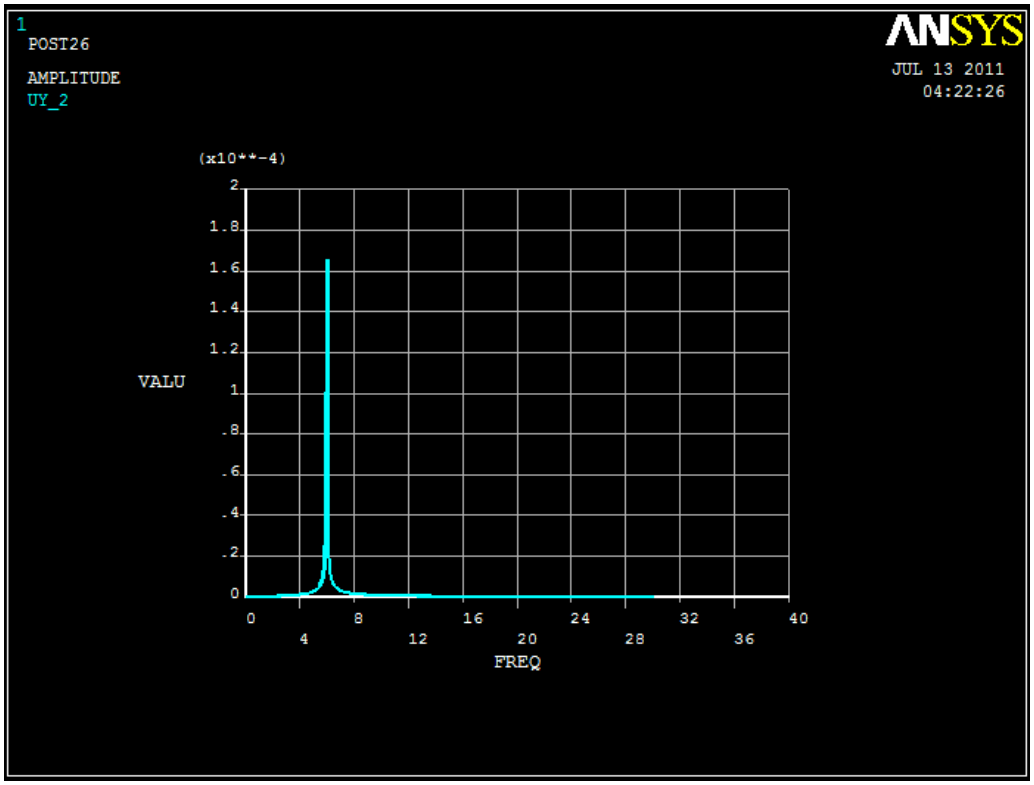

Fig 4.25 FRF graph of retrofitted beam 75% stressed at load 15.4kN

4.1.3.6 Load 24.8kN

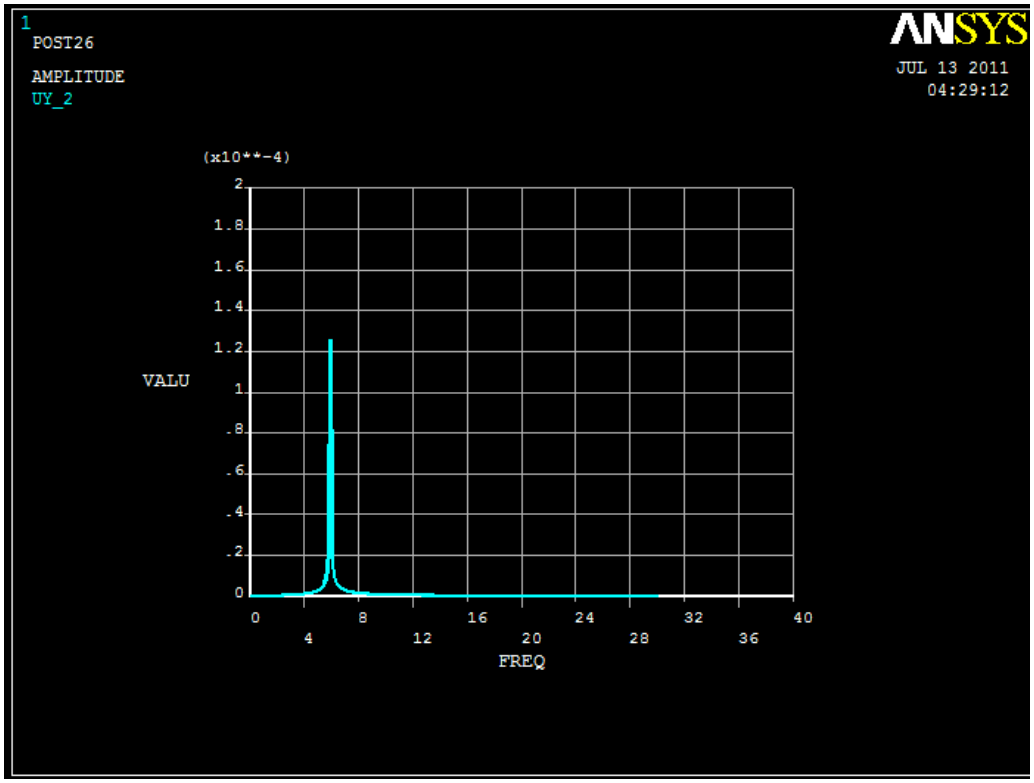

Fig 4.26 FRF graph of retrofitted beam 75% stressed at load 24.8kN

4.1.3.7 Load 30.1kN

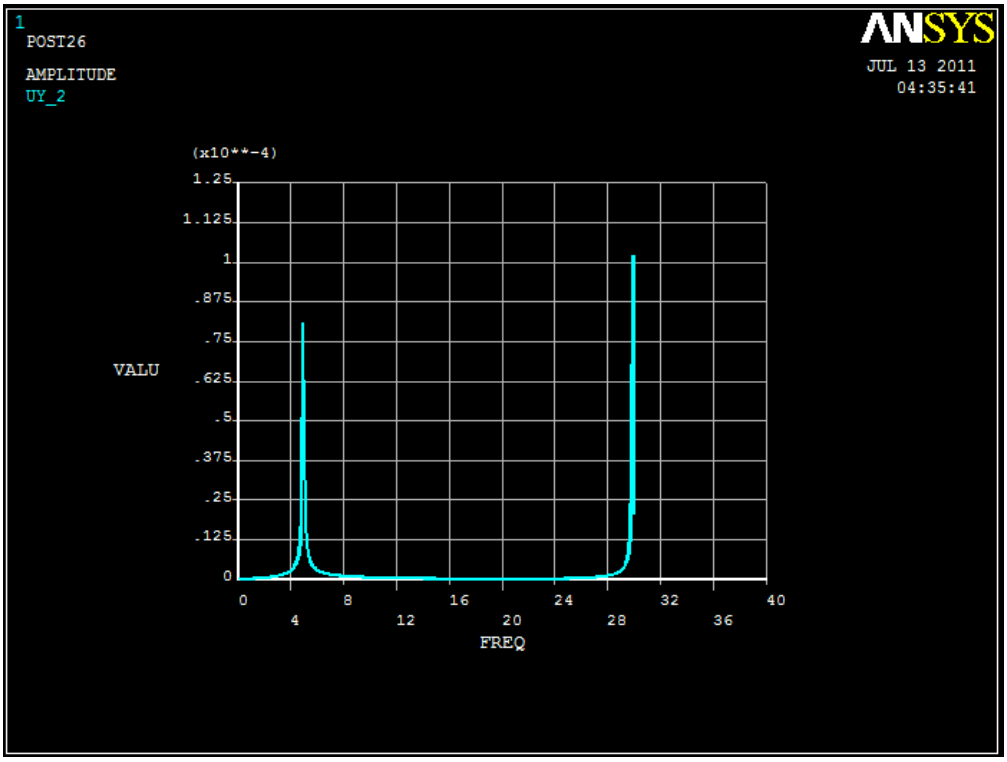

Fig 4.27 FRF graph of retrofitted beam 75% stressed at load 30.1kN

4.1.3.8 Load 33.6kN

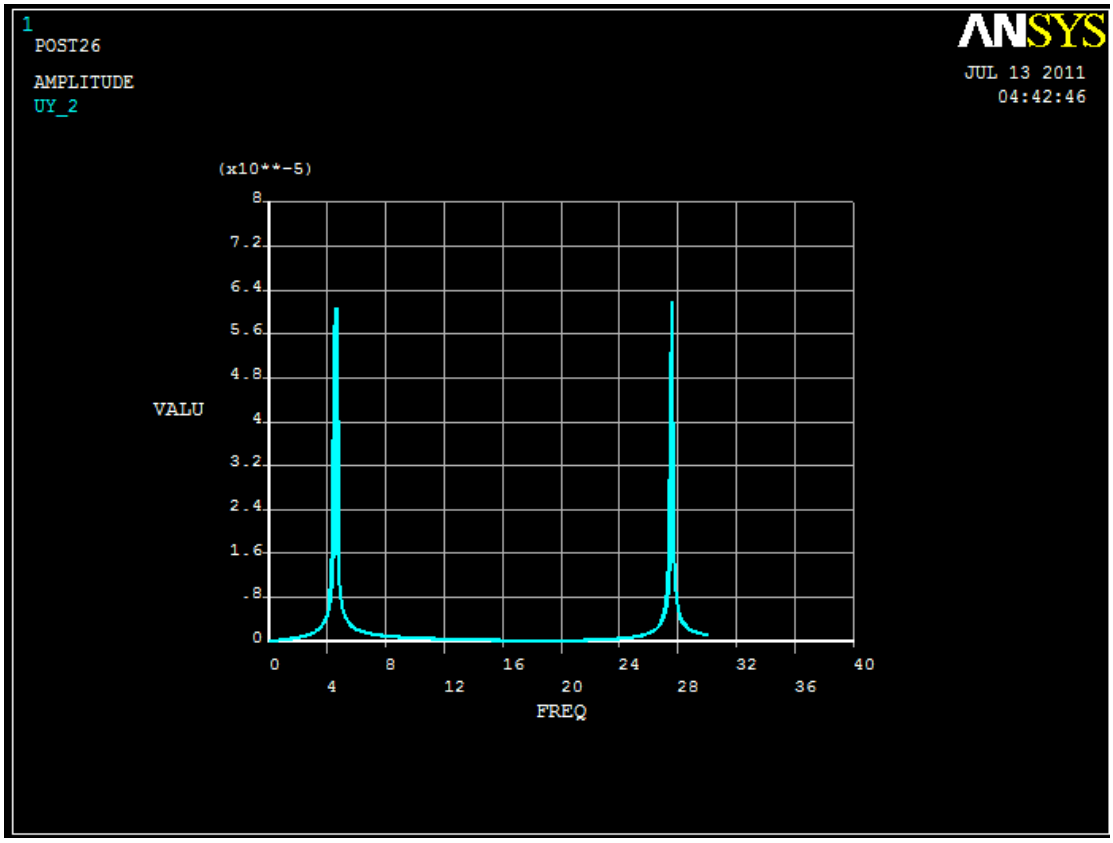

Fig 4.28 FRF graph of retrofitted beam 75% stressed at load 33.6kN

From the above graphs we can deduce the following

RETROFFIED BEAM AT 75%		
load (kN)	deflection (mm)	frequency
0	7.59E-05	6.1
4.6	7.33E-04	6
8.4	8.56E-05	6
13	9.14E-05	6
15.4	1.65E-04	6
24.8	1.26E-04	5.9
30.1	8.08E-05	4.9
33.6	6.07E-05	4.6

Table 4.6 Results of the retrofitted beam at 75% stressed

From the above table it can be observed that there is decrease in frequency as there is increase in load. There is also increase in amplitude during the increase in load at the start and then there is decrease as load is increased.

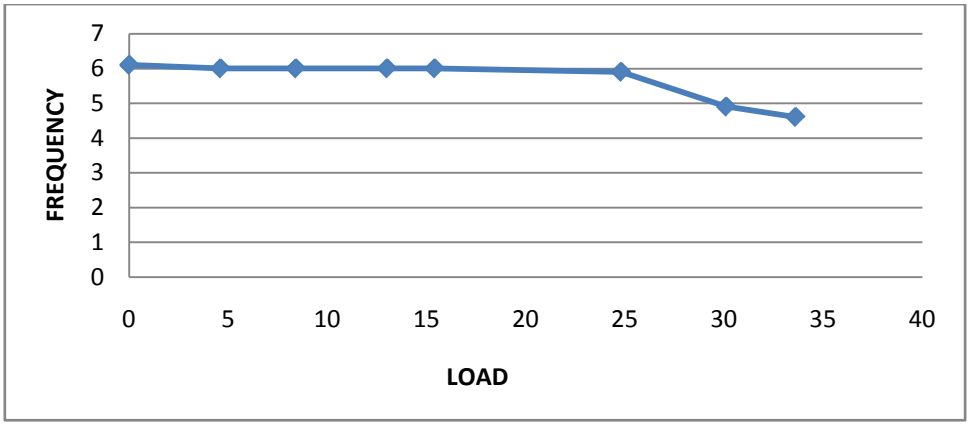

Fig 4.29 Load-frequency graph

From the above table we can see the variation in displacement with respect to frequency

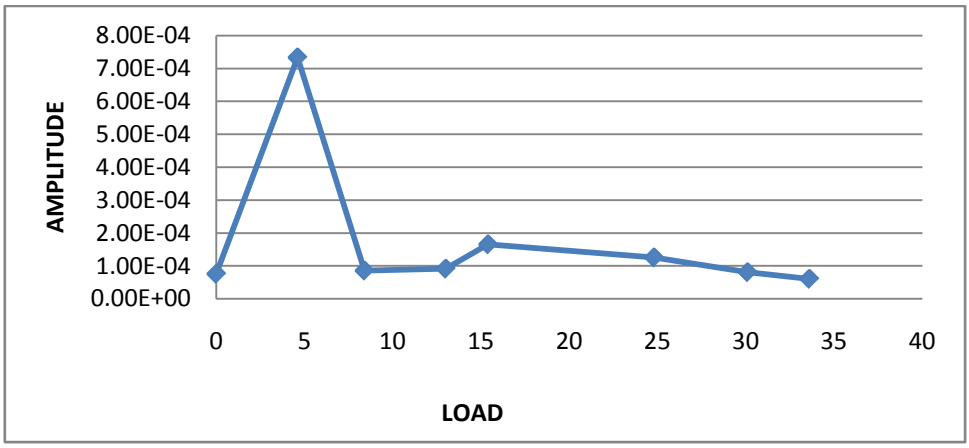

Fig 4.30 Amplitude-load graph

From the above table it can be observed that there is decrease in the frequency of the beam ass we increase the load. For load 4.6kN, 8.4kN, 13kN, 15.4kN, 24.8kN, 30.1kN, 33.6kN and the decrease in frequency is 1.6%, 1.6%, 1.6%, 1.6%, 3.2%, 19.6%, 24.5%

4.2 DAMAGE INDEX

Damage Index is defined as change in stiffness to the original stiffness i.e.

$$\text{Damage Index} = k''/k$$

where,
K'' = Original stiffness – Stiffness at different level
k = Original stiffness,

$$k = P/\Delta$$

where,
P = Load in kN
Δ = Deflection in mm

Load-deflection of a beam is taken from the deformation controlled non-linear analysis of beam. Damage index and frequency for controlled beam, retrofitted beam stressed at 90 and 75 percent are plotted below.

4.2.1 Control beam

CONTROL BEAM					
LOAD (kN)	DEFLECTION (mm)	Stiffness (kN/mm)	DAMAGE INDEX	FREQUENCY	AMPLITUDE
0	0	3.12	0	11.7	1.91E-04
5.6	1.42	2.31	0.25	10.2	1.95E-04
8.4	4.44	1.891	0.39	9.3	9.24E-04
13.2	12.26	1.07	0.65	7.3	6.55E-03
15.2	15.08	1.00	0.67	7.1	6.86E-04
19.9	43.43	0.45	0.85	5.3	9.88E-05

Table 4.7 Damage Index of control beam

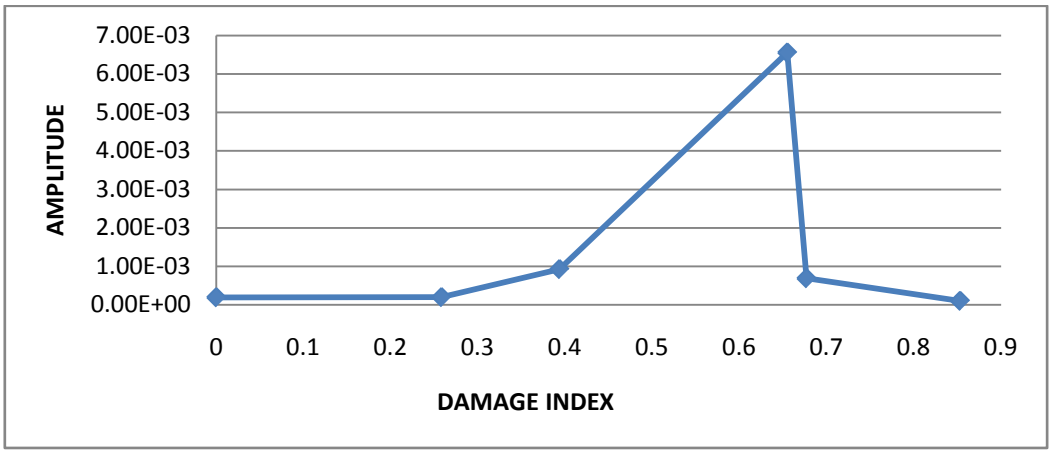

Fig 4.31 Change in Amplitude vs. Damage index of control beam

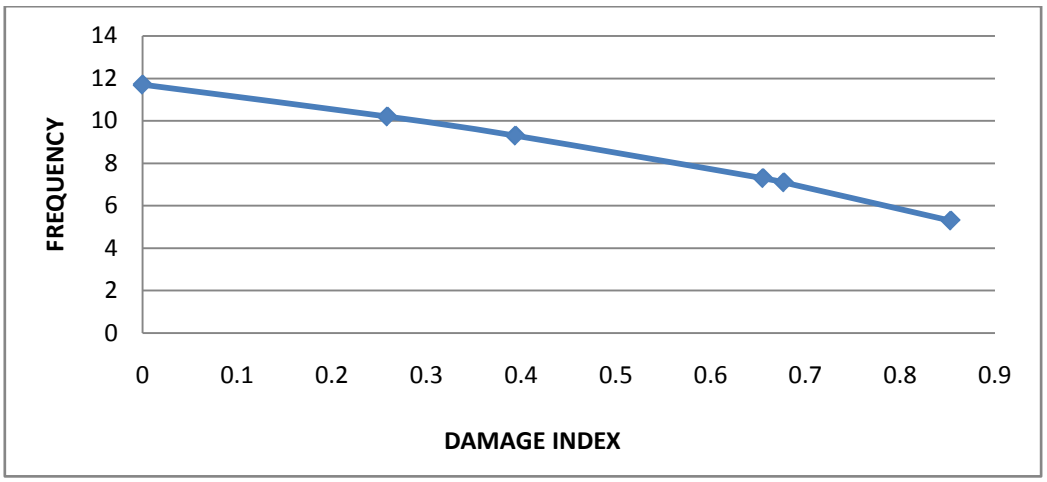

Fig 4.31 Change in Frequency vs. Damage index of control beam

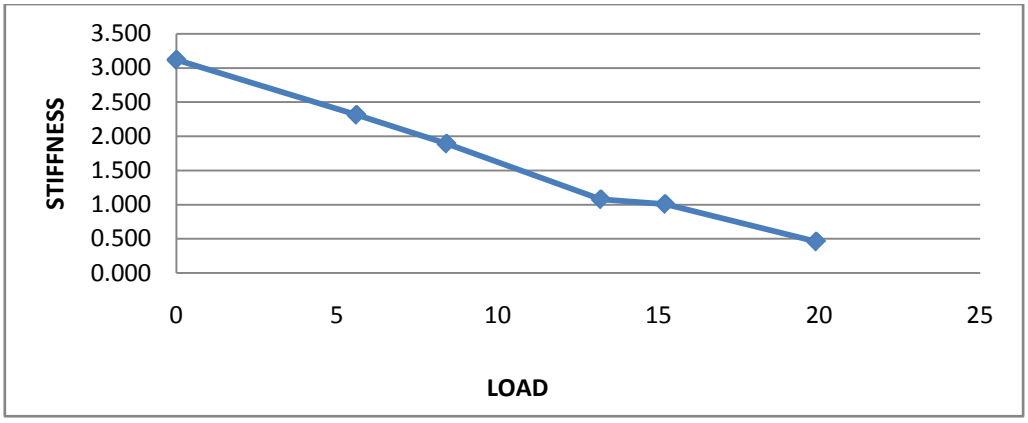

Fig 4.33 Change in Stiffness vs. Load of control beam

From the above plot it is seen that as we increase the load, the stiffness goes on decreasing which results in increasing in the damage factor. As this damage goes on increasing there is decrease in the frequency of the beam.

4.2.2 Retrofitted beam stressed at 90%

RETROFITTED BEAM 90%					
LOAD (kN)	DEFLECTION (mm)	STIFFNESS (kN/mm)	DAMAGE INDEX	FREQUENCY	AMPLITUDE
0	0	1.800	0.000	5.9	2.63E-04
4.6	8.2	0.561	0.688	5.7	8.10E-05
8.4	14.77	0.569	0.684	5.7	3.20E-04
13	23	0.565	0.686	5.7	1.31E-04
16	28	0.571	0.683	5.7	4.60E-03
23.4	44.2	0.529	0.706	5.5	6.38E-05
25.6	62.4	0.410	0.772	5.1	1.21E-04
31.6	96.3	0.328	0.818	4.7	1.39E-04

Table 4.8 Damage Index of retrofitted beam stressed at 90%

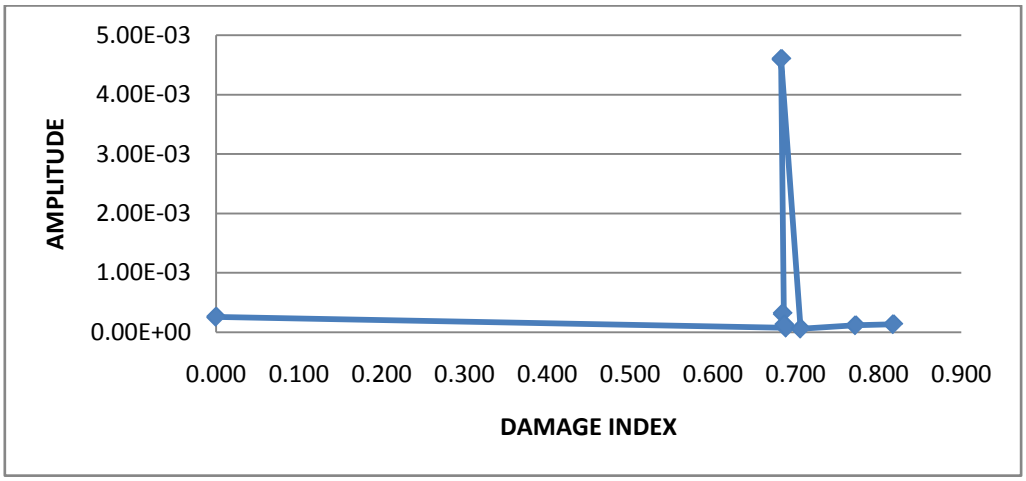

Fig 4.34 Change in Amplitude vs. Damage index of retrofitted beam stressed at 90%

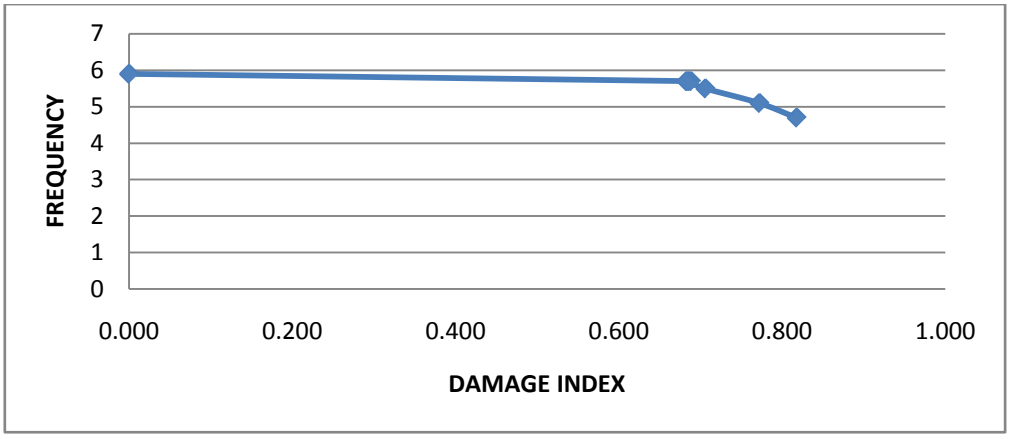

Fig 4.35 Change in Frequency vs. Damage index of retrofitted beam stressed at 90 %.

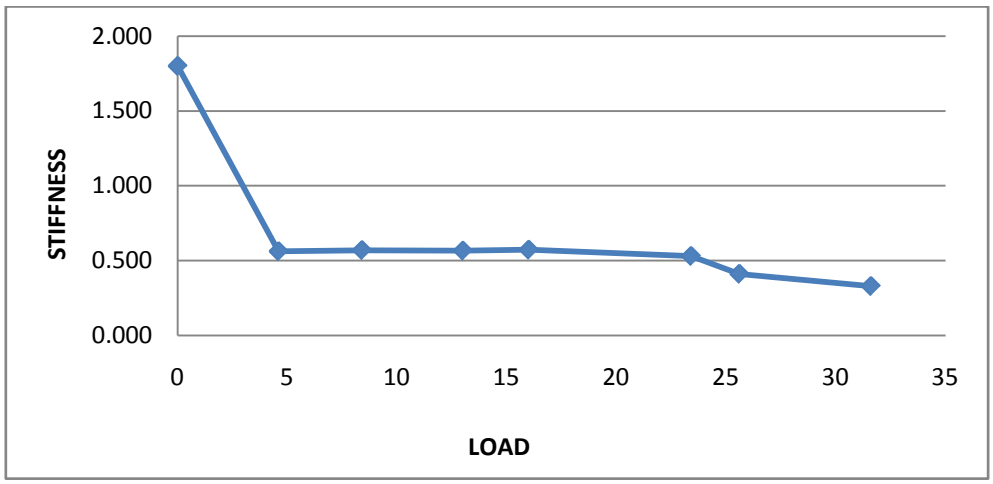

Fig 4.36 in stiffness vs. load of retrofitted beam stressed at 90 %.

From the above plot it is seen that as there is increase the load, the stiffness goes on decreasing which results in increasing in the damage factor. As this damage goes on increasing there is decrease in the frequency of the beam. Also it can be observed the amplitude increase where there is sudden decrease in frequency.

4.2.2 Retrofitted beam stressed at 75 %

RETROFITTED BEAM 75%					
LOAD (kN)	DEFLECTION (mm)	STIFFNESS (kN/mm)	DMAMGE INDEX	FREQUENCY	AMPLITUDE
0	0	1.800	0.000	6.1	7.59E-05
4.6	7	0.657	0.635	6	7.33E-04
8.4	13	0.646	0.641	6	8.56E-05
13	20.1	0.647	0.641	6	9.14E-05
15.4	23.66	0.651	0.638	6	1.65E-04
24.8	39.13	0.634	0.648	5.9	1.26E-04
30.1	79.85	0.377	0.791	4.9	8.08E-05
33.6	115.1	0.292	0.838	4.6	6.07E-05

Table 4.9 Damage index of retrofitted beam stressed at 75 %

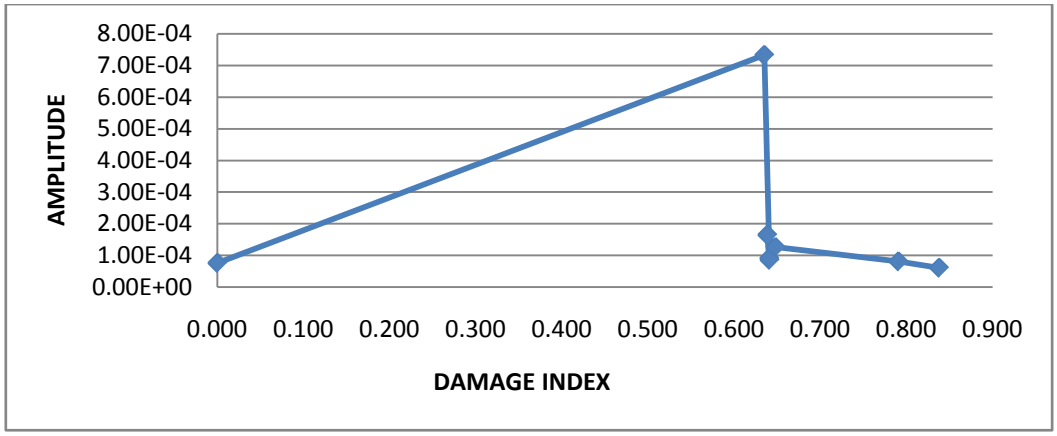

Fig 4.37 Change in amplitude vs. Damage index of retrofitted beam stressed at 75%

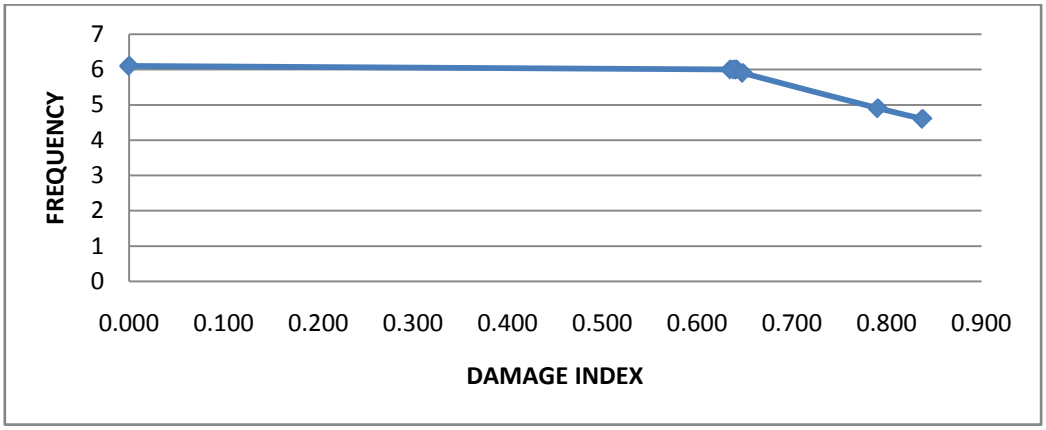

Fig 4.38 Change in frequency vs. Damage index of retrofitted beam stressed at 75%

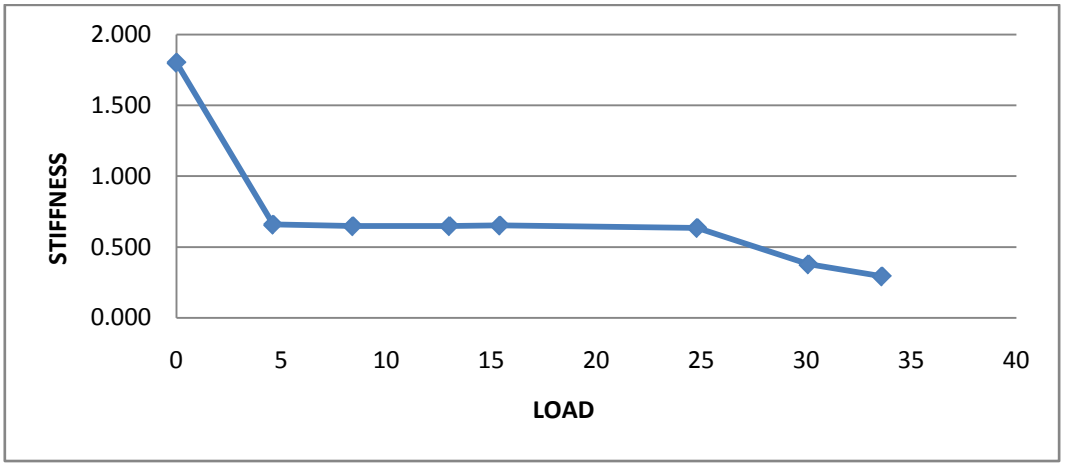

Fig 4.39 Change in stiffness vs. load of retrofitted beam stressed at 75 %.

Similar behaviour is observed for retrofitted beam stressed at 75 %.

4.3 COMPARISON BETWEEN EXPERIMENTAL AND ANALYTICAL WORK

In the experimental work Mr Ankush Goyal in his thesis "Structural health monitoring of retrofitted RCC beams using vibration measurements" conducted the vibration characteristics of a reinforced concrete beam eight channel FFT analyzer. The results of his experiment are stated below.

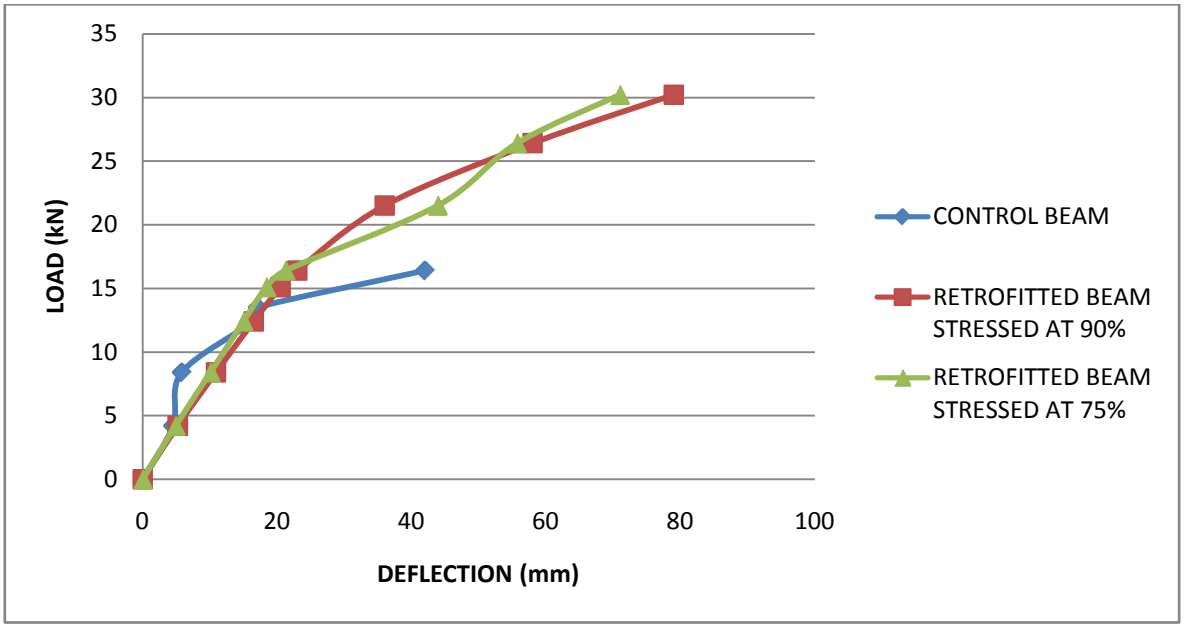

Fig 4.40 Load deflection curve (experimentally)

4.3.1 RETROFITTED BEAM STRESSED AT 90%

The experimental results of control beam is stated below

RETROFITTED BEAM 90%					
LOAD (kN)	DEFLECTION (mm)	STIFFNESS (kN/mm)	DAMAMGE INDEX	FREQUENCY	AMPLITUDE (mm/sec^2)
0	0	1.80	0.00	13.9	7.60E+00
4.2	5.2	0.81	0.55	13.5	5.00E+00
8.4	10.9	0.77	0.57	13.4	3.85E+00
12.4	16.5	0.75	0.58	13.3	2.85E+00
15.1	20.5	0.74	0.59	13.3	2.59E+00
16.4	23	0.71	0.60	13	1.14E+00
21.5	36	0.60	0.67	13	1.10E+00
26.4	58	0.46	0.75	13	8.56E-01
30.2	79	0.38	0.79	12.9	7.78E-01

Table 4.10 Experimental results of retrofitted beam stressed at 90%

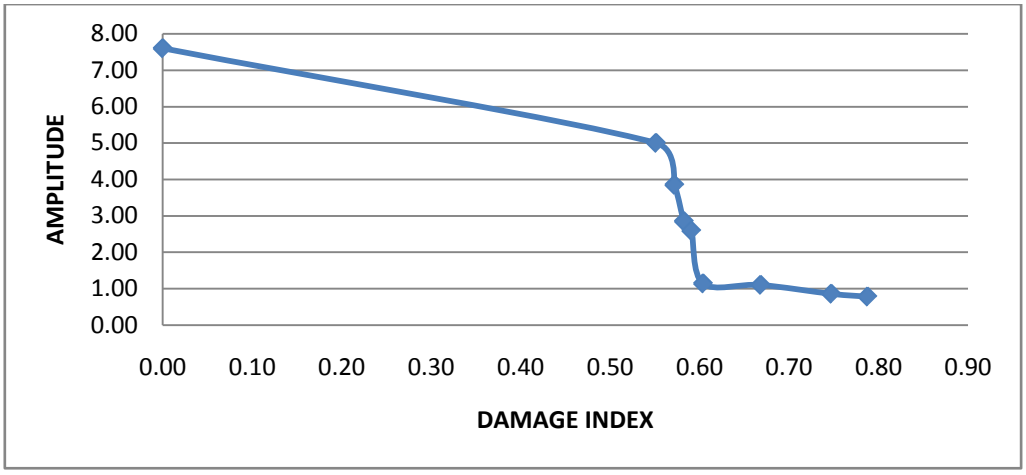

Fig 4.41 Change in amplitude vs. Damage index of retrofitted beam stressed at 90%

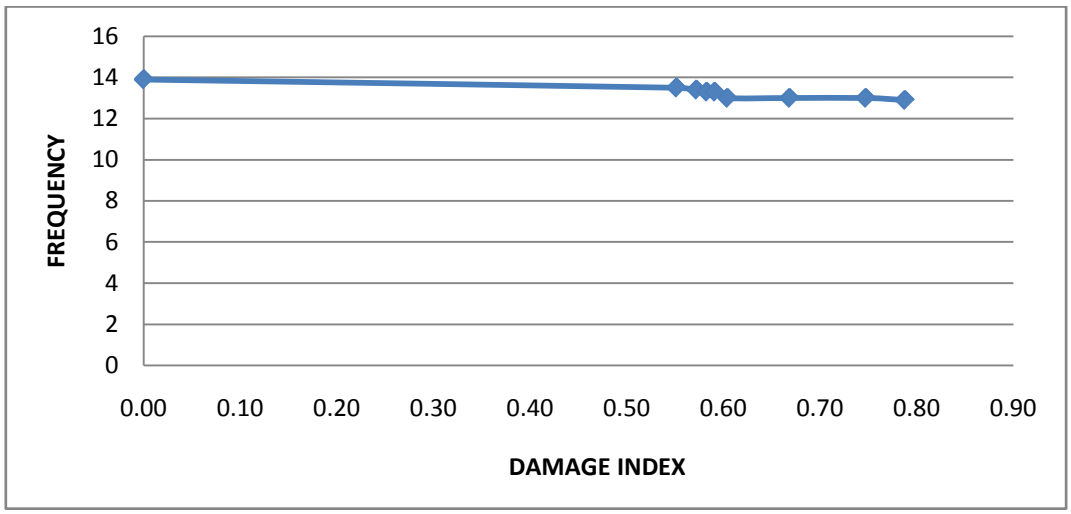

Fig 4.42 Change in frequency vs. Damage index of retrofitted beam stressed at 90%

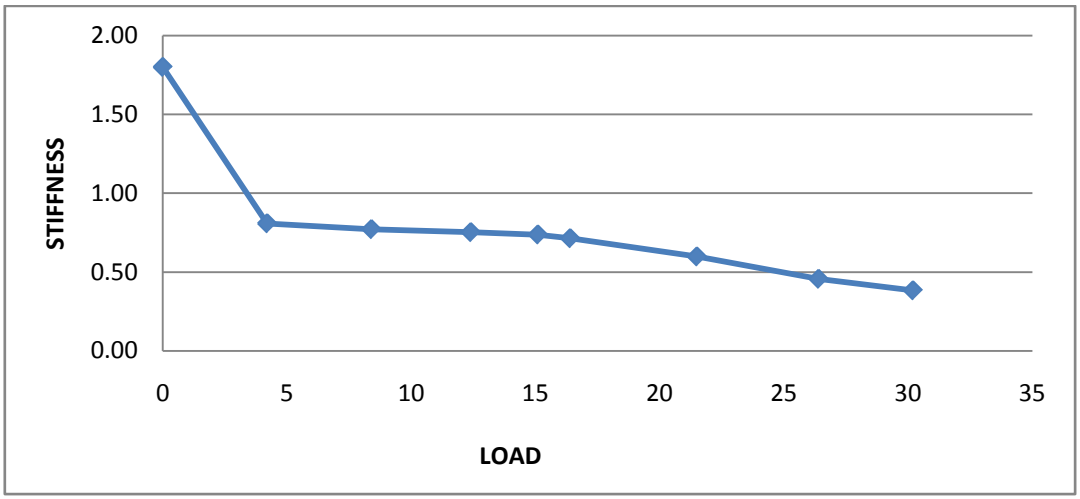

Fig 4.43 Change in stiffness vs. load of retrofitted beam stressed at 90%

4.3.2 RETROFITTED BEAM STRESSED AT 75%

The experimental results of control beam is stated below

RETROFITTED BEAM 75%					
LOAD (kN)	DEFLECTION (mm)	STIFFNESS (kN/mm)	DAMAMGE INDEX	FREQUENCY	AMPLITUDE (mm/sec^2)
0	0	1.80	0.00	15	7.30E+00
4.2	4.9	0.86	0.52	14.9	6.75E+00
8.4	10.1	0.83	0.54	14.9	6.25E+00
12.4	15	0.83	0.54	14.8	3.50E+00
15.1	18.4	0.82	0.54	14.8	2.05E+00
16.4	21.25	0.77	0.57	14.8	1.65E+00
21.5	43.9	0.49	0.73	14.8	1.55E+00
26.4	55.7	0.47	0.74	14.8	1.30E+00
30.2	71	0.43	0.76	14.7	8.80E-01

Table 4.11 Experimental results of retrofitted beam stressed at 75%

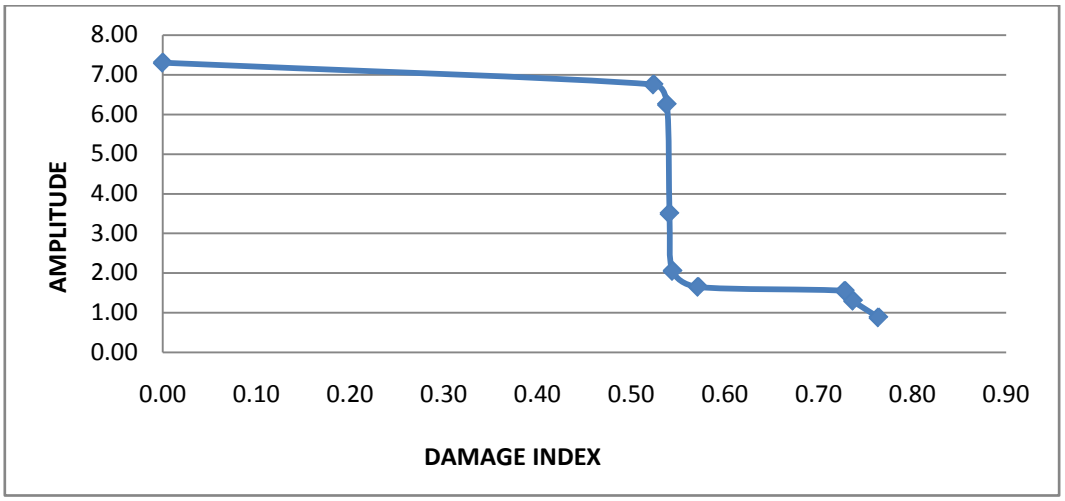

Fig 4.44 Change in amplitude vs. Damage index of retrofitted beam stressed at 75%

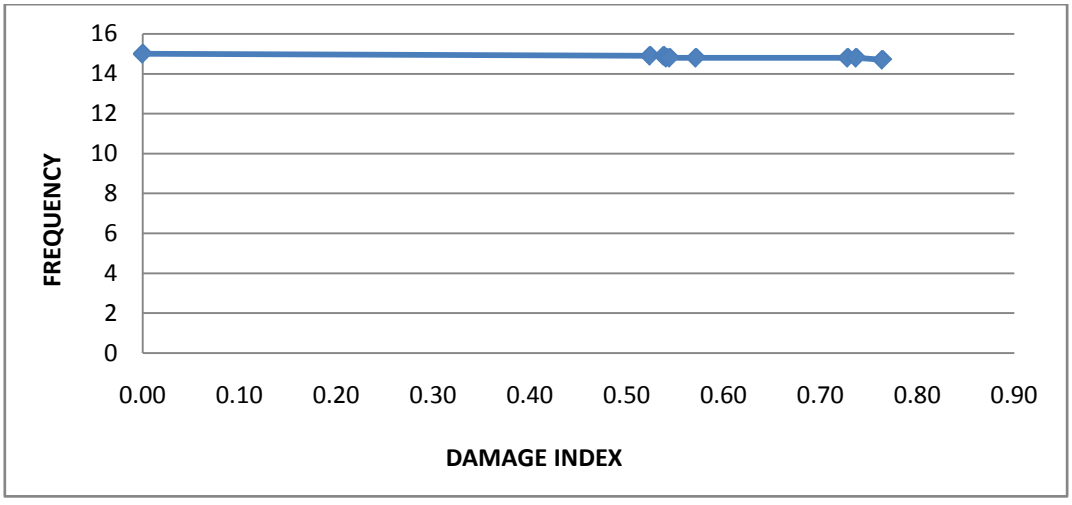

Fig 4.45 Change in frequency vs. Damage index of retrofitted beam stressed at 75%

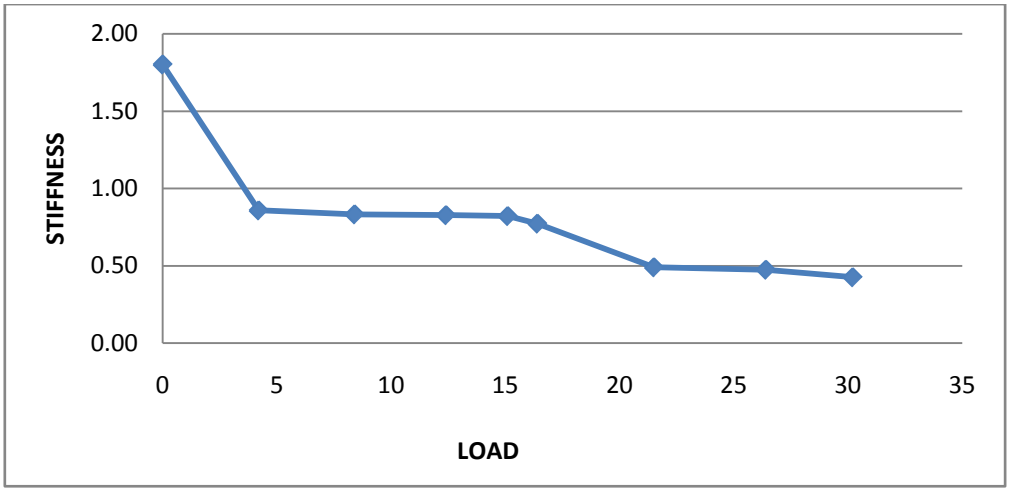

Fig 4.46 Change in stiffness vs. load of retrofitted beam stressed at 75%

Comparing the experimental work with analytical work it can be observed that the general behaviour of the finite element models represented by the load-deflection curves show good agreement with the experimental data from the full scale beam tests. Also analytical results of the stressed retrofitted beam at 75% and 90% of the ultimate load of the control beam show good agreement as the experimental results.

In case of experimental work the amplitude measured in acceleration while in case of analytical work the amplitude is measured in displacement. From both work it can be observed that the damage index at which the change in amplitude in analytical work is more than experimental work.

It can be noted that there is decrease in frequency with respect to damage index is observed in both experimental as well as analytical work.

CONCLUSION

5.1 GENERAL

An analytical study is carried out for FE modelling of the retrofitted RC beam.

In the first phase of the study, the control beam and the stressed retrofitted beam at 75%, and 90% of the ultimate load of the control beam are modelled and heir load deflection is analyzed.

In the second phase vibration characteristics are studies by doing the harmonic analysis.

5.2 CONCLUSION

The main conclusion drawn are summarized below:

1. For control beam for first load case, i.e. at 0 kN, the frequency is 11.7 Hz. Also as we increase the load the frequency goes on decreasing to 5.3 Hz for ultimate load.

2. For retrofitted beam stressed at 75 % it was found at the value of frequency decreases as there is increase in load.

3. Similar trend is observed for retrofitted beam stressed at 90 %.

4. From the load-deflection we concluded that there is there is increase in load carrying capacity of retrofitted beam as compare to control beam.

5. By observing the results we observe that there is sudden increase and decrease in amplitude in all beams at a particular load which is due to the sudden decrease in damage index at that location.

6. We observe that there is increase in stiffness in retrofitted beam as compared to control beam.

7. We can conclude as we monitor the health of retrofitted beam by measuring the vibration characteristics by increasing the load the frequency goes on decreasing as similar to that of control beam but the different percentage of variation.

8. The general behaviour of the finite element models represented by the load deflection curves show good agreement with the experimental data from the full scale beam tests.

10. In comparison with experimental data there is increase in damage index for analytical work than experimental.

11. Decrease in stiffness with increase in load can be observed for both experimental and analytical work.

REFERENCE

1. Balamuralikrishnani R and Jeyasehar C.A (2009),“ **Flexural behaviour of RC Beam Strengthened with Carbon Fibre Reinforced Polymer (CFRP) Fabrics**”, The Open Civil Engineering Journal pp 102-109.

2. Barbosa A.F a.d Ribeiro G.O (1998), “**Analysis of reinforced concrete structures using Ansys nonlinear concrete model**”, Computational Mechanics- New trends and applications, Barcelona, Spain.

3. Fassios C.R and Lieven N.A.J (2007),”**Time series methods for fault detection and identification in vibrating structures**” Phil. Trans. R. Soc. A, Vol. 365, pp. 411-448

4. Farrar C R and Worden K (2006),” **An introduction to structural health monitoring**”, Phil Trans Soc A, Vol. 365, pp 313-315

5. Friswell M.I (2007),”**Damage identification using inverse methods**” Phil. Trans. R. Soc. A, Vol. 365, pp. 393-410

6. Goyal Ankush (2007),”Structural Health Monitoring of retrofitted RCC beams using vibration measurements” Thesis, Thapar university, 2007

7. Hayton P, Utete S, King D, King S, Anuzis P and Tarassenka L (2007),”**Static and dynamic novelty detection methods for jet engine health monitoring**” Phil. Trans. R. Soc. A, Vol. 365, pp. 493-514

8. Ibrahim A.M and Mahmood M.S (2009) “**Finite Element Modeling of Reinforced Concrete beams Strengthened with FRP Laminates**”, Eurojournals 1450-216X Vol.30 No.4 pp 526-541

9. Irvine.T (1999),” **The Steady-state Response of a Single-degree-of-freedom System subjected to a Harmonic Force**” Vibrationdata.com Publications, 1999

10. Lee U, Jeong W and Cho J (2004), “**Frequency Response Function-Based Damage Identification Method for Cylindrical Shell Structures**”, KSME Internantional Journal, Vol. 18, No 12, pp 2114-2124

11. Liu X, Lieven N.A.J and Ambrosio P.J.E (2009),’ **Frequency response fuction shape based methods for structural damage localisation**” Mechanical systems and signal processing 23 pp 1243-1259

12. Lynch J.P (2007),” **An overview of wireless structural health monitoring for civil structures**” Phil. Trans. R. Soc., Vol. 365, pp 345-372

13. Maia N.M.M, Silva J.M.M and Almas E.A.M (2002),” **Damage detection in structures from mode shape to frequency response function methods**”, Mechanical systems and signal processing, Vol. 17, No. 3, pp 489-498

14. Mal A, Banerjee S and Ricci F (2007),"**An automated damage identification technique based on vibration and wave propagation data**" Phil. Trans. R. Soc. A, Vol. 365, pp-479-491

15. Park G and Inman D.J (2007)," **Structural health monitoring using piezoelectric impedance measurements**" Phil. Trans. R. Soc. A Vol. 365, pp 373-392

16. Saifullah I, Hossain M.A, Uddin S.M.K, Khan M.R.A and Amin M.A (2011),"**Nonlinear analysis of RC beam for different shear reinforcement patterns by finite element analysis**", UCEE-UENS, Vol.11 No. 1

17. Saikia B, Kumar P ,Thomsas J and Ramaswamy A (2005),"**Strength and serviceability performance of beams reinforced with GFRP bars in flexure**", Journal of construction and building materials, Vol. 21, pp 1709-1719

18. Schultz W, Dayan P and Montague P.R (1997),"**A neutral substrate of prediction and reward**", Sciencemag.com, science, Vol.275

19. Sohn H, Farrar C.R , Hemez F.M, Czarnecki J.J, Shunk D.D, Stinemates D.W and Nadler B.R (2003)," **A review of structural health monitoring literature:1996-2001**", Los Alamos National Laboratory Report, LA-13976-MS

20. Staszewski W.J and Robertson A.N (2007),"**Time frequency and time scale analysis for structural health monitoring**" Phil. Trans. R. Soc. A, Vol. 365, pp. 449-477

21. Tavio T and Tata A (2009)," **Predicting nonlinear behaviour and stress strain relationship of rectangular confined reinforced concrete columns with Ansys**" Civil engineering dimension, Vol. 11, No 1 pp 23-31

22. Todd M.D, Nichols J.M, Trickey S.T, Nichols C.J and Virgin L.N (2007),"**Braggrating based fibre optics sensors in structural health monitoring**" Phil. Trans. R. Sec. A, Vol. 365, pp. 317-343

23. Worden K and Manson G (2007),"**The application of machine learning to structural health monitoring**" Phil. Trans. R. Soc. A, Vol. 365, pp. 515-537